Lancaster University
MSc by Research Thesis

Synthesis and Characterisation of Cyclometallated Iridium (III) Tris-triazole Bidentate Complexes and Exploratory Attempts Towards Chromium (III) Analogues

Amber Makin

For the degree of MSc by Research in Chemistry

31st December 2025
Word count:25090

Keywords: iridium, triazole, meridional, facial, carbene, chromium

Acknowledgements:

Dr Nicholas Fletcher for his supervision, guidance and support throughout this project.

Andrew Stocker for his support and supervision in the lab.

Khaleel Zareen for his previous work and the data provided for comparisons discussed in this report.

Dr Nathan Halcovitch for obtaining and processing the crystal structure discussed in this report.

Dr David Rochester for obtaining and processing the mass spectra discussed in this report.

Abstract:

Cyclometallated iridium(III) complexes containing N-heterocyclic carbene (NHC) ligands have gained significant research interest due to their highly tuneable photophysical properties and potential applications in areas such as organic light-emitting diodes (OLEDs), photocatalysis, and bioimaging. Despite this, controlling emission behaviour, quantum efficiency, and geometric structure through ligand design remains an important challenge in the development of high-performance phosphorescent materials. In addition, extending these design principles to earth-abundant first-row transition metals such as chromium(III) could provide access to more sustainable luminescent systems.

This research investigates how the modification of cyclometallating NHC ligands influences the structure, geometric isomer distribution, and photophysical behaviour of luminescent iridium(III) complexes and further goes on to explore whether these ligand design strategies can be transferred to chromium(III) systems to produce analogous complexes. A range of substituted 1,2,4-triazolium precursors were synthesised and subsequently functionalised to produce six cyclometallating NHC ligands with one of three electronic phenyl substituents (H, CF_3, NO_2) and one of two different steric substituents on the triazole (methyl or benzyl).

These ligands underwent complexation with iridium(III) to yield six novel tris-cyclometallated complexes, with isolable *mer* and *fac* isomers obtained for four complexes and pure *mer* isomers obtained for the other two. The observed *mer*/*fac* ratios were found to be strongly dependent on ligand substitution. Increasing steric bulk was found to favour the formation of the *mer* isomer under kinetic control, while installing electron-withdrawing substituents promoted *fac* isomer formation in the less sterically hindered systems. Single-crystal X-ray diffraction showed a clear correlation between ligand substitution, geometric distortion, and crystal packing, including evidence of stabilising π- π stacking interactions in the benzyl-substituted *mer* isomers.

Photophysical studies on these complexes demonstrated that while electron-withdrawing substituents significantly influence absorption characteristics, emission maxima remained largely unchanged when modifying the non-coordinating ligand substituents. This is consistent with what is expected of emission from a triplet metal to ligand charge transfer (MLCT) state. Emission efficiencies, however, were found to be strongly affected by steric bulk and geometric isomerism through their influence on non-radiative decay pathways.

Attempts to extend these ligand frameworks to chromium(III) complexes were generally unsuccessful, but highlighted fundamental differences in coordination chemistry between Ir(III) and Cr(III), including slower ligand substitution kinetics, hard-soft acid–base mismatch, and extreme air sensitivity. Overall, this work establishes clear relationships between the structure and properties of Ir(III) NHC emitters and defines the key challenges faced in extending these ligand design strategies to the synthesis of analogous NHC-based earth-abundant metal systems.

Abbreviations:

^{1}H NMR	Proton nuclear magnetic resonance
^{13}C NMR	Carbon nuclear magnetic resonance
a.u.	Arbitrary units
Bn	Benzene
$CDCl_3$-*d*	Deuterated chloroform
CF_3	Trifluoromethyl
COSY	Correlation Spectroscopy
Cr(III)	Chromium(III)
DCM	Dichloromethane
DMSO	Dimethyl Sulphoxide
EDG	Electron-Donating Group
EWG	Electron-Withdrawing Group
Fac	Facial
HMBC	Heteronuclear Multiple Bond Correlation
HOMO	Highest Occupied Molecular Orbital
HSAB	Hard soft acid base (theory)
HSQC	Heteronuclear Single Quantum Coherence Spectroscopy
Ir(III)	Iridium(III)
IR	Infrared
LCDs	Liquid crystal display
LEDs	Light emitting diode
LUMO	Lowest Unoccupied Molecular Orbital
Me	Methyl
MeCN	Acetonitrile
Mer	Meridional
MLCT	Metal to Ligand Charge Transfer
NHC	N-Heterocyclic Carbene
NMR	Nuclear Magnetic Resonance
NO_2	Nitro group
NOESY	Nuclear Overhauser Effect Spectroscopy
OLED	Organic Light-Emitting Diode
Pet Ether	Petroleum Ether
PLQY	Photoluminescent Quantum Yield
THF	Tetrahydrofuran
TLC	Thin-Layer Chromatography
UV	Ultra-Violet
UV/Vis	Ultraviolet/Visible
ε	Molar absorbance coefficient
λ	Wavelength

Ligand and Ir(III) complex abbreviations:

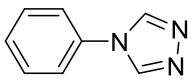

H-PTz

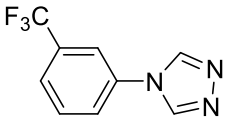

CF_3-PTz

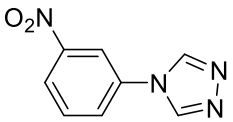

NO_2-PTz

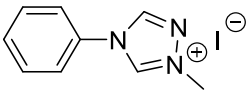

H-PTz-Me

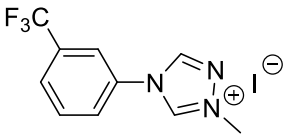

CF_3-PTz-Me

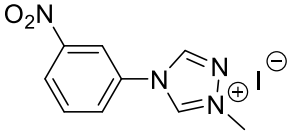

NO_2-PTz-Me

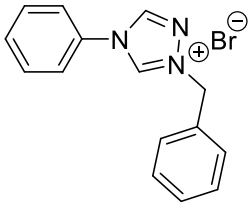

H-PTz-Bn

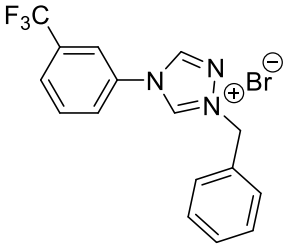

CF_3-PTz-Bn

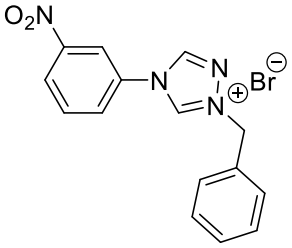

NO_2-PTz-Bn

Ir(H-PTz-Me)$_3$

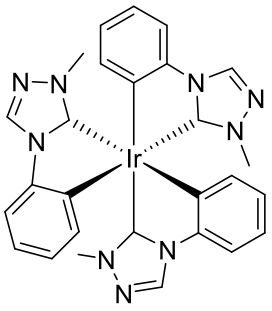

fac

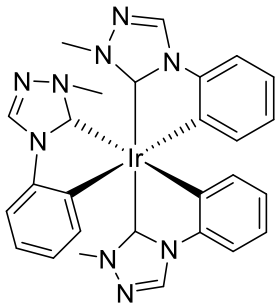

mer

Ir(H-PTz-Bn)$_3$

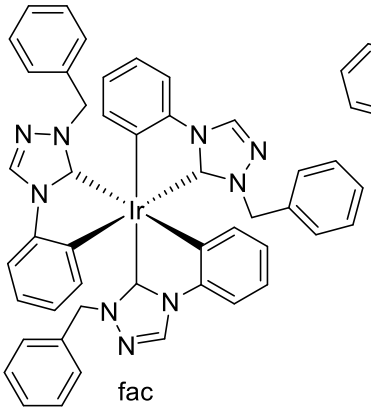

fac

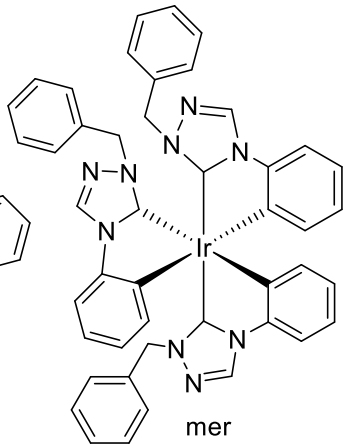

mer

Ir(CF$_3$-PTz-Me)$_3$

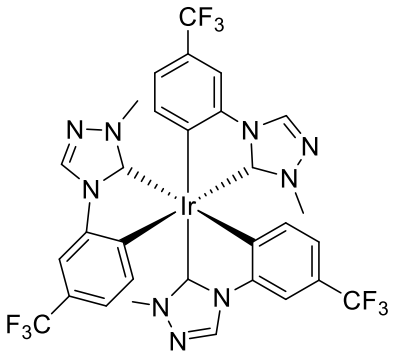

fac

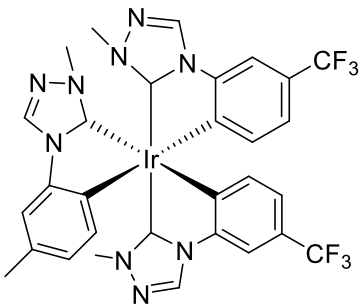

mer

$Ir(CF_3\text{-}PTz\text{-}Bn)_3$

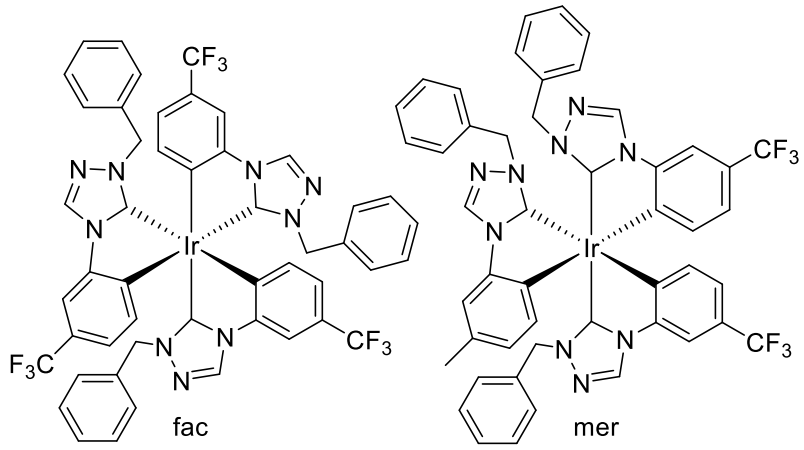

$Ir(NO_2\text{-}PTz\text{-}Me)_3$

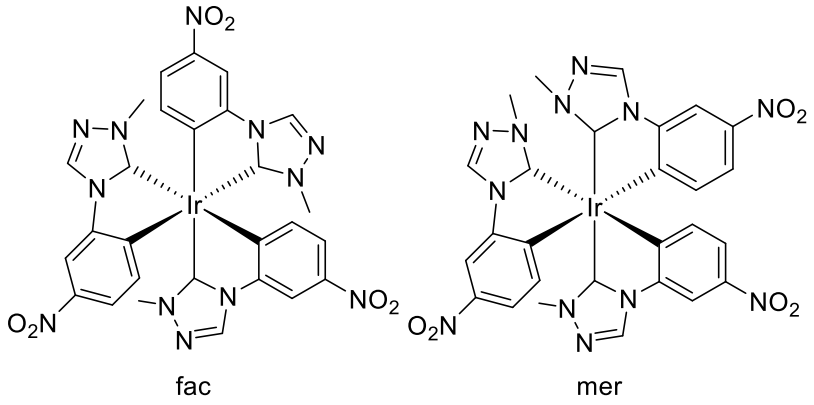

$Ir(NO_2\text{-}PTz\text{-}Bn)_3$

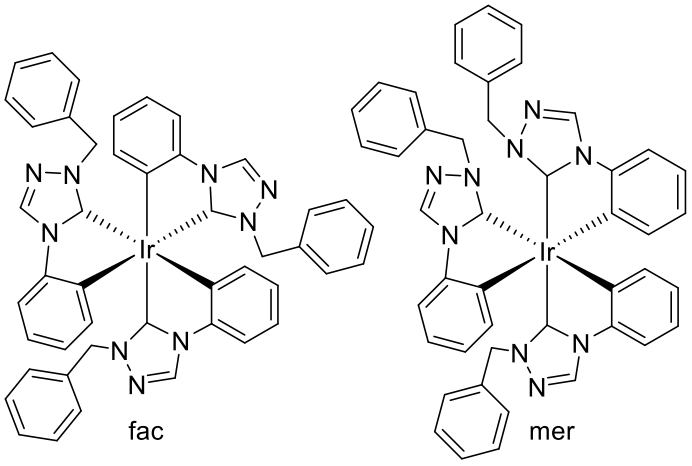

Contents

1. Introduction and background

1.1. Introduction of luminescent materials

Luminescent compounds have become essential in the modern world, from OLEDs and LEDs to sensors, decontamination agents, and luminescent biomarkers. Their use spans a wide range of industries and applications, with different emission wavelengths offering unique functionalities.[1-7] Whilst red and green emitting devices are more abundant and are known to be relatively stable, their blue emitting counterparts are found to be much less robust.[8-10] This is highlighted by their increased susceptibility to degradation and in the limited number of reported blue emitting compounds.[11, 12]

These discrepancies are driven by the unique challenges faced during the creation of blue emitting devices. The large energy gap between the highest occupied molecular orbital (HOMO) and the lowest unoccupied molecular orbital (LUMO) required for blue light emission is difficult to overcome. As a result these devices typically exhibit short emission lifetimes, low emission colour purity and a reduced stability, resulting in bond breakage and consequently a shorter device lifetime.[8, 10, 12, 13] Their inability to produce the desired deep blue emission, coupled with their poor efficiency leaves a considerable gap in the development of these compounds for a stable long-lived blue emitting device.[7, 10, 14]

The difficulties in producing blue emission however is not the only noticeable gap in this field, as red emitting devices, despite being more abundant, face their own set of unique challenges due to having low quantum yields and high thermal quenching.[15, 16] In addition, many red emitting devices often rely on expensive rare materials and harsh conditions such as Eu(III) doped nitrides which are synthesised at high temperatures and pressures which can be both costly and impractical for the manufacturer.[15, 17, 18]

It is also important to consider the environmental implications of continuing to use these devices. In today's landscape of chemical research, with its heavy emphasis on sustainability, it becomes apparent that we need alternatives to these devices made from cheaper, more abundant materials with less extreme reaction conditions.[19-21]

1.2. Blue emissive complexes and the challenges in blue emission

Various heavy metals have been studied for the purpose of producing compounds capable of red and blue emission. One example of a blue emissive compound is the zinc(II) Schiff-base and azomethine complexes as reported by Srinivas *et al.* in 2017 (**Figure 1**).[22, 23] These complexes feature a zinc(II) metal centre and are coordinated to two organic ligands with bidentate covalent bonds. These complexes were reported to show blue light emission at 468-436 nm via a ligand centred fluorescence as opposed to a metal to ligand charge transfer (MLCT). This is caused by their d^{10} closed shell electronic configuration, which enables a radiative decay without substantial spin-orbit coupling contributions from the metal centre. Despite being deep blue emitting, relatively inexpensive and easily

sourced owing to the use of zinc, these complexes have several limitations with regards to their stability and colour purity.[8, 22] As their excited states are not stabilised by heavy-atom effects, their excited states are easily distorted leading to broad emission bandwidths meaning that the colour purity and brightness is poor. In addition, these compounds show lower photostability due to singlet excited electrons remaining in higher energy states that are more reactive. This contrasts with complexes which have heavy metal spin orbit coupling, where the electrons undergo inter-system crossing (ISC) to lower energy triplet states that are more stable.[9, 11, 23] The electrons residing in these higher energy states make the organic ligands more prone to damage and will also limit the maximum internal efficiency of the complex.[11, 22, 23]

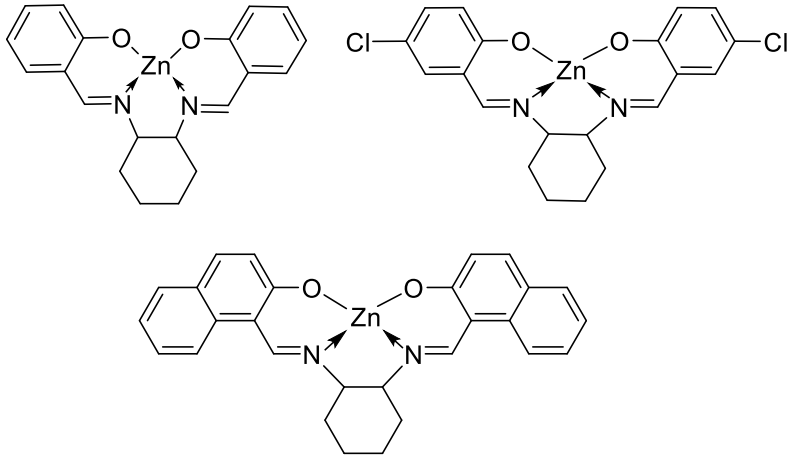

Figure 1: The Zinc(II) Schiff-base and azomethine complexes reported by Srinivas *et al.*[22]

Similarly, the three-coordinate Cu(I) NHC complexes synthesised by Krylova *et al.* in 2010 (**Figure 2**) also showed blue/green emission, this time via a phosphorescence arising from MLCT and ligand to ligand charge transfer (LLCT) transitions which are altered through ligand design. [24] However, these complexes have limitations, as they suffer from poor colour purity, increased non radiative decay and lower photoluminescence quantum yields caused by the distortion of the complex geometry upon reaching the excited state. [9, 25]

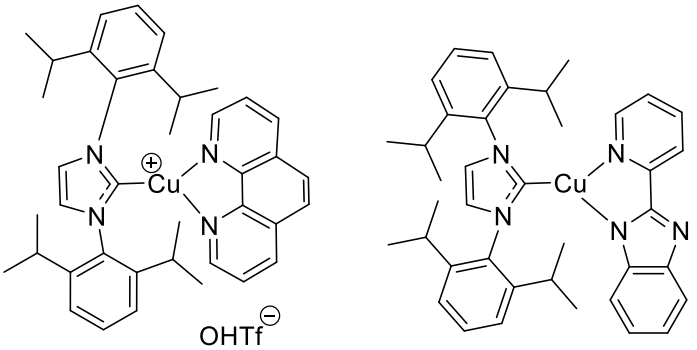

[(IPr)Cu(phen)]OTf (IPr)Cu(pybim)

Figure 2: Three-coordinate Cu(I) NHC complexes synthesised by Krylova *et al.*[24]

More recently coinage metals became a focus for synthesising blue emissive compounds, such as the two coordinate Cu, Ag, and Au benz-imidazolyl-carbene complexes made by Hamze *et al.* in 2020 (**Figure 3**).[26] They reported these complexes gave deep-blue emission around 430 nm with high photoluminescence quantum yields due to the rigidity of the geometry of the complexes and the choice of ligands which prevented non-radiative decay pathways.[26, 27] Despite ticking many boxes for a perfect blue emitting device, these complexes have other limitations that hinder their practical application, most notably the complexity of their synthesis.[26] Additionally, as the complexes are only able to coordinate to two chelating ligands, the ligands must be substantially bulkier than in complexes with more coordination sites to prevent decomposition.[26, 28] The largest limitation associated with using coinage metal complexes for emissive compounds is that under excitation the complexes become susceptible to ligand dissociation, structural distortion and rearrangements due to the metal centres being soft metals. This results in metal-ligand bonds that are shorter and more labile, meaning that when charge transfers to the ligand π* orbitals during excitation the bonds weaken and can distort and break.[9, 25-27]

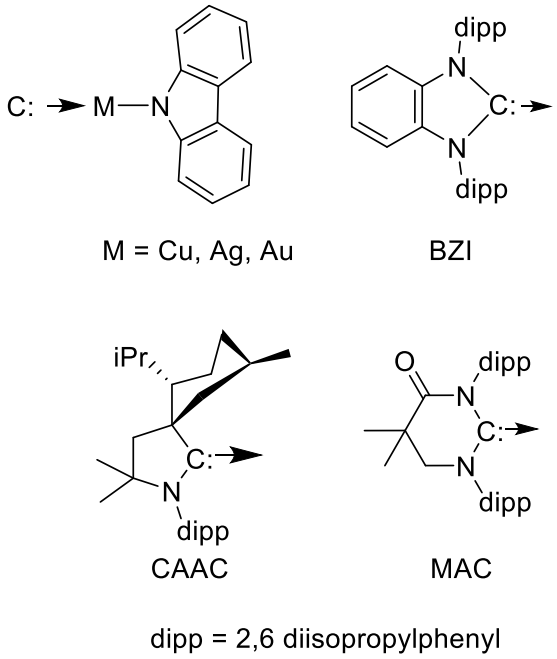

Figure 3: The two coordinate Cu, Ag, and Au benz-imidazolyl-carbene complexes made by Hamze *et al.*[26]

1.3. Blue emissive Ir(III) compounds

1.3.1. Advantages of Ir(III) for Blue emission

As seen in the examples explored thus far, amongst others, many blue emitters are good choices from a cost and sustainability standpoint, but their performance is constrained by a common series of challenges namely; poor colour purity, low photostability and broad emissions.[9-11] Consequently, the focus has shifted to the use of iridium as an alternative for luminescent cyclometallated complexes.[4, 29] The benefit of using iridium over other heavy metals is that is has strong spin orbit coupling due to its high atomic number which promotes ISC from singlet to triplet states significantly increasing internal quantum efficiency.[25, 30-32] Furthermore, strong spin orbit coupling acts to reduce the lifetime of the triplet excited state. The benefit of this is that radiative decay occurs quickly therefore the time available for quenching to occur is minimised thereby reducing the level of non-radiative decay that occurs. [31, 33-35]

As well as being thermally and chemically stable, iridium(III) is capable of forming incredibly stable complexes with a wide variety of cyclometallating ligands such as 2-phenylpyridine (ppy),[36] benzo[*h*]quinoline (Bq)[37] and the phenyl-substituted imidazolylidene complexes formed by Stringer *et al.* in 2014[38] to name a few. Compared to other heavy metals such as Pt(II), Pd(II), Re(I) or Os(II), which are restricted by square-planar or highly rigid pseudo-octahedral geometries, iridium(III) can support a wide range of cyclometallated ligands.[39, 40] This means that by using Ir(III) it allows a wider scope for tuning and tailoring complexes for specific properties such as emission colour and quantum lifetimes.[38 41-44] Moreover, with cyclometallating ligands, Ir(III) forms complexes with an octahedral geometry which is desirable because it is significantly more robust and can accommodate multiple bidentate or tridentate cyclometallating ligands without destabilising the metal centre.[36, 45] In contrast, metals such as Pd(II) and Pt(II) typically adopt square-planar geometries, which despite being capable of producing highly blue emissive complexes, are more limited in the number and type of cyclometallating ligands they can support due to having stricter bite angle and steric constraints[39, 40, 46] making Ir(III) significantly more versatile for synthesising complexes with structurally diverse and highly rigid ligand environments. As the Ir(III) octahedral geometry is significantly more rigid it means that the excited triplet state is stabilised within the rigid octahedral field. This reduces the strain on the ligands during excitation making the complexes more resistant to non-radiative decay and improves quantum yield and gives a better colour purity for these complexes.[40, 47-50]

1.3.2. Ligand field control and NHC based Ir(III) complexes

An example of an iridium(III) centred emissive metal complex in recent literature is the *fac*-Ir(flz)$_3$ complex synthesised by Sajoto *et al.* (**Figure 4**).[51] This complex uses fluorenyl-substituted pyrazolyl ligands to form an emissive blue compound that emits at 480 nm and has a photoluminescence quantum yield of 0.38.[51] However owing to the structural flexibility of the five-membered pyrazolyl chelating ligands, and their medium ligand field strength, the complex is susceptible to geometric distortion in the excited state broadening emission and increasing non-radiative decay pathways leading to poorer colour purity and a red shift to a green/blue

emission as opposed to deep blue.[51, 52] To overcome this, alternative research used N-heterocyclic carbene (NHCs) based ligands that have a much stronger ligand field strength and have very strong σ-donation abilities leading to favourable radiative decay pathways resulting in bright, strongly emissive complexes.[27, 31, 52] For example, Sajoto *et al.* in 2005 demonstrated that replacing cyclometallating pyrazolyl ligands with strongly σ-donating NHC ligands in Ir(III) complexes, yields efficient blue to near-UV phosphorescence, suggesting that the strong ligand-field strength and σ-donation of NHCs can promote favourable radiative decay pathways.[51, 52] Other examples of this can be seen in the work of Sebris *et al.* who synthesised a homoleptic purine-based NHC Ir(III) complex (**Figure 5**)[53] which showed deep-blue emission at 437–466 nm with excellent quantum yields due to the strong σ-donation and rigid geometry of the NHC ligands.[53] A similar complex was synthesised by Idris *et al.* who produced triazolyl–pyridine Ir(III) complexes[13] emitting in a sky-blue colour which had high device efficiencies with values over 15% external quantum efficiency owing to the strong ligand field which pushes non-emissive metal-centred excited states to higher energies preventing emission quenching.[13]

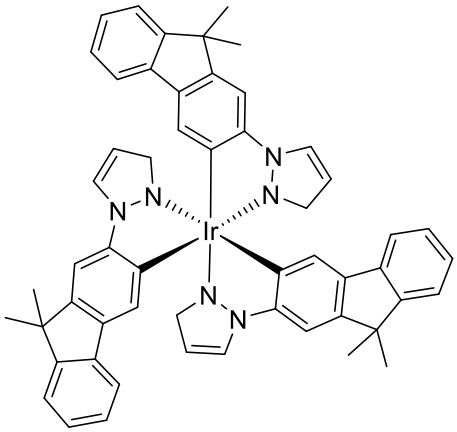

Figure 4: *Fac*-Ir(flz)$_3$ complex synthesised by Sajoto *et al.*[51]

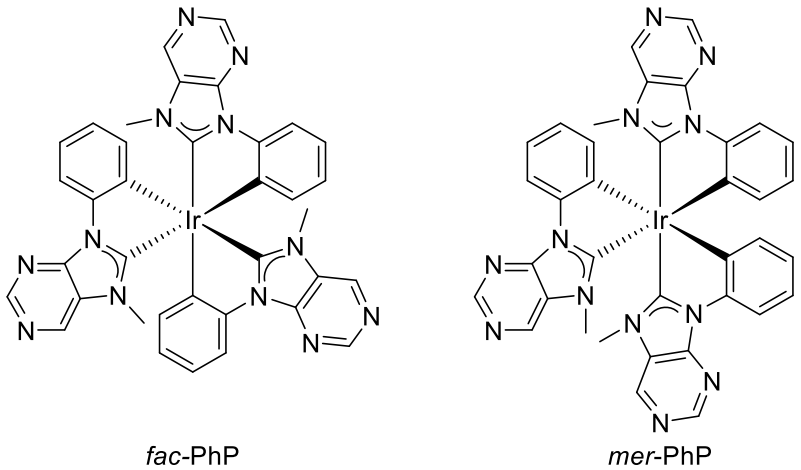

fac-PhP *mer*-PhP

Figure 5: The homoleptic purine-based NHC Ir(III) complex synthesised by Sebris *et al.*[53]

Using a bis-tridentate NHC ligand, Kuo *et al.* produced similarly efficient blue emitting Ir(III) NHCs (**Figure 6**).[54] In the process, they showed the benefits of a fully saturated coordination sphere for these complexes and demonstrated that the octahedral geometry is far superior to the square planar geometries of other luminescent complexes when it comes to minimising vibrational relaxation. This results in narrow, high colour purity emission and improved complex stability.[54] In contrast, Jin *et al.* in 2022 showed that the distortion of the excited state seen in other emissive compounds can be harnessed and controlled in iridium(III) complexes to form hyperphosphorescent blue complexes. In this context, hyperphosphorescence refers to an extremely bright, narrowband, and short-lifetime phosphorescence arising from the Ir(III) unit acting as a triplet sensitiser and transferring triplet energy to the organic emitter.[31, 55] They showed that they could increase the energy of the metal centred excited states by strengthening the ligand field by using increasingly more rigid and strongly donating ligands which made the metal centred excited state thermally inaccessible improving both efficiency and colour purity.[52, 55]

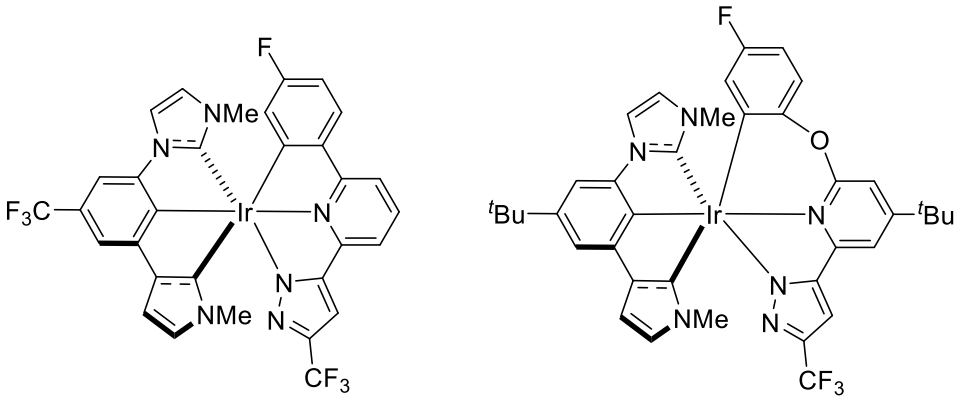

Figure 6: Ir(III) complexes with bis-tridentate NHC ligands synthesised by Kuo *et al.*[54]

Perhaps the most significant research in this area comes from Thompson and co-workers whose work has formed the basis for most modern day blue-emissive Ir(III) complexes.[31, 36, 52] Their paper from 2005 identified two key strategies for achieving blue and near-UV emission in Ir(III) complexes.[52] First, they demonstrated that the strengthening of the ligand field through the use of NHC donor ligands, which at the time was a big discovery, produced high-energy phosphorescence with short lifetimes, something that was previously unachievable with classical cyclometallating ligands such as the 2-phenylpyridine (ppy) ligands.[51, 52] They also explored the use of pyrazolyl ligands which have high energy π–π* orbitals and electron deficient heterocycles. Together these features raise the energy of the ligand centred excited state and increase the energy of the emissive triplet state showing pyrazolyl complexes to be excellent candidates for blue emission even without the use of strong σ-donors. Their research produced blue emitting complexes in the 480nm region.[51, 52]

In their more recent work, Thompson and co-workers developed these ideas further by exploring the effects of ligand modification to tune the electronic structure and therefore the chemical properties, and the effects of isomerism on

emission.[13, 45, 56] The results gave sky blue emissive complexes with external quantum efficiencies above 15% with isolatable *mer* and *fac* isomers in a 3:1 ratio.[13] Both the *mer* and *fac* isomers produced blue phosphorescence and it was concluded after electrochemical and photochemical analysis that the *fac* isomer showed a greater emission energy and longer lifetimes than its *mer* counterpart suggesting that the *fac* isomer is the most desirable.[13, 45] This observation is attributed to the small difference in the HOMO-LUMO gap.[13, 52] This research shows that high efficiencies can be reached without using incredibly rigid ligands therefore offering a more favourable synthetic approach to a blue emissive device.[13, 36]

Although significant progress has been made on the road to produce an efficient deep blue emissive complex, the research still has drawbacks when compared with the earlier pyrazolyl complexes.[13, 51] One issue is that they suffer from small quantum yields and excited state distortion of the complex geometry.[13, 53] Even the complexes reported in 2021, while showing better quantum efficiencies, still suffer from issues with colour purity failing to reach a deep blue colour.[9, 13] Additionally, they show significant environmental sensitivity meaning that the emission colour and device efficiency varied depending on environmental conditions such as the polarity or the rigidity of the structure.[9, 13, 57]

1.3.3. Remaining challenges of blue emissive Ir(III) complexes

Despite these advances, iridium blue emitters still face many limitations, most notably is the challenge of balancing the high triplet energies with structural robustness.[50, 57] Synthesising deep blue Ir(III) complexes requires very strong ligand fields and highly rigid ligands in order to prevent non-radiative pathways.[52, 58, 59] However, in working to prevent this by increasing rigidity this can restrict the tunability of the complex and leads to concentration induced quenching caused by strong intermolecular interactions.[50, 57, 60] Conversely using ligands with very strong ligand fields for the high triplet energies means that there is an increased risk of ligand degradation and loss during excitation as the triplet energy reaches the threshold for bond dissociation leading to reduced device lifetimes.[50, 58, 61] Consequently, this trade-off between deep blue emission and device stability is the biggest roadblock to forming efficient and effective Ir(III) blue phosphors.[57, 60, 62, 63]

1.4. Red Emitters and Their Limitations

Despite being more abundant, red emissive compounds often rely on the use of rare and expensive metals such as Ir(III), Ru(II) and Os(II)[1, 23, 27, 64-67] and in cases such as Eu(III) and other rare-earth phosphors, harsh synthetic conditions.[68-70] Some examples of common red phosphors are the tris-cyclometallated Ir(III) complexes such as $Ir(piq)_3$ and $Ir(btpy)_3$ which are common phosphors in OLEDs due to their ability to achieve high radiative decay rates and external quantum efficiencies between 10-14% [35, 71] Similarly, Ru(II) polypyridyl complexes, like $[Ru(bpy)_3]^{2+}$ show thoroughly studied photophysics,[64, 72] while Os(II) complexes such as $[Os(phen)_3]^{2+}$ (**Figure 7**) have been shown to push emission wavelength into the deep red to near-infrared region.[1, 65, 73-75]

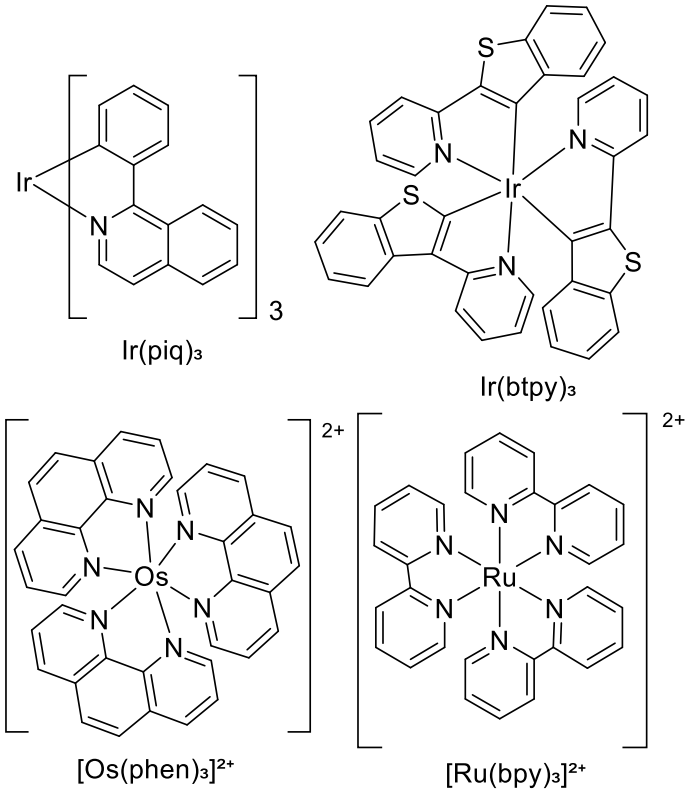

Figure 7: Common red phosphors consisting of tris-cyclometallated Ir(III), Ru(II)and Os(II) complexes.

However, despite their excellent photophysics, these traditional red emitters face several key limitations. One example is the lower quantum yields and increased non-radiative decay seen in many red phosphors as red emission is a much lower energy emission than blue or green. This means that the energy gap between the excited state and ground state are much smaller, which leads to an increase in the thermally induced deactivation pathways.[76-78] This can be seen in Ir(III) systems where red emission occurs from a ligand centred or MLCT state which lies very close in energy to the non-emissive metal centred state which results in quenching at room temperature.[33, 79-82] This is also seen in the Ru(II) complexes which show a decline in quantum yield as the emission wavelength shifts into the red region. This shift makes the MLCT states more thermally accessible to the metal centred states therefore reducing emission efficiency.[83-86]

Thermal quenching observed in deep red emitters occurs as the thermal energy increases as molecules can more easily populate non-radiative pathways.[33, 48, 87] A good example of this is seen in Os(II) complexes such as those produced by Borisov *et al.* in 2016 and more recently those synthesised by Roque *et al.* in 2020. The small gap between the emissive ^{3}MLCT state and the low-lying ^{3}MC states leads to a rapid quenching at raised temperatures, meaning these complexes are very temperature dependant and will perform well only at low temperatures which is problematic when used as an emitting device as their temperature fluctuates due to its usage.[88, 89]

Furthermore, many highly efficient red emitters are based on rare earth ions, most commonly Eu(III).[90, 91] Eu(III)-doped materials, such as Eu^{3+} activated nitrides are an excellent example of this, giving narrow band red emissions with a high colour

purity. These materials are typically prepared through high temperature solid-state synthesis, although many molecular Eu(III) complexes can be synthesised under much milder conditions. However, because these Eu(III) phosphors operate via a lanthanide f–f transition they have a fundamentally different photophysical mechanism compared to molecular transition-metal complexes like those made with Ir(III) and Cr(III) reliant on strongly absorbent ligands to allow excitation via the antenna effect. Therefore, while worth mentioning they are less relevant in this context as they provide a very limited insight into the ligand field tuning strategies that are central to the Ir(III) complexes. Additionally, from a sustainability perspective the use of Eu(III) is not desirable due to it being geographically restricted in the areas it can be found and therefore subject to geopolitical and market instability.[92-94]

1.5. Chromium(III) Complexes as Red Emitters

1.5.1. Motivation for Cr(III) as a sustainable red emitter

As a result of these issues there is a growing push toward earth-abundant alternatives for red emitters. One promising direction for this is the use of chromium(III) complexes, which offer the potential for red emission[64, 95] while avoiding the economic and environmental drawbacks associated with conventional heavy-metal phosphors.[96-99]

1.5.2. Photophysical limitations of Cr(III) complexes

Although chromium(III) is an attractive alternative for synthesising sustainable red emitting materials, its photophysical behaviour has thus far been inferior to that of 4d and 5d metal complexes such as those made with Ru(II), Os(II), and Ir(III).[64, 65, 96, 98] The reason for this is that in an octahedral ligand field Cr(III) possesses a d^3 electron configuration, which produces the spin-forbidden $^2E/^2T_1 \rightarrow {}^4A_2$ transitions that are responsible for luminescence.[100, 101] For efficient phosphorescence to occur, these doublet states must have considerable separation from the non-radiative $^4T_2$ state.[64, 102-104] However, in most Cr(III) complexes such as the $[Cr(H_2O)_6]^{3+}$ and $[Cr(NH_3)_6]^{3+}$ complexes investigated by Kirk and Porter,[100] the ligand field strength is too weak to create a large enough gap between the emissive $^2E/^2T_1$ levels and the thermally accessible $^4T_2$ state resulting in population of the $^4T_2$ state where decay occurs non-radiatively lowering the emission intensity (**Figure 8**).[96, 98, 100]

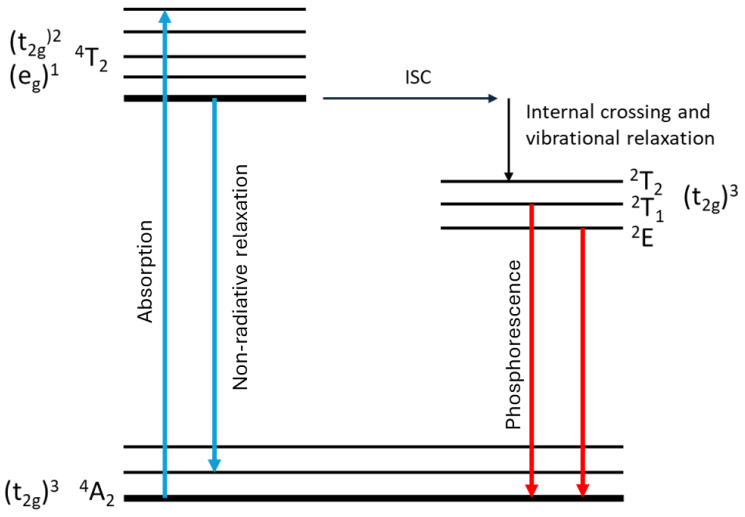

Figure 8: A simplified energy level diagram of Cr(III) showing the spin-allowed $^4T_2 \rightarrow {}^4A_2$ absorption and the spin-forbidden $^2E/^2T_1 \rightarrow {}^4A_2$ luminescent decay. Efficient emission requires a large energy gap between the emissive doublet states and the thermally accessible $^4T_2$ state as reported by Otto *et al.*[95]

A good example of these limitations comes from the widely studied tris-bipyridine $[Cr(bpy)_3]^{3+}$ and tris-phenanthroline $[Cr(phen)_3]^{3+}$ complexes.[100] These complexes consist of relatively flexible five-membered chelating rings around a chromium centre.[64, 96] The flexibility of the ligands causes distortions on the octahedral geometry weakening the ligand field and reducing the energy gap between the ^2E and $^4T_2$ states. This leads to low quantum yields, short lifetimes and very weak room temperature emissions which are hard to detect.

For example, the $[Cr(bpy)_3]^{3+}$ complex shows phosphorescence for only 63-74 µs at room temperature with a vanishingly low intensity due to the energy gap being too small to prevent non-radiative decay. Similar issues are observed in the $[Cr(phen)_3]^{3+}$ complexes, which still do not have a strong enough ligand field strength to stabilise the emissive doublet states despite having a more rigid ligand framework than the $[Cr(bpy)_3]^{3+}$ complexes.[64, 96, 100] The combination of weak ligand fields and small energy gaps between ground and excited states, along with the high amounts of rapid non-radiative relaxation observed in these complexes has historically prevented Cr(III) complexes from being considered as practical red emitters.

Recent research has aimed to overcome these limitations by using strong field ligands in order to increase the $^2E/^4T_2$ energy gap. These ligands have strong σ donation or π acceptance and hence act to raise the energy of the metal centred $^4T_2$ state thereby widening the energy gap. The benefits of this are that back intersystem crossing into the $^4T_2$ state becomes thermally inaccessible therefore supressing non-radiative decay and increasing emission intensity.[64, 65, 95, 105]

Another method to overcome these limitations suggested by researchers is to choose ligands with a more rigid framework and/or larger bite angles such as tridentate ligands as shown with the $[Cr(ddpd)_2]^{3+}$ complexes made by Otto and Wenger in 2015 (**Figure 9**).[95] The more rigid the ligand framework is the less

distortion occurs during excitation resulting in less non-radiative decay and an increase in the emission lifetimes and quantum yields. By using tridentate ligands, such as ddpd, this gives a larger bite angle and creates a more rigid geometry, thereby minimising excited state distortion. This rigidity helps to stabilise the emissive ^2E state in Cr(III) complexes, resulting in longer lived and more efficient spin-flip ($^2E \rightarrow {}^4A_2$) phosphorescence. Moreover, using tridentate ligands increases the metal to ligand orbital overlap strengthening the ligand field further while also raising the energy of the metal centred state making them less thermally accessible hence improving emission quantum yield from the excited states.[64, 65, 97, 102, 105]

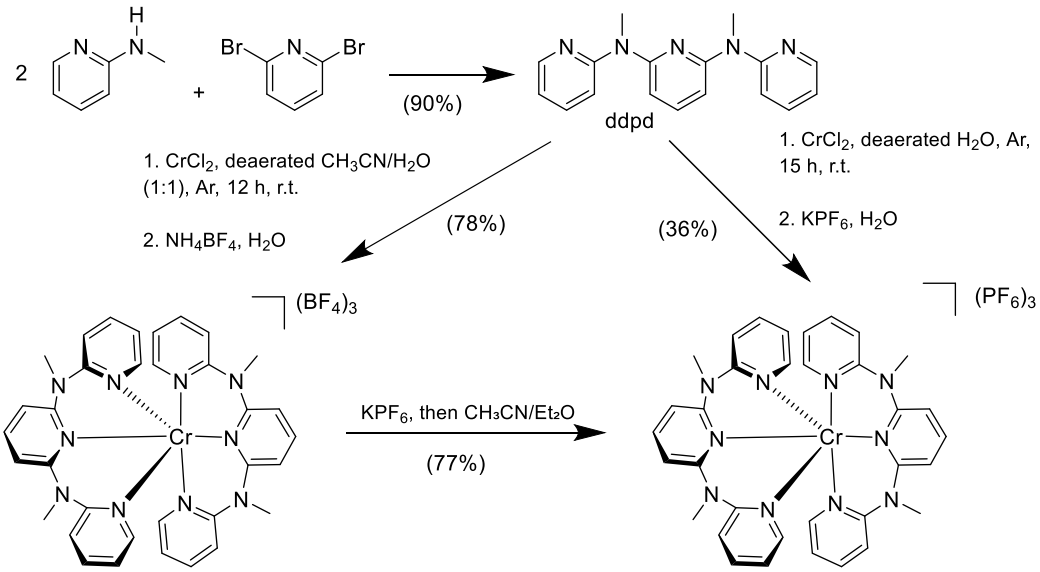

Figure 9: Synthesis of the tridentate ddpd ligand and its corresponding Cr(III) complexes as reported by Otto and Wenger.[95]

Similarly, heteroleptic tris-bidentate and bis-terpyridyl systems such as those reported by Doistau *et al.* have shown that careful ligand design can tune the Cr(III) emission wavelength from the near-infrared into the deep-red region possibly providing a more sustainable pathway into red emission.[65, 95, 96, 106-110]

Although Cr(III) red emitters still struggle to rival the brightness and efficiency of its Ir(III) or Ru(II) analogues, the combination of a lower cost synthesis, the availability, and the gradual improvement of its photophysical properties achieved in recent years particularly in the alteration of ligand-field strength places chromium as a promising alternative for sustainable red emissive devices.[65, 96]

1.6. Photophysical Mechanisms in Ir(III) and Cr(III)

In order to understand the importance of ligand choice and how different ligands will affect the HOMO to LUMO energy gap and subsequently the emission wavelength, it is important to understand how complexes of both iridium and chromium luminescent species emit light.[44, 64, 98, 103] Cyclometallated Ir(III) complexes emit light by phosphorescence via a MLCT.[29, 36] The excited triplet states are readily populated via an intersystem crossing driven by the strong spin orbit coupling of the iridium(III).[23, 31, 33] As the LUMO is centred on the ligands this

means that the HOMO-LUMO energy gap is largely controlled by the rigidity and substituents of the ligands allowing tuning of the emission wavelength by way of altering the size of this energy gap. [42, 48, 111]

In contrast Cr(III) complexes emit light through a different mechanism arising from their d^3 electronic configuration.[64, 100] Upon excitation electrons initially populate the high energy quartet ligand-field states ($^4T_2$ or $^4T_1$), which then proceed to undergo intersystem crossing into the lower-lying doublet states (^2E or $^2T_1$)(**Figure 10**).[100, 101] However, direct excitation into the doublet manifold is both Laporte-forbidden and spin-forbidden, and therefore inefficient. [100, 101] In most emissive Cr(III) complexes the population of the ^2E state occurs indirectly via a MLCT state which undergoes rapid intersystem crossing to a short-lived doublet charge separated state that then relaxes into the long-lived ^2E ligand field state.[64, 96] When relaxation from these doublet states to the quartet ground state ($^4A_2$) occurs, this results in an emission of light. This is also known as a spin-flip emission as the spin multiplicity changes between the transition from doublet to quartet states. This is a spin forbidden d-d transition and hence the radiative decay from the $^2E/^2T_1$ states to the $^4A_2$ ground state is very slow. [100, 101] However, in most Cr(III) complexes this slow radiative decay competes with fast non-radiative vibrational decay which dominates, resulting in an emission that is weak and a short excited-state lifetime**.** [64, 96] Consequently, emissive Cr(III) complexes require strong-field, rigid ligands that can increase the small $^2E/^4T_2$ energy gap and therefore suppress non-radiative vibrational decay.[96, 104, 112, 113] Strong σ-donating ligands or those with large bite angles such as ddpd have shown to be excellent ligand choices producing complexes capable of room temperature spin-flip phosphorescence with longer lifetimes and much improved quantum yields.[95, 97, 105, 107, 114]

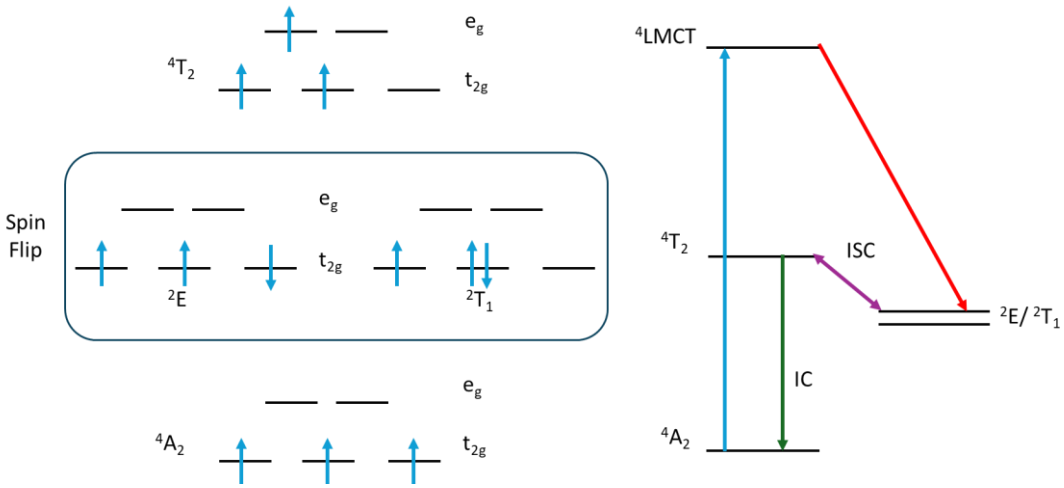

Figure 10: A simplified ligand field energy level diagram showing the photophysical mechanism of Cr(III) spin-flip emission as described by Ghodrati *et al.*[115] Excitation causes population of the high energy quartet ligand field states ($^4T_2$ / $^4T_1$), which undergo intersystem crossing to the lower lying doublet states (^2E / $^2T_1$). From the spin-forbidden doublet states radiative decay to the quartet ground state ($^4A_2$) occurs resulting in a long-lived phosphorescence. Strong σ-donating ligands and rigid ligands increase the ^2E-$^4T_2$ energy gap, suppressing non-radiative decay enabling room-temperature Cr(III) emission.

These mechanisms of light emission in both Ir(III) and Cr(III) complexes highlight the importance of controlling the ligand environment by developing ligands with rigid structures and strong ligand fields in order to produce the most efficient emissive complexes.[36, 96]

1.7. N-Heterocyclic Carbenes (NHCs) as Ligands for Luminescent Complexes

N-Heterocyclic carbenes (NHCs) consist of a strong σ-donating carbene centre flanked by two nitrogen atoms (**Figure 11**) that forms structures with robust metal to carbon bonds that have high dissociation energies.[116-123] By varying the substituents attached to the NHC a wide variety of analogues can be formed and the ligand altered to achieve specific properties.[116-118] NHCs have become prominent ligand choices for luminescent compounds of heavy metal complexes as they offer many significant advantages over other traditionally used ligands such as phosphines and diamine ligands.[27, 51, 124, 125] Most notably the inherent robustness of these ligands provides complexes with thermal and chemical resistance[120, 121] and effectively promotes efficient radiative decay by creating a stronger ligand field which works to increase the MLCT character of the emissive triplet state and destabilise the non-radiative metal-centred states. [27, 51, 117, 119, 124, 125] This is far superior to the previously favoured phosphine ligands which have weaker metal to carbon bonds and are thus more susceptible to oxidative degradation which has the knock-on effect of limiting the device lifetimes achievable with these complexes.[120-122]

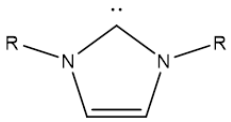

Figure 11: The general structure of an NHC.

1.7.1. Tunability and Ligand Modification

The biggest advantage of using NHCs over more traditional ligands is their ability to be readily tuned for specific desirable electronic and steric properties. Multiple studies such as the work done by of Liu *et al.* [37] and Leuthäusser *et al.* [126] have shown the effects of incorporating an electron donating groups or electron withdrawing groups on the HOMO to LUMO energy gap and the subsequent emission wavelength.[37, 126] In other studies, such as that reported by Idris *et al.* [13] and Mathew *et al.*[117] show that increased steric bulk can suppress intermolecular quenching and improve quantum yields of luminescent complexes. This ability to fine tune the ligand framework makes these ligands much more modular and therefore more versatile than many classical ligand systems.[13, 117, 127]

Another important consideration of being able to alter steric effects is that this also translates to the ability to control the *mer* to *fac* isomer ratio of cyclometallated complexes. Typically, NHC complexes such as the complexes reported by Mackenzie *et al.*[124] and Tamayo *et al.*[56] give greater amounts of the *mer* isomer close to the expected 3:1 statistical ratio with Mackenzie observing *mer*:*fac* mixtures of around 3.5:1 and 5.5:1 for two benzyl-substituted Ir(III) based NHC complexes.[45, 56, 124, 128] Electronically NHCs are strongly σ donating which would normally favour the *fac* isomer as in a *fac* arrangement no carbene donors

lie *trans* to one another. However, as *mer* is the kinetic product and has a lower barrier to initial formation, it dominates over *fac* under standard synthetic conditions.[56, 129] In cases where the N-substituents are bulky the *mer* isomer becomes favoured as there is an increase in steric repulsion between N-substituents across the Ir-C axis causing the *fac* geometry to become destabilised despite the *fac* isomer being more favourable as it avoids any *trans*-carbene arrangement.[124, 128] This effect is shown well in the work by Osiak *et al.* who observed the ratio switching from *fac* to *mer* in Ir(III) NHC complexes as the steric demand of the N-substituents increased.[130, 131]

Generally, the *fac* isomer, with its C_3 axis of symmetry, is considered to be more desirable due to its stronger ligand-fields,[24, 51, 56]wider HOMO-LUMO gap[13, 132] and less radiative decay pathways compared to its *mer* counterpart.[71, 128] For this reason, there have been multiple attempts to produce a specific isomer, *fac* for example, or otherwise convert one isomer into another such as the Brønsted acid induced isomerisations studied by groups such as Osiak *et al.*[128] (**Figure 12**) and the acid-base switching reactions shown by Gitlina *et al.*[133] (**Figure 13**) which can produce reversible isomerisation under kinetic control. Although isolated examples exist where the *mer* complexes outperform their *fac* analogues such as the study in 2023 by Sebris *et al.*, the typical trend for Ir(III) luminescent compounds shows *fac* geometries are favoured for achieving very bright and efficient phosphorescence.[53]

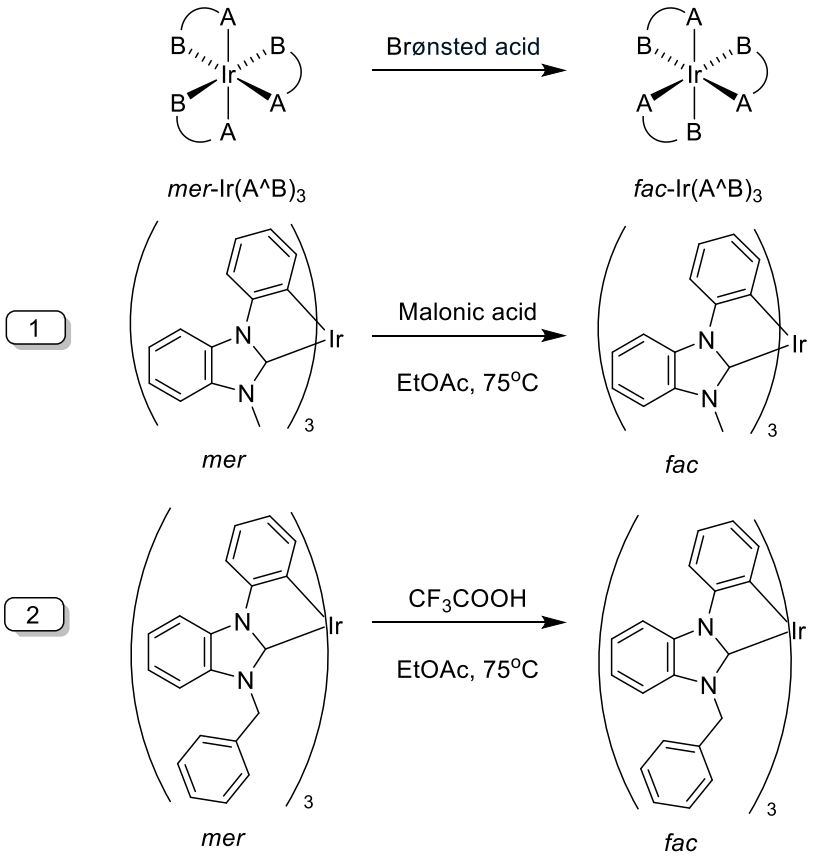

Figure 12: Brønsted acid induced *mer* → *fac* switching in Ir(III) NHC complexes as reported by Osiak *et al.*[128]

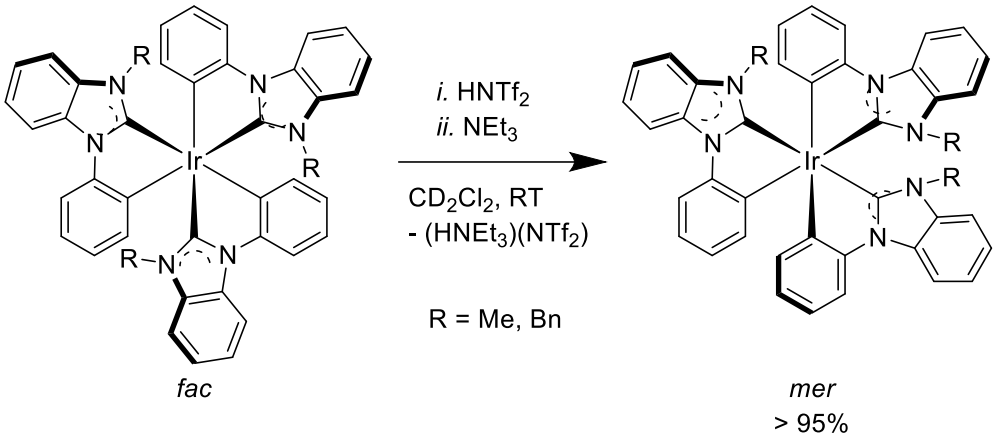

Figure 13: Acid-base reversible isomer switching in Ir(III) NHC complexes as reported by Gitlina *et al.*[133]

1.8. Previous Work

Previous work in the Fletcher group in this area focused on the synthesis of the novel NHC precursor ligand, 3-nitrophenyl-1,2,4-triazole (NPTz) and the subsequent formation of new unreported 1,2,4-triazolyl ligands (**Figure 14**). Further work was undertaken with these ligands to synthesise blue emissive iridium complexes. This work displayed evidence that these ligands are capable of forming tris-bidentate emissive iridium complexes that form both the *mer* and *fac* stereoisomers with the *mer* isomer as the kinetically favoured product, being isolated in greater yields than the *fac* isomer.

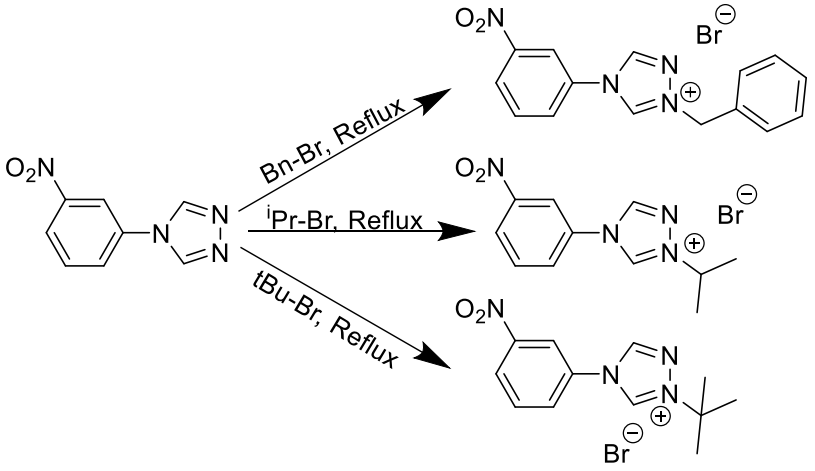

Figure 14: 3-nitrophenyl-1,2,4-triazole (NPTz) structures previously synthesised by the Fletcher group (unpublished).

A key finding of this research was that increasing steric bulk prevented the complexation of the ligands to iridium, with ^{i}Pr ligand complexes showing very small yields compared to the complexes with less bulky Bn substituents, while the ^{t}Bu substituted ligand complexes did not form at all instead favouring decomposition. Furthermore, it was seen that the use of Ag_2O as a base to

deprotonate the ligands in order for them to coordinate to iridium, caused competing decomposition reactions. This, along with the presence of air and moisture during the reaction, led to additional decomposition by-products as well as the iridium complexes (**Figure 15**)

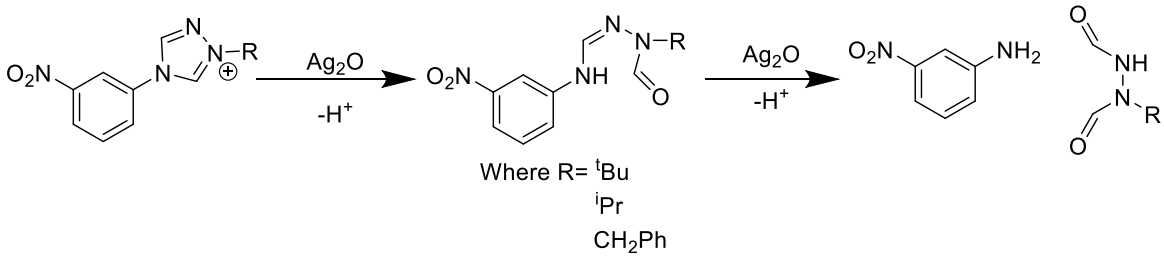

Figure 15: The proposed degradation pathway of the ligand to the tosylate salt then back to the starting materials.

Preliminary luminescence studies on these complexes suggest that the Bn substituted ligand is favoured over the Me substituted ligand for luminescence as it showed a much more intense spectrum. However, the presence of the NO_2 group proved to be problematic as the MLCT emission occurs in the same region as the n to p* ligand transition absorption causing a re-absorbance of the emitted light limiting their effectiveness as blue emitters.

1.9. Project aims

The proposed project involves the synthesis and subsequent optimisation and characterisation of novel blue luminescent iridium(III) complexes with unreported chelating NHC ligands. Where appropriate the geometric isomers will be isolated followed by an assessment and comparison of their photophysical properties both between isomers and between the different complexes.
The project further aims to synthesise the analogous chromium(III) complexes testing various reaction pathways with the aim of using the same blue shift effect seen in the iridium complexes to create a novel red emitting chromium NHC complex.
The key objectives of this research were:

- Synthesis of novel 1,2,4-triazolyl ligands from NHC precursor ligands
- Coordination of 1,2,4-triazolyl ligands to an iridium metal centre
- Isolation of geometric isomers
- Analysis of photophysical properties of the iridium(III) complexes to determine the effect of introducing EWG/EDG R-groups and bulky R'-groups to the chelating NHC ligands on the luminescence and ratio of geometric isomers obtained of the synthesised iridium complexes.

Through these objectives this project aims to improve the understanding of the relationship between chemical structure, isomer distribution and the photophysical properties of metal NHC complexes.

2. Results and discussion

2.1. Ligand synthesis

2.1.1. Synthesis of ligand precursors

The NHC precursor ligands were synthesised via a procedure adapted from Becker and co-workers (1988)[134] involving the reaction of substituted aniline compounds with diformylhydrazine (**Scheme 1**) and were successfully obtained in yields of 19% for the unsubstituted triazole (H-PTz) and 52% for the CF_3-substituted triazole (CF_3-PTz), following isolation via silica column chromatography. Whilst the NO_2 substituted triazole (NO_2-PTz) was not synthesised as material was supplied by Nick Fletcher from previous group work.

The low yield obtained for the H-PTz ligand may be due to competing side reactions during synthesis and most likely the reaction not going to completion as earlier fractions showed significant quantities of starting material. In addition to this product was lost during the work-up and purification process, for example during column chromatography. CF_3-PTz was isolated in a significantly higher yield of 52% compared with H-PTz, although this still remained relatively moderate. This could be attributed to the increased steric bulk of the CF_3 group, which may have caused slower reaction kinetics or the reaction not running to completion. Additionally, the solubility of CF_3-PTz in the solvents used could have influenced the efficiency of the reaction and purification steps. Further optimisation of these reaction conditions by adjusting temperature and solvent choice, could help improve these yields.

Of the three ligand precursors H-PTz and NO_2-PTz have been previously reported[135-137] while CF_3-PTz is yet to be reported in the literature. This procedure proved to be robust, synthesising the desired triazolium precursors in consistently good to moderate yields from a range of aniline starting materials. Successful synthesis was confirmed via ^{1}H NMR analysis showing the key singlet triazolium proton peak at 8.50 ppm integrating for two protons, which was further used to determine the success of the later substitution reactions to form the 1,2,4-triazolyl ligands. With these triazolium precursors further N-alkylation reactions were performed to synthesise the corresponding 1,2,4-triazolyl ligands.

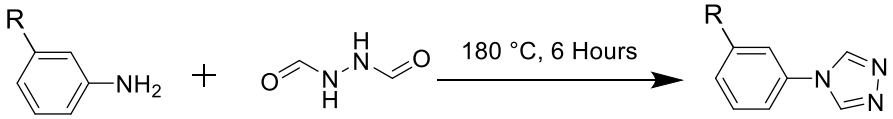

Where R=H
R=CF_3
R=NO_2

Scheme 1: Scheme of the synthesis of the R substituted ligand precursors adapted from the original synthesis by Becker *et al.* [134]

2.1.2. Synthesis of 1,2,4-triazolyl ligands

Each of the precursor ligands were subject to two separate substitution reactions to install a methyl group or a benzyl group at the R' position, giving a total of six novel 1,2,4-triazolyl ligands all six of which are unreported. These ligands were synthesised via reactions with the alkyl halides MeI and BnBr in acetonitrile, according to experimental procedures adapted from Becker[134] (**Scheme 2**).

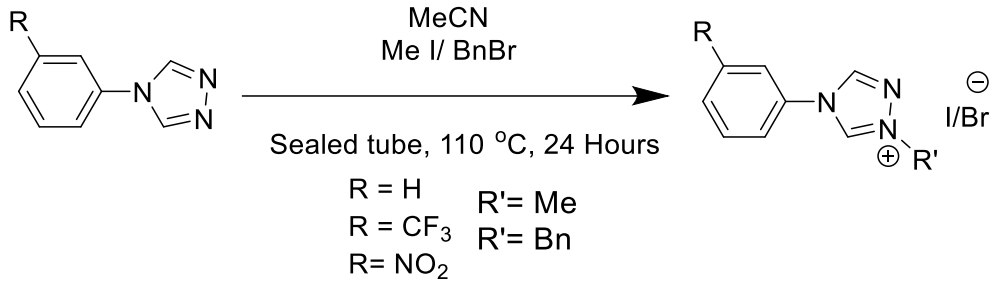

Scheme 2: The synthesis of the pre-ligands from the ligand precursors that undergo substitution reactions to functionalise the ligands at position R'. Each of the three precursor ligands was subjected to separate methylation and benzylation reactions at the R' position, producing a total of six novel 1,2,4-triazolyl ligands as shown below:

Ligand	R	R'
H-PTz-Me	H	Me
H-PTz-Bn	H	Bn
CF_3-PTz-Me	CF_3	Me
CF_3-PTz-Bn	CF_3	Bn
NO_2-PTz-Me	NO_2	Me
NO_2-PTz-Bn	NO_2	Bn

The benzyl group was installed via a standard reflux reaction between the ligand precursor and benzyl bromide in acetonitrile. In contrast the installation of the methyl group involved the reaction of MeI with the ligand precursor in acetonitrile and required the use of an ACE pressure tube. Previous work in the Fletcher group showed that benzyl bromide reacts readily with the ligand precursors under standard reflux to give the ligand in high purity with all three benzyl bromide ligands giving yields above 80 % with the highest being H-PTz-Bn with a yield of 89%.

In comparison, the methyl iodide only formed the methylated ligand with use of the ACE pressure tube due to its reduced reactivity for N-alkylation under standard reflux conditions despite its low steric bulk. The success of these reactions was monitored by ^{1}H NMR analysis, comparing with the precursor ligand spectra as the singlet triazolium proton peak at 8.50 ppm corresponding to the starting material disappears and is replaced by two singlet peaks at around 9.80 ppm and 10.80ppm, as the triazolium protons become

inequivalent and additional peaks appear corresponding to the protons on the added R' groups.

The yields of the methylation reactions were generally good with the lowest being H-PTz-Me at 60 %. This lower yield could be attributed to competing side reactions such as degradation or over-alkylation. In comparison the yields for the CF_3 and NO_2 substituted ligands were relatively high, suggesting that these substitutions do not hinder the alkylation reactions as much. The benzyl substituted compounds showed slightly higher yields than the methyl substituted compounds which could be explained by the steric bulk of the benzyl group facilitating better reaction conditions or reducing side reactions competing with the ligand reaction when compared to the methyl group. Despite the good to moderate yields observed, in some cases, residual starting material was observed, and purification proved challenging due to similar solubilities of the ligands and the starting material. Therefore, alternate purification techniques such as anion metathesis is suggested as a potential strategy to improve isolation and yield pure ligand material.

The functionalisations at R and R' were carefully chosen in order to explore the effects of both, different chemical environments and different steric environments on the photophysical properties and ratio of geometric isomers of the resulting metal complexes. On the phenyl side of the ligands the R group was functionalised with three separate groups with varying degrees of electron donating capabilities. The nitro group was chosen due to there being a gap in the literature for nitro functionalised luminescent NHC complexes[138] and its strong electron withdrawing character, as well as the advantage provided during purification as these complexes are an intense yellow colour and thus are more easily seen.[139, 140] The trifluoromethyl group was chosen to enable comparison with other similar luminescent NHC complexes in the literature such as those synthesised by Chi *et al.*[141] The final R group used was the native proton to allow comparison between the complexes in order to determine the effect of adding an EWG.

As well as the inclusion of these groups the positioning of the substitution was specifically chosen in order to place the R group para to the metal centre in the metal complexes. The benefit of this is that the EWGs will stabilise the HOMO as this lies on the phenyl ring and d orbitals of the metal thereby increasing the HOMO–LUMO energy gap causing a blue shift in emission wavelength, a feature exploited in these complexes.[142, 143] On the triazole side of the ligands the group R' is functionalised with a methyl group and a benzyl group to explore and observe the effects of increasing steric bulk. With the pre-ligands synthesised, they were subsequently used in complexation reactions with Ir(III) and Cr(III) metal centres to investigate how controlling electronic and steric modifications influence complex structure, photophysical behaviour and isomer distribution.

2.2. Ir complexes

2.2.1. Complex synthesis and optimisation

Using the synthesised pre-ligands, complexation reactions with an iridium(III) metal centre were undertaken following an experimental procedure adapted from Thompson and co-workers.[13] Their research was highly influential and formed the basis for many subsequent studies into luminescent NHC iridium(III) complexes. In 2005 Thompson *et al.* performed a research study that provided evidence that triscyclometallated iridium(III) complexes could be successfully tuned for deeper blue phosphorescence by using cyclometallating NHC ligands. The strong σ-donating character of the NHC strengthens the ligand field at the

iridium centre and modifies the metal-ligand electronic structure, increasing the energy of the emissive MLCT state, resulting in a deeper blue phosphorescence. These complexes however suffered from relatively low quantum yields and short excited state lifetimes.[51] Using insights from their previous study, in 2021 Thompson and co-workers reported the synthesis of blue-emitting iridium(III) carbene complexes with isolatable *mer* and *fac* isomers. In this study a series of cyclometallating NHC ligands (**Figure 16**) were complexed to iridium(III) to investigate the influence of ligand structure on emission colour, excited state lifetime and isomer distribution. They showed that the complexation of these ligands produces both the *mer* and *fac* geometric isomers which could be isolated and characterised allowing a direct comparison of the photophysical properties. They concluded that the *fac* isomers generally showed greater photoluminescence quantum yields and longer excited state lifetimes than the *mer* isomer attributed to the stronger, more symmetrical ligand field of the *fac* isomer. However, despite the *fac* being photophysically favourable, the *mer* isomer was the kinetically favoured product and formed in three times the quantity of the *fac* isomer.[13]

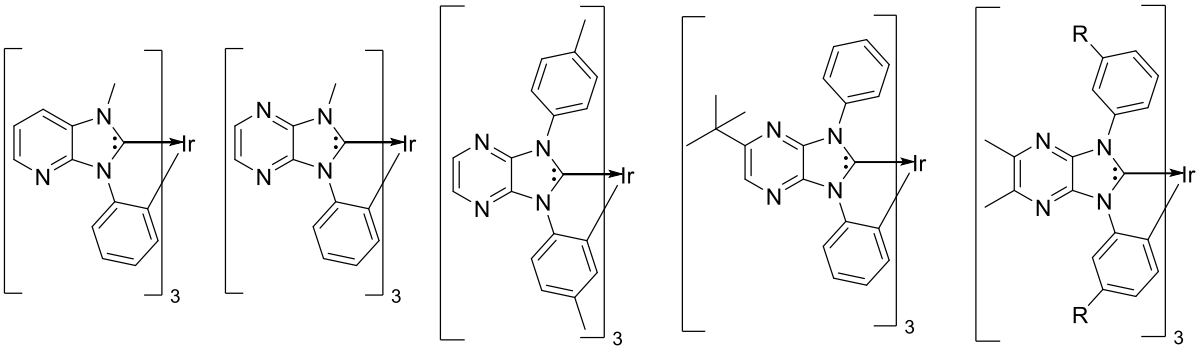

Figure 16: Cyclometallating NHC ligands complexes to Ir(III) as reported by Thompson *et al.*[13]

Building upon these findings in 2023 Mackenzie *et al.*[124] reported the synthesis of NHC ligands with bulky substituents with the goal of exerting control over the isomer distribution of the subsequent iridium(III) blue emissive complexes. As they increased steric bulk this increased the steric repulsion between ligands across the Ir-C axis therefore destabilising the *mer* geometry making it unfavourable and shifting the ratio in favour of the formation of the *fac* isomer. They reported that this led to increased selectivity for the *fac* isomer and resulted in higher quantum efficiencies. However, while increased steric bulk improved isomer control and suppressed non-radiative decay pathways by providing steric protection to the metal centre and reducing intermolecular quenching, the emission colour did not reach the deepest blue region achieved in earlier systems. This highlights the challenge of achieving the careful balance between electronic tuning in order to access the high energy emissive states needed for deep blue emission and the design of steric environments to suppress non-radiative deactivation pathways and control isomer formation.[124, 144]

In line with this research the novel NHC ligand frameworks developed in this work seek to allow the tuning of both electronic and steric ligand properties. When coordinated to iridium(III),these ligands aim to improve blue emission efficiency, control *mer*/*fac* isomer ratios, and extend excited-state lifetimes. To this end, an adapted one pot synthetic procedure based on that reported by Thompson *et al.* in 2021 was developed leading to

the synthesis of 12 novel iridium(III) complexes. The synthesis involved refluxing the ligand precursor with iridium trichloride hydrate in the presence of silver tosylate (AgTos) and potassium carbonate (K_2CO_3) (**Scheme 3**), followed by purification and isomer separation via column chromatography.

In this reaction the silver tosylate was chosen in place of silver oxide in an attempt to optimise this reaction after previous attempts in the Fletcher group noted that using silver oxide led to significant decomposition of the ligands which competed with the iridium complexation reactions. It was suggested that a base perhaps was not necessary as the Lewis acidity of the iridium may be strong enough to deprotonate the ligands alone however experiments run without a base present showed no evidence of complexation so it was a determined that a weaker base was needed. Therefore, AgTos was chosen as it is a much weaker base than silver oxide and hence did not cause the triazole five membered ring to open but was still strong enough to abstract the acidic triazole protons while the K_2CO_3 was used to scavenge the HI/HCl acid produced during the cyclometallation in order to maintain reaction conditions preventing the build-up of acid that could reprotonate the carbene or decompose ligands.

The progress of this reaction was monitored by ^{1}H NMR spectra in which several distinct peaks gave evidence of successful complexation. Most notably the peak associated with the triazole proton is the biggest indicator of a successful reaction as prior to isomer separation this peak is seen as four distinct singlet peaks, one corresponds to the *fac* isomer as due to its C_3 symmetry all three triazole protons of the attached ligands are chemically equivalent giving one singlet peak, whilst the other three peaks correspond to the *mer* isomer as the *mer* isomer does not have this symmetry hence the protons are chemically inequivalent and appear as three distinct triplets amongst all the other *mer* NMR peaks that appear in triplicate for this same reason. Other notable peaks are those such as the ones at around 3.2 - 3.4 ppm that correspond to the methyl group in methyl substituted complexes and the CH_2 of the benzyl group of the benzyl substituted complexes found at around 4.7 - 4.9 ppm. These peaks lie well out of the way of the aromatic region and thus are easy to see and characterise.

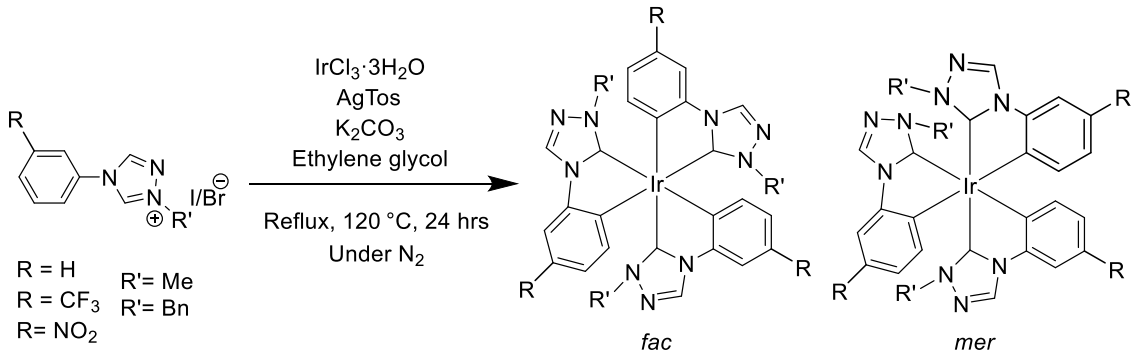

Scheme 3: The Synthesis of Ir(III) complexes from the functionalised ligands to produce a mix of *mer* and *fac* isomers.

2.2.2. *Mer*/*fac* isomer distribution

The ratio of *mer* to *fac* isomers is not consistent across the complexes suggesting that the ratio has been affected by bonded substituents. Statistically the ratio of *mer* to *fac* isomers is expected to be close to 3:1 as the reaction is under kinetic control meaning that the ligands coordinate to the metal centre and do not drop off or rearrange once coordinated unlike in thermodynamically controlled reactions where ligands are subject to rearrange until the most thermodynamically stable product is formed. The crude *mer*/*fac* isomer distributions determined by ^{1}H NMR integration for the synthesised complexes are summarised in **Table 1**.

Table 1: Crude yields and *mer*/*fac* isomer distributions of the synthesised iridium(III) complexes determined by ^{1}H NMR integration prior to chromatographic separation.

Complex	Crude isolated yield[a] (%)	[b]*Mer* (%)	[b]*Fac* (%)
$Ir(H\text{-}PTz\text{-}Me)_3$	65	55	45
$Ir(CF_3\text{-}PTz\text{-}Me)_3$	84	45	55
$Ir(NO_2\text{-}PTz\text{-}Me)_3$	90	52	48
$Ir(H\text{-}PTz\text{-}Bn)_3$	59	82	18
$Ir(CF_3\text{-}PTz\text{-}Bn)_3$	110	88	12
$Ir(NO_2\text{-}PTz\text{-}Bn)_3$	23	82	18

[a]Crude yields greater than 100 % are attributed to residual solvent and/or moisture retained within the isolated products. *Mer*/*fac* ratios were determined by ^{1}H NMR integration of the crude reaction mixtures prior to chromatographic separation.
[b] Percentages rounded to nearest whole percent

In complexes substituted with the benzyl group the *mer* to *fac* ratio was seen to favour the *mer* isomer much more than the expected statistical 3:1 ratio with the *mer* isomer appearing four to seven times more than the *fac* isomer with the $Ir(CF_3\text{-}PTz\text{-}Bn)_3$ giving the highest ratio of 7.2:1 . $Ir(H\text{-}PTz\text{-}Bn)_3$ showed a substantially greater proportion of *mer* isomer than its comparable less substituted $Ir(H\text{-}PTz\text{-}Me)_3$ counterpart, providing strong evidence that steric bulk on the triazole fragment tips the isomer distribution towards the *mer* isomer.

Due to the small scale of this work owing to the expense and rarity of the iridium, and the low concentration of *fac* isomer produced, it was found almost impossible to isolate the *fac* isomer of these compounds with only one successful isolation, that of the $Ir(CF_3\text{-}PTz\text{-}Bn)_3$. A possible explanation for these observations is that steric bulk crowds the coordination sphere during ligand approach increasing steric repulsion close to the Ir-C axis. This raises the kinetic barrier to the formation of the *fac* isomer therefore making it harder for the complex to adopt the *fac* arrangement where the three bulky ligands are packed *cis* to one another.

It is also seen that the complexes that are also substituted at the R position with EWG are seen to have a much greater effect on pushing the isomer distribution towards *mer* than those without as the $Ir(CF_3\text{-}PTz\text{-}Bn)_3$ complex has a much larger ratio difference of 6.9:1 compared to the unsubstituted $Ir(H\text{-}PTz\text{-}Bn)_3$ which had a ratio of 4.7:1. This could be due to the decrease in lability of the aryl Ir-C bond caused by the presence of the EWG. This results in the kinetically formed *mer* isomer being “trapped” into the configuration as the

energetic driving force for the *fac* rearrangement is lowered hence less rearrangement to the *fac* isomer will occur leading to higher concentrations of the *mer* isomer.

Despite both complexes bearing EWG giving greater *mer* ratios than the complex without an EWG, between the two EWG the CF_3 prevailed as causing the greatest shift towards *mer* isomerism despite the NO_2 group being more electron withdrawing. This could be because this effect is not only controlled by the strength of its electron withdrawing ability but also how it changes the kinetics and rearrangement ability of the complex. CF_3 is strongly electron withdrawing predominantly through negative inductive effects, drawing electron density away from the rest of the ligand through σ bonds due to its high electronegativity. On the other hand, the NO_2 group has a strong negative inductive effect but also has a strong negative mesomeric effect as the group is π-withdrawing. This means it can change the electronic distribution of the cyclometallating aryl ring making it more activated towards metalation which could make the rearrangement towards the *fac* geometry occur more readily than in the CF_3 substituted complexes. Despite this, the overall net effect results in it still tending towards the *mer* isomer, though not as strongly as with the CF_3 complex as it is negated in part by this strong mesomeric effect.

Another factor to consider is the polarity and π withdrawing character of the groups. Unlike the CF_3 group the NO_2 group exerts both strong negative inductive and mesomeric effects. This may alter the electronic distribution within the cyclometallating aryl ring and consequently influence the kinetics of ligand rearrangement and therefore contributing to the differing *mer*/*fac* ratios observed between the CF_3 and NO_2 substituted complexes. Moreover, although the intended effect of the inclusion of these groups was not to study steric effects, it is important to note that the CF_3 group is sterically bulkier than the NO_2 group which may also have had an effect in increasing steric congestion meaning that *mer* approach geometries would be favoured as they would minimise the steric interactions therefore pushing the observed *mer*/*fac* ratio further in favour of the *mer* isomer.

When looking at the effects of the substituents on the phenyl ring where the triazole substituent is a methyl group, which provides minimal steric effects, the changes seen to the isomer ratios must arise primarily from electronic effects of the phenyl substituents. There is strong evidence to suggest that electron withdrawing substituents cause an increase in *fac* isomerism with the *mer* to *fac* ratio approaching 1:1 for the $Ir(CF_3\text{-PTz-Me})_3$ complex. This is a major shift in the observed *mer*/*fac* ratio towards the *fac* isomer giving three times more *fac* isomer than statistically expected for these compounds.

Notably, the unsubstituted $Ir(H\text{-PTz-Me})_3$ complex already displayed a high *fac* ratio (1.2:1) rather than the statistically expected 3:1 ratio however given that the reaction was refluxed for 24 hrs in the presence of silver tosylate, there may have been significant interconversion of the *mer* isomer to the *fac* due to the reaction conditions used (24 hrs at 120 ^{o}C in ethylene glycol). Ethylene glycol is a polar solvent with a high boiling point and is capable of stabilising ion-pair and coordinatively labile intermediates and thus with prolonged heating this may facilitate ligand reorganisation to the thermodynamically favoured product, the *fac* isomer. This is in line with observations seen in similar research studies such as that by McDonald *et al.* who reported that under standard thermal conditions tris-cyclometallated iridium(III) complexes undergo changes in isomer distribution from favouring *mer* to *fac* when increasing temperature, showing that prolonged heating in a coordinating solvent can promote the rearrangement into the more thermodynamically favoured *fac* isomer.[45]

Moreover, the introduction of EWG on the phenyl ring was shown to cause a notable shift towards an increase in the formation of the *fac* isomer the most pronounced shift occurring for the CF_3 substituted complex. One possible explanation for this is that EWG on the phenyl ring, such as CF_3 and the NO_2, alter the electronic properties of the NHC ligand influencing the metal-ligand interactions within the complex. The presence of EWGs reduces the electron density at the carbene carbon thereby reducing the π-donation into the carbene centre. The consequence of this is it weakens the NHC σ-donating ability which reduces the destabilisation usually associated with *trans* carbene-carbene interactions. However, these substituents may also increase the π-accepting character of these complexes influencing the metal-ligand back-bonding interactions, therefore the overall electronic effects are much more complex than a simple inductive withdrawal through the σ system alone and would require further study to determine.

Amongst the substituents studied the CF_3 group produces the greatest reduction in NHC σ-donation due to its aforementioned strong negative inductive effects therefore giving a larger *fac* ratio compared to the NO_2 substituted complexes which withdraw less electron density from the carbene due to the competing resonance effects resulting a shift towards *fac* isomer distribution but weaker than that caused by the CF_3. This effect is also supported by the findings of Kearney *et al.* who found that CF_3 substitutions strongly withdraw electron density from the complex via inductive effects, thereby reducing the σ-donation of the NHC, influencing metal-ligand interactions to a greater degree than NO_2 substitutions as their electron withdrawing effects are caused by a mixture of inductive and resonance effects.[145]

2.2.3. Structural analysis

The insights into the steric and electronic effects on isomer distribution are also supported by the crystallographic data obtained. All complexes managed to grow crystals of their isolated *mer* and *fac* isomers (**Figure 17-19**) and the crystal data tabulated (**Tables 2-3**), except for the *fac* isomers of the Ir(H-PTz-Bn)$_3$ and Ir(NO_2-PTz-Bn)$_3$ complexes which were not isolated as was discussed previously. The crystals show that these complexes have a distorted octahedral geometry at the Ir centre with the *mer* isomers exhibiting a more distorted geometry than the *fac*, with larger bond angles between the metal and ligand atoms, which is consistent with the steric repulsion caused by the *trans* carbene-carbene interactions. In contrast, the *fac* isomers have a more symmetrical arrangement, correlating to the stabilisation provided by the symmetrical ligand field, providing structural evidence for the preferential formation of *fac* isomers in these systems.

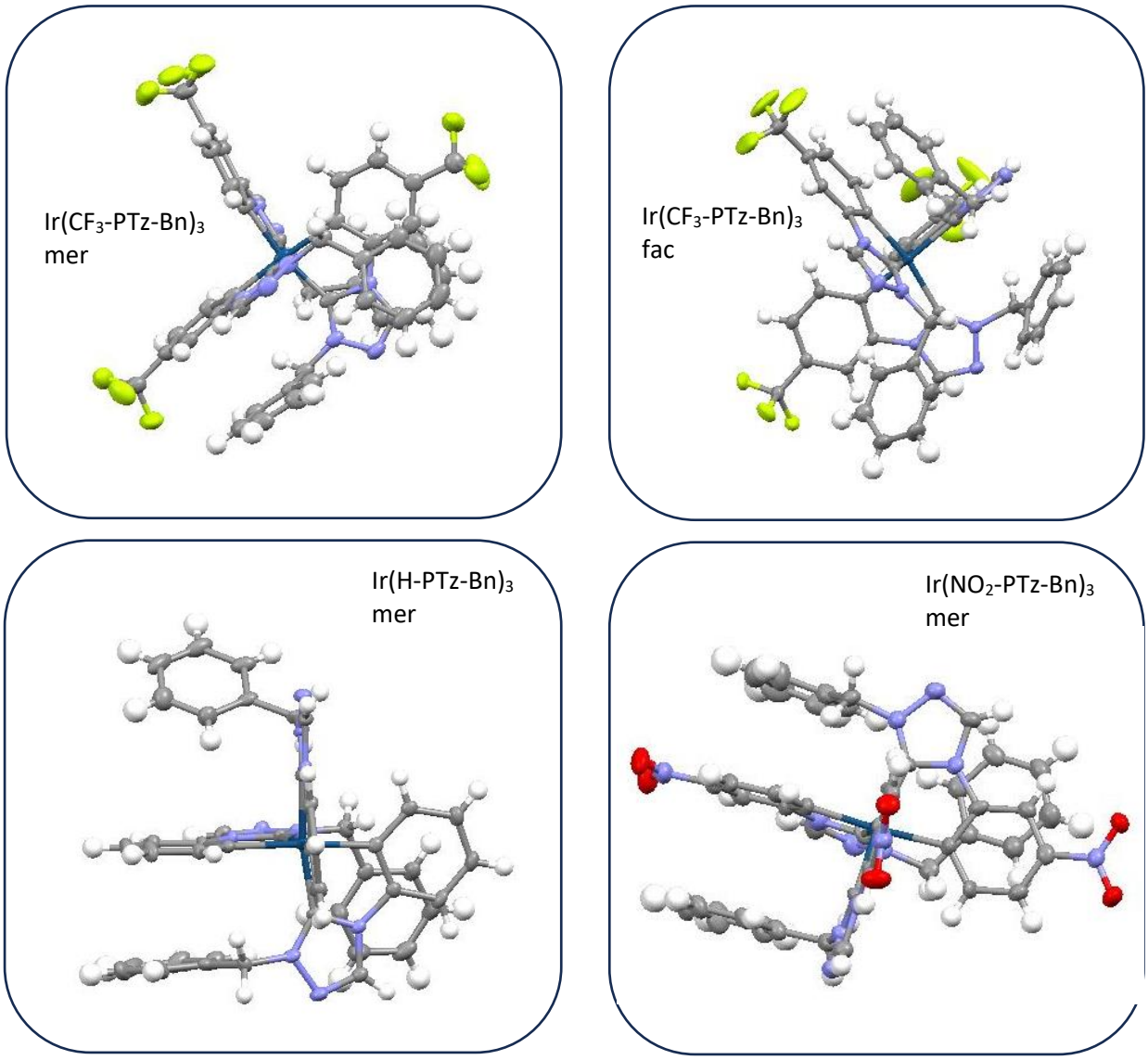

Figure 17: The isolated *mer/fac* isomer crystal structures of the benzyl-substituted Ir(III) complexes with the R groups, H,CF_3 and NO_2

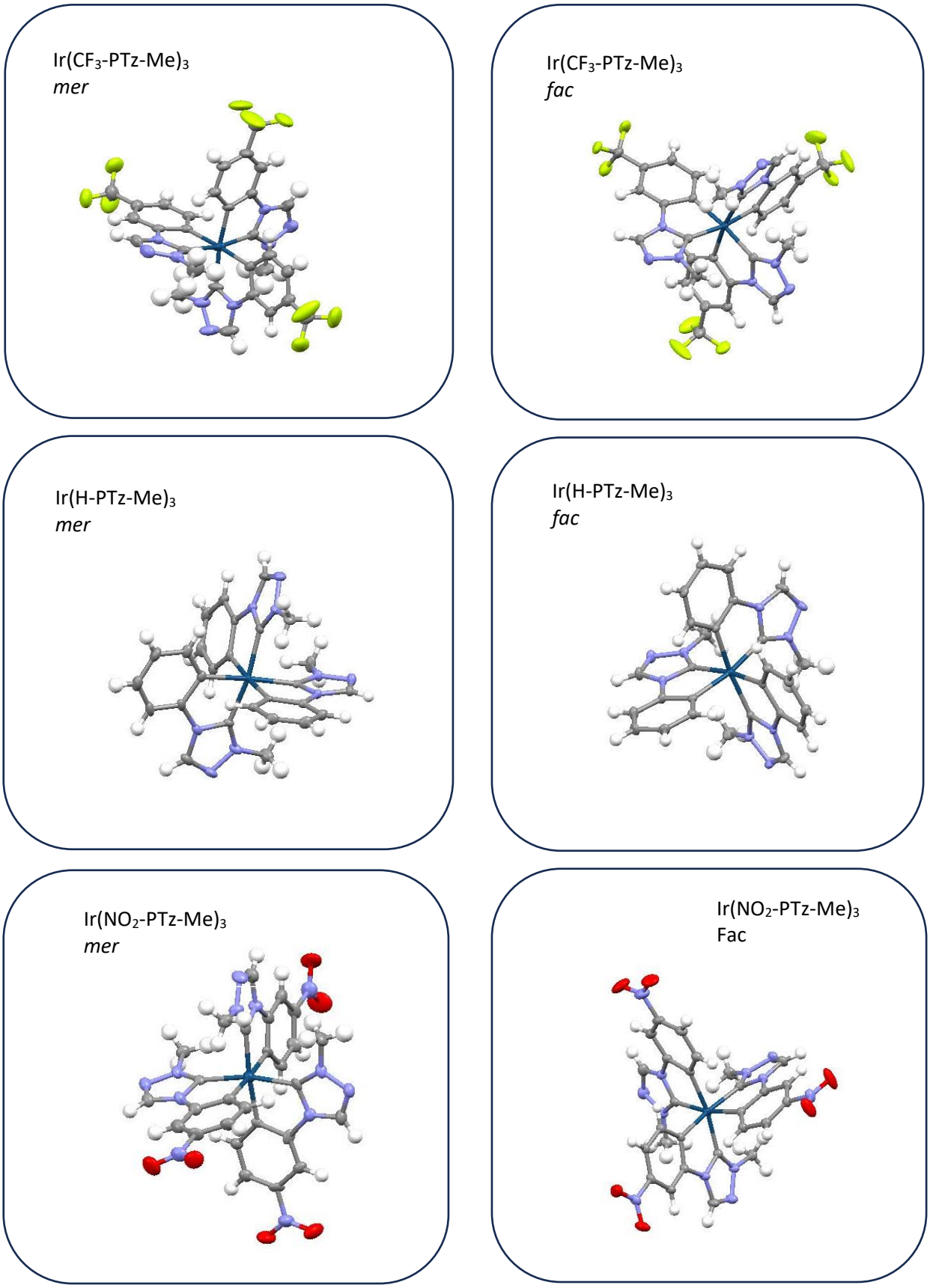

Figure 18: The isolated *mer/fac* isomer crystal structures of the methyl-substituted Ir(III) complexes with the R groups, H,CF_3 and NO_2

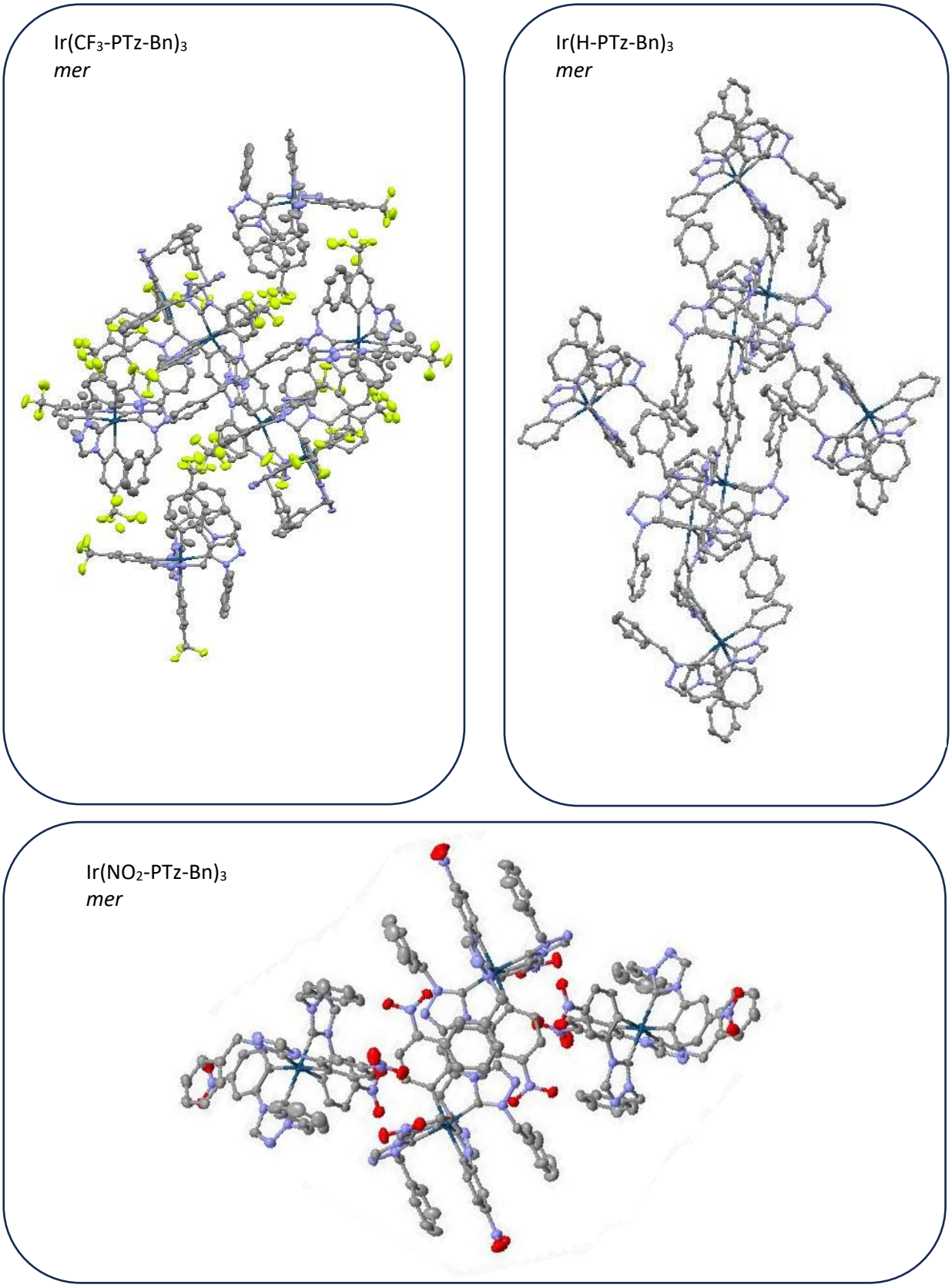

Figure 19: Crystal packing structures of all three isolated Ir(III) complexes with both a benzyl substitution and a *mer* isomer.

Table 2: A condensed crystallographic table showing key values for the *mer* and *fac* isomers of the methylated complexes with a H and CF_3 substituent and the *fac* isomer of the benzylated CF_3 complex.

	Ir(CF_3-PTz-Me)$_3$ *Fac* + acetone	Ir(CF_3-PTz-Me)$_3$ *Mer* + 0.75 Water	Ir(H-PTz-Me)$_3$ *Fac*	Ir(H-PTz-Me)$_3$ *Mer*	Ir(CF_3-PTz-Bn)$_3$ *Fac* + Chloroform
Formula Formula Moiety	C_{33} H_{27} F_9 Ir N9 O C_{30} H_{21} F_9 Ir N_9, C_3 H_6 O	C_{30} H_{21} F_9 Ir N_9 O C_{30} H_{21} F_9 Ir N_9, 0.75 H_2O	C_{27} H_{24} Ir N_9 C_{27} H_{24} Ir N_9	C_{27} H_{24} Ir N_9 C_{27} H_{24} Ir N_9	C_{49} H_{34} C_{13} F_9 Ir N_9 C_{48} H_{33} F_9 Ir N_9, C H C_{13}
Crystal system	Monoclinic 14	Monoclinic 14	Triclinic 2	Orthorhombic 33	Triclinic 2
Space group	P 1 21/c 1	P 1 21/n 1	P -1	P n a 21	P -1
a (Å)	11.46850	11.16340	9.7135	16.6933	11.7749
b (Å)	19.17030	17.7407	11.2263	14.05564	13.4960
c (Å)	15.70610	15.9857	14.1452	10.56950	15.6037
α (o)	90	90	89.514	90	75.727
β (o)	96.9510	97.7460	89.554	90	73.937
γ (o)	90	90	83.307	90	79.425
V (Å^3)	3427.68	3137.02	1531.88	2479.97	2291.52
R1 (for I > 2σ)	0.0284	0.0500	0.0232	0.0257	0.0446
wR2	0.0753	0.1062	0.0528	0.0594	0.1189
S	1.111	1.308	1.065	1.041	1.020
Largest difference peak/hole (e–Å^{-3})	-2.447, 0.868	-1.429, 1.417	-1.442, 1.145	-1.412, 1.125	-1.765, 3.414

Table 3: A condensed crystallographic table showing key values for the *mer* isomers of the benzylated complexes with a H and CF_3 substituent as well as the *mer* isomer of the methylated NO_2 complex along with its *fac* counterpart and the *mer* isomer of the benzylated NO_2 complex.

	$Ir(CF_3\text{-}PTz\text{-}Bn)_3$ *Mer*	$Ir(H\text{-}PTz\text{-}Bn)_3$ *Mer* +solvents incuded	$Ir(NO_2\text{-}PTz\text{-}Me)_3$ *Fac* +0.75 water	$Ir(NO_2\text{-}PTz\text{-}Me)_3$ *Mer*	$Ir(NO_2\text{-}PTz\text{-}Bn)_3$ *Mer* +Water
Formula	$C_{48}\ H_{33}\ F_9\ Ir\ N9$	$C_{45}\ H_{36}\ Ir\ N_9$	$C_{27}\ H_{22.5}\ Ir\ N_{12}\ O_{6.75}$	$C_{27}\ H_{21}\ Ir\ N_{12}\ O_6$	$C_{45}\ H_{35}\ Ir\ N_{12}\ O_7$
Formula Moiety	$C_{48}\ H_{33}\ F_9\ Ir\ N_9$	$C_{45}\ H_{34}\ Ir\ N_9$, + Solvents	$C_{27}\ H_{21}\ Ir\ N_{12}\ O_6$, + 0.75 H2O	$C_{27}\ H_{21}\ Ir\ N_{12}\ O_6$	$C_{45}\ H_{33}\ Ir\ N_{12}\ O_6,\ H_{20}$
Crystal system	Monoclinic 14	Monoclinic 15	Monoclinic 14	Monoclinic 14	Monoclinic 14
Space group	P 1 21/c 1	C 1 2/c 1	P 1 21/n 1	P 1 21/c 1	P 1 21/c 1
a (Å)	18.30370	38.4189	15.79100	11.2165	15.3730
b (Å)	22.18010	9.35242	13.56110	20.5659	13.2769
c (Å)	21.31420	21.8265	27.9666	17.0167	20.8302
α (o)	90	90	90	90	90
β (o)	98.44	102.7717	97.3790	107.257	103.426
γ (o)	90	90	90	90	90
V ($Å^3$)	8559.34	7648.42	5939.26	3748.66	4135.34
R1 (for I > 2σ)	0.0339	0.0381	0.0194	0.0504	0.0641
wR2	0.0826	0.0948	0.0499	0.1150	0.1493

The influence of the EWGs, CF_3 and NO_2, on the phenyl ring can be seen in the crystal packing and molecular interactions of the complexes. For example, the $Ir(CF_3\text{-}PTz\text{-}Bn)_3$ complex exhibits a more ordered packing structure, with shorter intermolecular distances which reflects the stronger electron-withdrawing effect of the CF_3 group. This effect promotes a more symmetrical packing, stabilising the *fac* isomer. In comparison, the $Ir(NO_2\text{-}PTz\text{-}Bn)_3$ complex shows a less compact crystal packing, in line with what is expected as the electron-withdrawing effect of NO_2 is weaker than that of CF_3 due to its resonance properties. This results in less stabilisation of the *fac* isomer, and giving a more distorted packing arrangement as is observed in the crystal structure.

An interesting feature of the benzyl-substituted complexes, specifically in the *mer* isomers, is the presence of π-π stacking interactions between adjacent phenyl rings. These interactions promote a closer packing and stabilise the crystal lattice reducing steric strain. The steric bulk of the benzyl groups positions the aromatic rings on top of one another allowing for optimal overlap meaning that π-π stacking is favoured in the *mer* isomer. The stabilising effect of the π-π stacking interaction may explain why the formation of the *mer* isomer over the *fac* isomer is favoured in these complexes. The *fac* isomer does not allow the same degree of π-π stacking due to the spatial positioning of the benzyl groups, which could lead to a less favourable crystal packing arrangement in despite the *fac* isomer's more symmetrical and seemingly favourable geometry.

In the CF_3 substituted complexes, the bond lengths of the *fac* isomers show relatively consistent Ir-C bond lengths ranging from 2.048 Å to 2.088 Å. In contrast, the *mer* isomer shows slightly longer Ir-C bonds, ranging from 2.025 Å to 2.123 Å. These differences in bond lengths suggests that the *mer* isomers in these complexes experience more strain and less favourable bonding which could be explained by the less symmetrical arrangement of the ligands compared to the *fac* isomer where its ligands are arranged more symmetrically around the Ir(III) centre.

The bond angles further support this idea as the *fac* isomer displays Ir-C-Ir bond angles that are consistent with typical octahedral geometry, ranging from 78.33° to 172.19°, which suggests the steric repulsion between the ligands is balanced. In contrast, the *mer* isomer shows more varied bond angles, such as bond angles C1-Ir1-C7 = 78.6° and C9-Ir1-C11 = 78.2°, which shows that the *mer* isomer has a more distorted geometry. This distortion could explain why the isomer ratio sits closer to 1:1 in these complexes as the *fac* isomer geometry is more favoured. This distortion effect is also seen in the NO_2 substituted complexes but to a lesser degree which could explain why the CF_3 complexes give a larger *fac* ratio compared the NO_2 complexes despite them being more electron withdrawing.

The unit cell parameters further emphasise the differences in the crystal packing arrangements between the *mer* and *fac* isomers. For example, the *mer* Ir(CF_3-PTz-Me)$_3$ complex has unit cell dimensions of a = 11.16 Å, b = 17.74 Å, c = 15.99 Å, with a volume of 3137.02 Å^3 and four formula units per cell (Z = 4), this reflects a unit cell that is compact with an ordered packing arrangement. In contrast, the *fac* Ir(CF_3-PTz-Me)$_3$ complex has unit cell parameters of a = 11.47 Å, b = 19.17 Å, c = 15.71 Å, and a volume of 3427.68 Å^3, showing it has a larger unit cell volume and less close packing, which can be attributed to the more symmetric geometry of the *fac* isomer. This is further seen in the benzyl substituted complexes which have even larger unit cell volumes such as the *fac* Ir(CF_3-PTz-Bn)$_3$ (a = 11.77 Å, b = 13.50 Å, c = 15.60 Å). This shows that there is an expansion in the crystal lattice due to the increase in steric bulk caused by the CF_3 and Bn groups. This suggests that the more symmetrical packing of the *fac* isomer might make it more energetically stable in the crystalline state.

In contrast, the *mer* isomers, such as *mer* Ir(NO_2-PTz-Me)$_3$, show a much tighter unit cell packing with a = 15.37 Å, b = 13.28 Å, c = 20.83 Å, and a volume of 4135.34 Å^3. This tighter packing suggests that the intermolecular interactions such as the observed π-π stacking, contributes to the stabilisation of the *mer* isomer. These interactions likely influence the *mer*/*fac* isomer distribution as they promote a more compact packing helping to stabilise the more compact and distorted geometry of the *mer* isomer.

Through examining the bond lengths, bond angles, and the unit cell data, it becomes clear that the *mer* isomer is generally more stable in the solid state due to the stronger intermolecular interactions it experiences, while the *fac* isomer, though more symmetrical, is less densely packed and displays a less efficient crystal packing making the *mer* isomer the dominant isomer. However, upon the introduction of EWG crystal lattice becomes stabilised by the electronic effects of the NO_2 and CF_3 groups influencing both the isomer distribution and the crystal symmetry, with CF_3 stabilizing the *fac* isomer more effectively due to its stronger electron-withdrawing properties. Whilst increasing steric bulk of compounds via the introduction of a benzyl substituent has the opposite effect pushing the isomerism in favour of the *mer* isomer due to the π-π stacking between triazole rings and phenyl groups.

2.3. Ir Photophysical Data

Preliminary qualitative photoluminescence was also observed for the iridium(III) complexes where blue emission was visible when examined under a handheld UV lamp. While this observation confirms that the complexes are emissive, the emission observed under these conditions is likely dominated by ligand fluorescence rather than MLCT phosphorescence. This is supported by the emission spectroscopy discussed in the following sections, where high energy excitation shows a strong ligand-centred emission. The emission data presented in this section should be considered preliminary. Although UV excitation below 400 nm was readily accessible and allowed the probing of ligand centred and MLCT emission in the iridium complexes, further investigations are needed as the available instrumentation was limited in its ability to excite and detect emission at longer wavelengths. As such we are awaiting additional data from a collaborator with the necessary equipment to perform excitation studies at these shorter wavelengths.

2.3.1. UV/Vis absorption

The geometric isomers of the synthesised iridium complexes were purified and separated via column chromatography on silica column with an eluent composed of 40:60 pet ether:ethyl acetate to afford pure *mer* and *fac* isomers of four of the complexes and pure *mer* isomers of the Ir(H-PTz-Bn)$_3$ and Ir(NO_2-PTz-Bn)$_3$ complexes. These isomers were subject to preliminary UV/Vis and emission studies in order to determine the effect of the electronic and steric substituents on the photophysical properties of these compounds.

The UV/Vis spectra were recorded to evaluate the absorption characteristics of each of the isomers in order to determine how different substituent groups such as electron-withdrawing CF_3 and NO_2 on the phenyl rings or the sterically bulky Bn group on the triazole rings, impact the absorption wavelengths.
The UV/Vis spectra were recorded in solutions of acetonitrile to evaluate the absorption characteristics of each of the isomers in order to determine how different substituent groups such as electron withdrawing CF_3 and NO_2 on the phenyl rings or the sterically bulky Bn group on the triazole rings, impact the absorption wavelengths (**Figure 20**). All of the complexes showed three absorption bands corresponding to the ligand centred $\pi \rightarrow \pi^*$ transitions at around 220 nm, the MLCT transitions in the region of 260-280 nm and a $n \rightarrow \pi^*$ transition found above 290 nm with the exact positioning differing by complex.

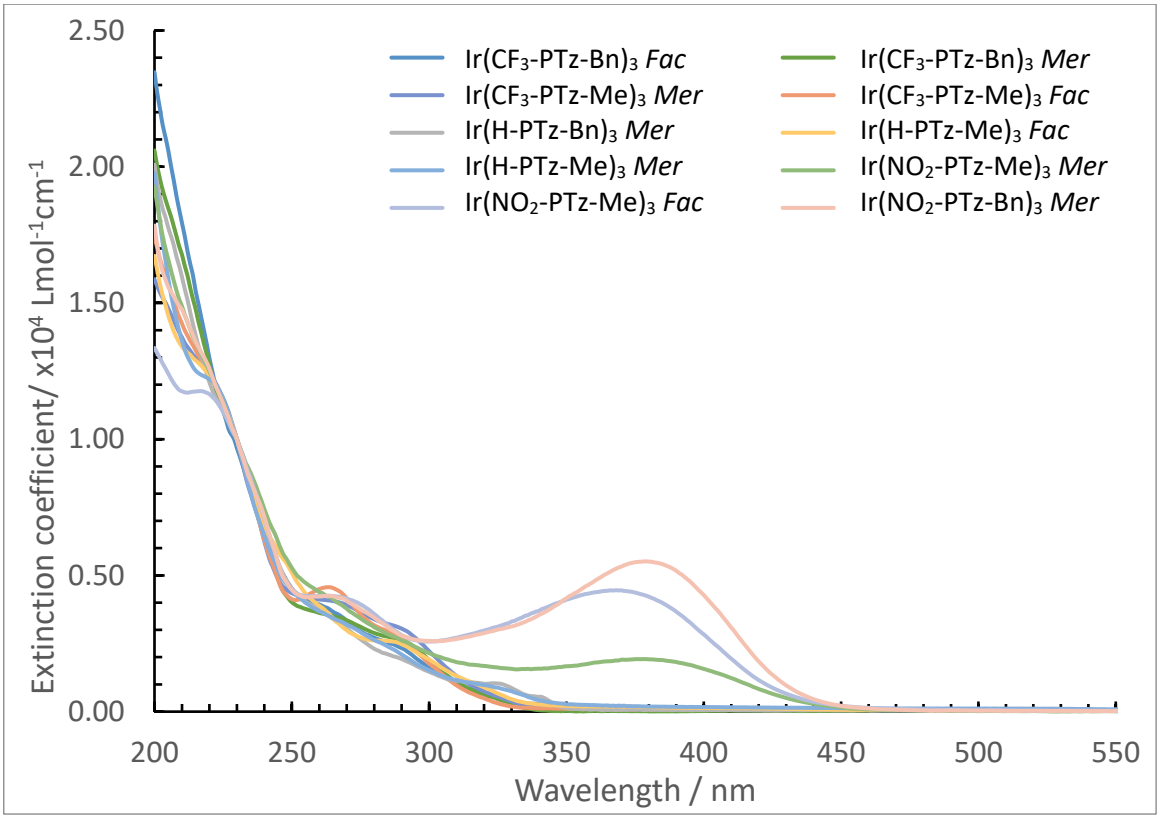

Figure 20: The UV/Vis absorption spectra of the isolated Ir(III) complexes.

The presence of the different substituents can be seen to significantly affect the absorption behaviour of these complexes. Most notably then NO_2 substituted complexes show a substantial red-shift in wavelength for the n→ π* transitions compared to the CF_3 and unsubstituted analogues. The n→ π* bands of the NO_2 complexes are found between 370-390 nm which means there are shifts of approximately 50 + nm higher than the closest analogue. This finding is consistent with what would be expected from the strong π withdrawing nature of the NO_2 groups as the group stabilises the π* orbitals meaning that electronic transitions that are lower in energy become more accessible due to the stabilisation of ligand-based π* orbitals involved in the n → π* transition, therefore the n→ π* absorptions are shifted to longer wavelengths. This shift was also seen in the CF_3 substituted complexes but to a much lesser extent which is reflective of the inductive electron withdrawing behaviour of the CF_3 group.

A comparison between spectra of the methyl and benzyl substituted complexes shows that there is little to no effect on the position of the absorption bands as both the π → π* and MLCT transitions occur at similar wavelengths for all the complexes. This suggests that substituents on the triazole do not significantly alter the electronic structure of the coordinating ligand, which is expected as they are not directly conjugated to the ligand π system that is coordinated to the iridium centre. However, differences can be seen when comparing the relative intensities of the peaks. In general, methyl substituted complexes display higher MLCT intensities than their benzyl analogues, a detail particularly seen in the *fac* isomers. This reduction in intensity of the benzyl substituted complexes is due to the increased steric bulk caused by these groups which distorts the complex geometry reducing the metal-ligand overlap consistent with the crystallographic observations discussed previously. In contrast, the steric congestion and intermolecular π–π interactions

have a more significant role in the *mer* isomers, where these structural factors can cause stronger variation in the absorption intensity and band shape of these transitions.

When looking for differences in the spectra between the geometric isomers it becomes evident that geometric isomerism does have a small effect on the absorption energies although this is to a much lesser extent than that caused by the ligand substitution. When looking at the CF_3 substituted geometric isomers the *fac* isomers are generally have higher intensity MLCT transitions than their *mer* counterparts an observation especially seen in the Ir(CF_3-PTz-Me)$_3$ complexes where the *fac* isomer has an extinction coefficient 415 $Lmol^{-1}$ cm^{-1} higher than the *mer* isomer. In contrast the NO_2 substituted complexes show greater absorption intensities in the n→ π* transitions for the *mer* isomers particularly when looking at the benzyl substituted complex. This reflects the increased contribution of the ligand centred excited states introduced by the strongly π-withdrawing NO_2 substituent. The presence of these states may also contribute to the excited state quenching pathways via interactions with the emissive MLCT state.

In conjunction with the observations made it should be noted that analysis across the full set of complexes should be interpreted with caution as unintended minor variations in concentrations may have altered observed intensities, particularly with the complexes of Ir(H-PTz-Me)$_3$ *mer* and Ir(NO_2-PTz-Me)$_3$ *mer* which showed lower intensities than expected. However, normalised to 230 nm and a concentration of 100 µM, the band shapes and positions are still comparable and the overall trends amongst the other complexes clearly show the effect of phenyl substitutions with electron withdrawing effects increasing absorption behaviour whilst steric substitutions on the triazole and geometric isomers influence MLCT intensity via secondary structural effects. These trends are consistent with previous reports on cyclometallated Ir(III) NHC complexes, which showed that introducing electron withdrawing substituents on the cyclometallating aryl ring can red shift the wavelengths of the ligand-centred and charge-transfer transitions as shown in the research by Chi in 2010.[141] The absorption trends highlighted here provide important context for interpreting the emission behaviour discussed in the following section.

2.3.2. Emission under excitation at 280 nm

Emission measurements were taken initially at 280 nm using solutions with absorbances of 0.10 ± 1% for all samples to ensure any differences observed in intensity were reflective of the photophysical behaviour of the complexes and not due to concentration variations. The complexes showed two emission bands the first a high energy band centred approximately around 307 nm caused by ligand centred fluorescence and a second weaker absorption emission band within the range of 380-420 nm dependant on the complex (**Figure 21a-c and Figure 21d-f**).

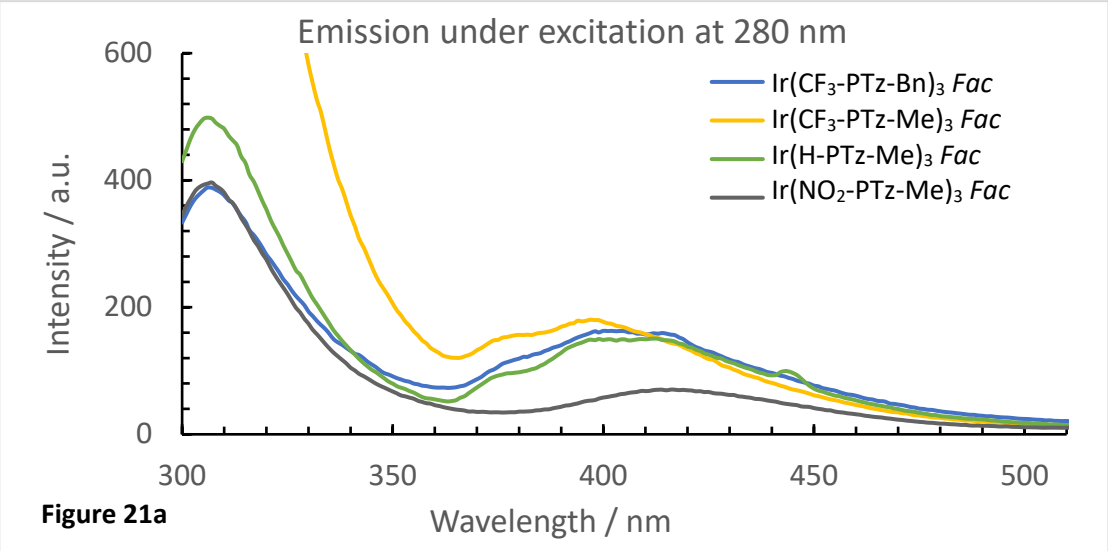

Figure 21a

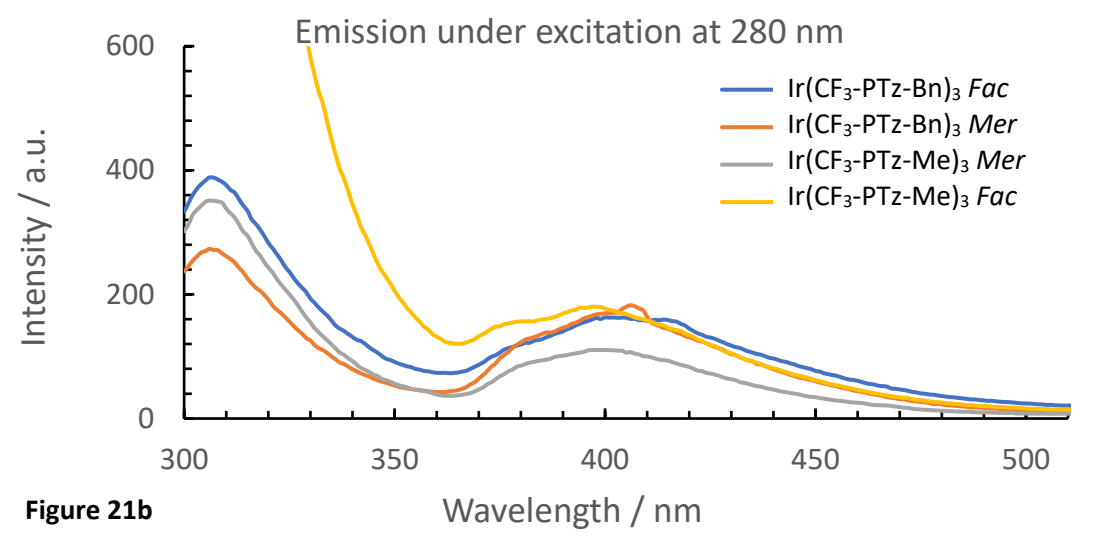

Figure 21b

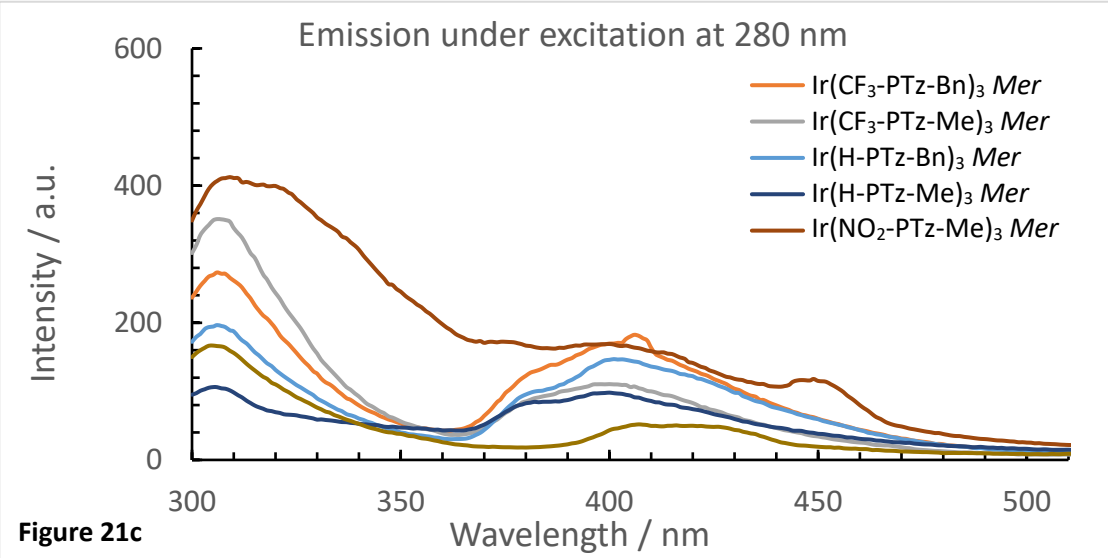

Figure 21c

Figure 21a-c: The emission spectra of the isolated *mer/fac* Ir(III) complexes recorded in a MeCN solution exciting at 280nm, split into spectra a-c for ease of comparison. Sample concentrations were adjusted to give absorbance values of 0.1 prior to measurement

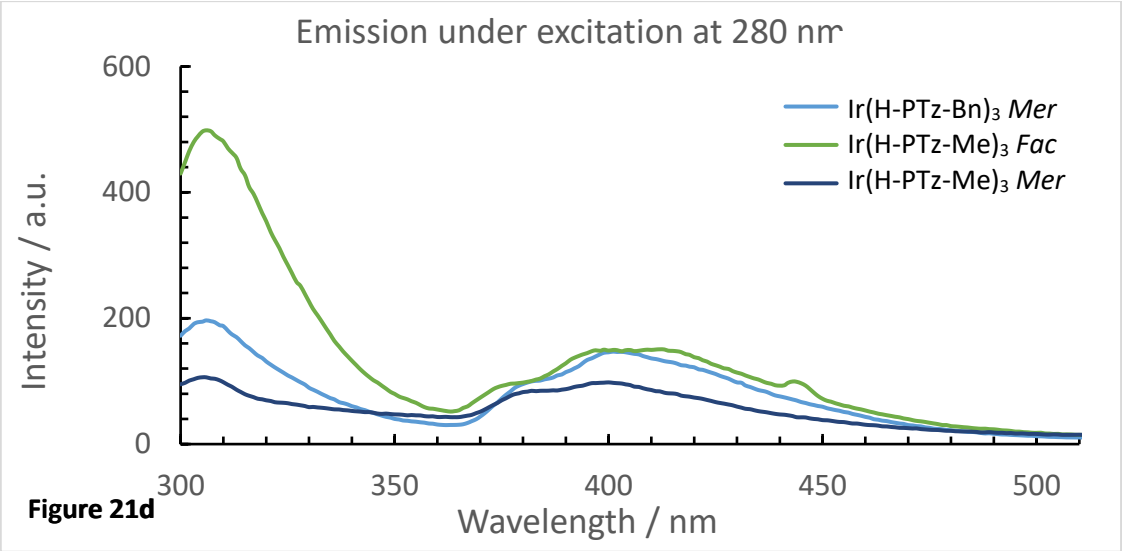

Figure 21d

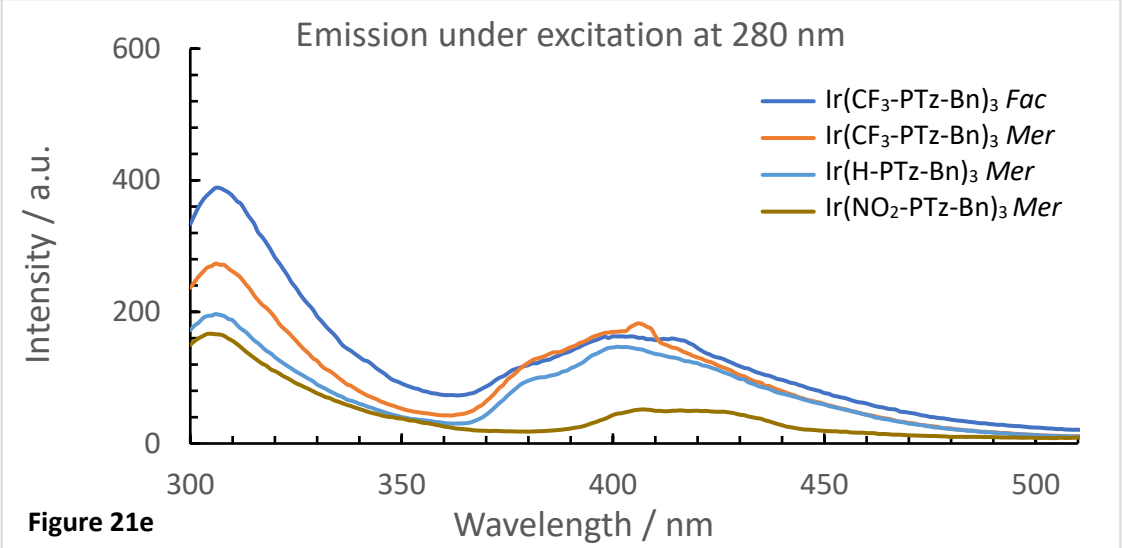

Figure 21e

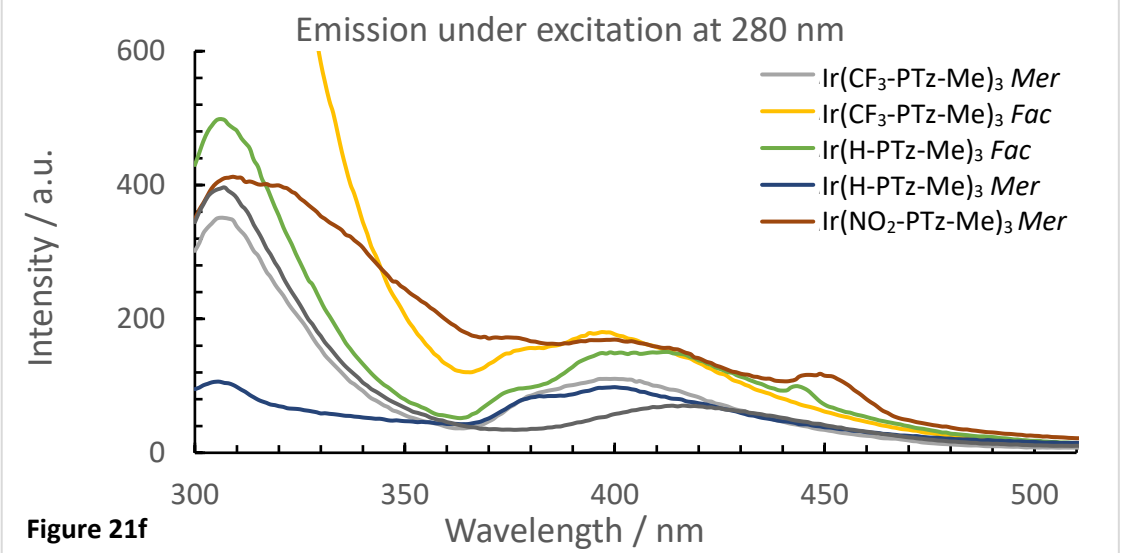

Figure 21f

Figure 21d-f: The Emission spectra of the isolated *mer/fac* Ir(III) complexes recorded in a MeCN solution at 280 nm and split into spectra d-f for ease of comparison. Sample concentrations were adjusted to give absorbance values of 0.1 prior to measurement.

The intensity of the ligand centred emission band is seen to fluctuate between the complexes depending on the attached substituents and geometric isomerism. Generally, the *fac* isomers are seen to have more intense ligand fluorescence than the *mer* isomers which is expected due to the symmetry and rigidity of the coordination environment of the *fac* isomer leading to a suppression of the non-radiative decay pathways. This difference is most easily observed in the $Ir(CF_3\text{-}PTz\text{-}Me)_3$ complex in which the *fac* ligand shows an extremely intense ligand fluorescence relative to the *mer* complex but this is not the only instance as many of the *fac* isomers such as $Ir(H\text{-}PTz\text{-}Me)_3$ *fac* show a more intense fluorescence than their *mer* counterpart but to a lesser extent only being 490 a.u. higher compared to the 650 a.u. shift seen in the $Ir(CF_3\text{-}PTz\text{-}Me)_3$ complexes which represents an extreme but chemically consistent case, which can be explained by the simultaneous compounding effects of stabilisation of the electronic states, geometric symmetry, and lack of steric disruption.

When comparing the emission of the different phenyl ring substitutions it becomes evident that the CF_3 substituted complexes give the most intense ligand fluorescence followed by the unsubstituted complexes whilst at the other end NO_2 substituted complexes result in the smallest ligand fluorescence intensities. This can be explained by the significant overlap of the NO_2 emission and absorption bands resulting in the re-absorbance of emitted light in addition to the increase in available non-radiative decay pathways due to the low-lying $n\rightarrow\pi^*$ states. Despite showing a heavily dampened emission the geometric effect on emission can still be seen in these complexes which show an inversion of the usual trend to give the *mer* isomer as the more intense ligand fluorescence. This is caused by the strong π-withdrawing and excited state quenching of the NO_2 group in the *fac* isomer as the ligand is more effectively coupled to the metal centre due to stronger metal-ligand orbital overlap. This results in the enhancement of the emission quenching through charge-transfer processes. In contrast the *mer* isomer which has a more distorted octahedral geometry which means it has less effective metal–ligand orbital overlap which weakens the influence of the NO_2 group on the excited state meaning the excited state retains more ligand-centred character hence the ligand fluorescence is still observed.

All the complexes showed a weak emission band in the region of 380-420nm that varied in intensity and position due to substituent and isomer effects. However, when exciting at 280 nm the ligand fluorescence dominates the photophysics and whilst it is possible to determine trends in the MLCT emission the phosphorescence is obscured. Therefore, the measurements were retaken with the same solutions exciting at 320 nm (**Figure 22a-c and Figure 22d-f**) as this lies outside the strongest ligand-centred absorption region allowing selective population of the charge-transfer excited states to give clearer observations of the MLCT emissions allowing a more reliable comparison of the emission energies and intensities between the different complexes.

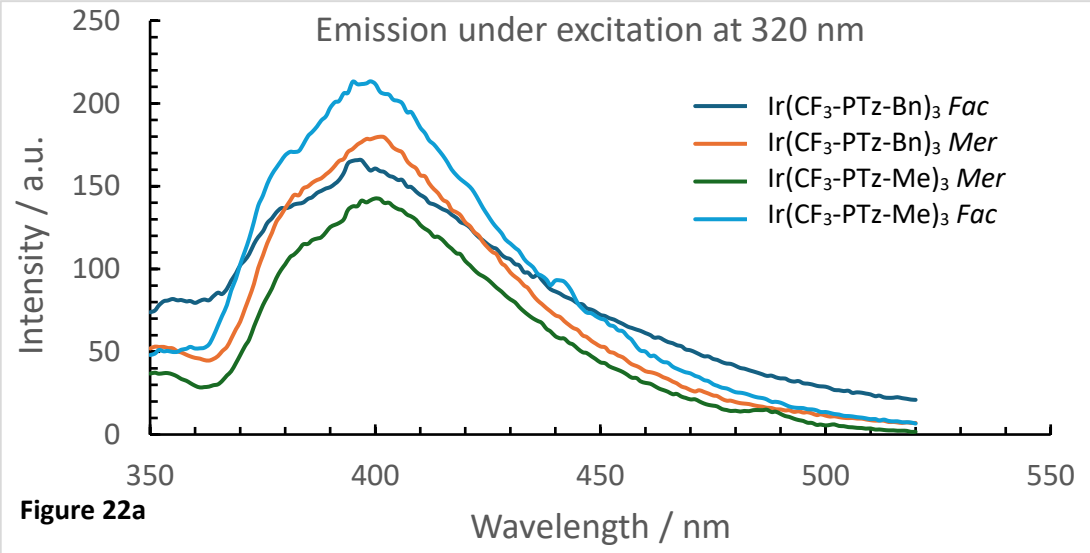

Figure 22a

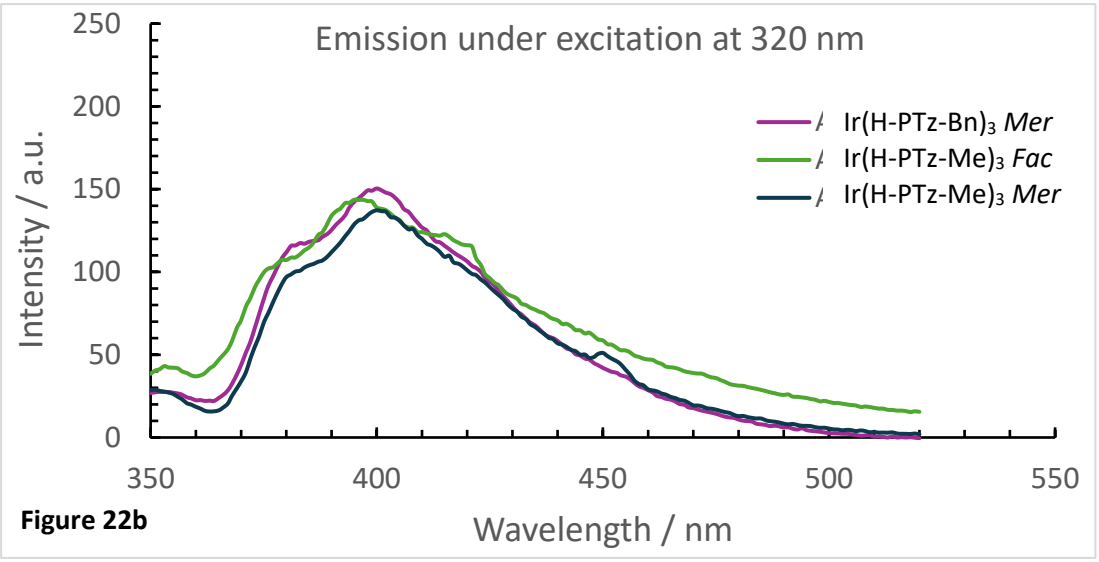

Figure 22b

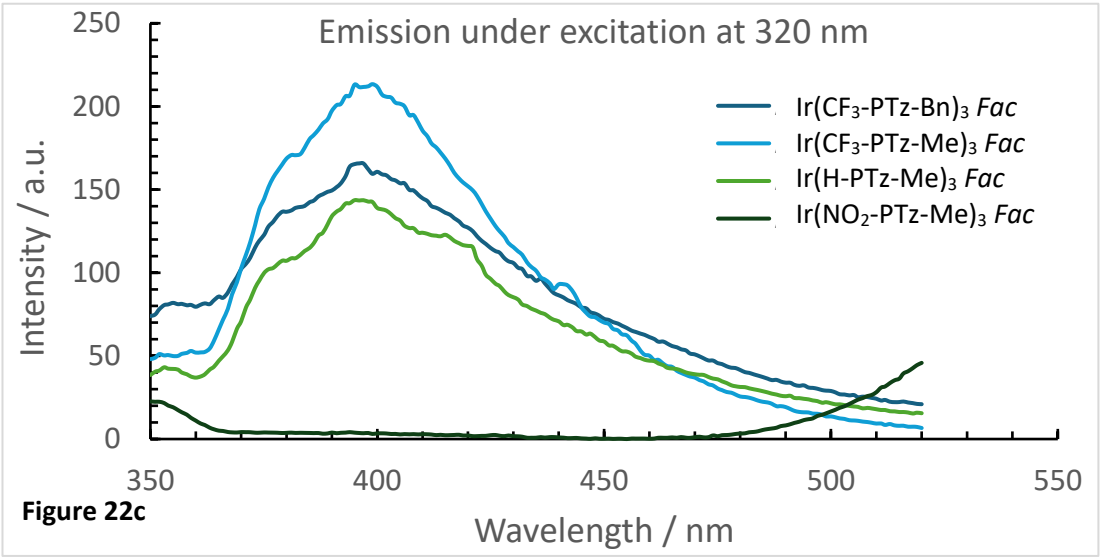

Figure 22c

Figure 22a-c: The Emission spectra of the isolated *mer*/*fac* Ir(III) complexes recorded in a MeCN solution at 320 nm and split into spectra a-e for ease of comparison. Sample concentrations were adjusted to give absorbance values of 0.1 prior to measurement.

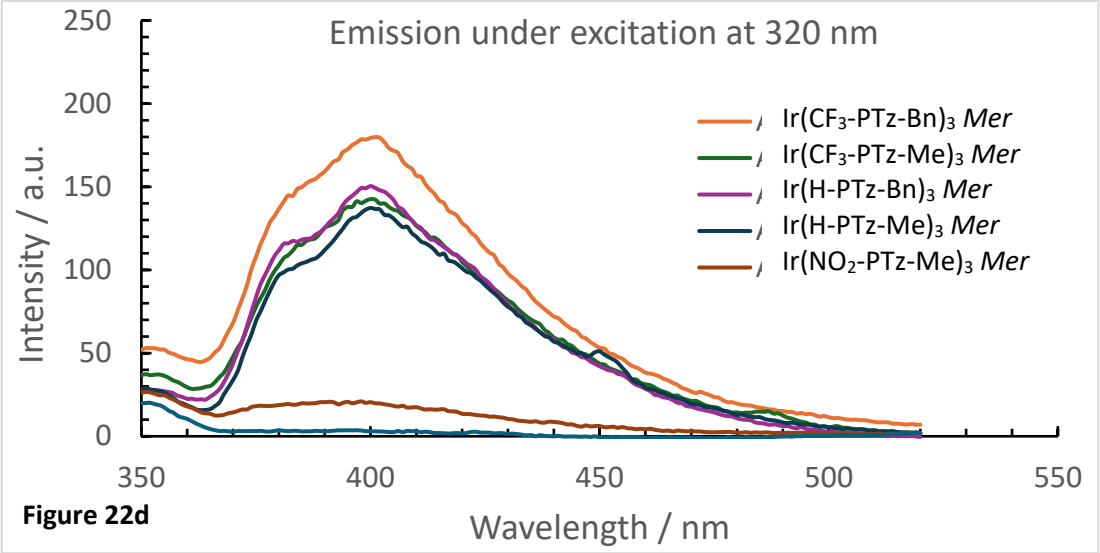

Figure 22d

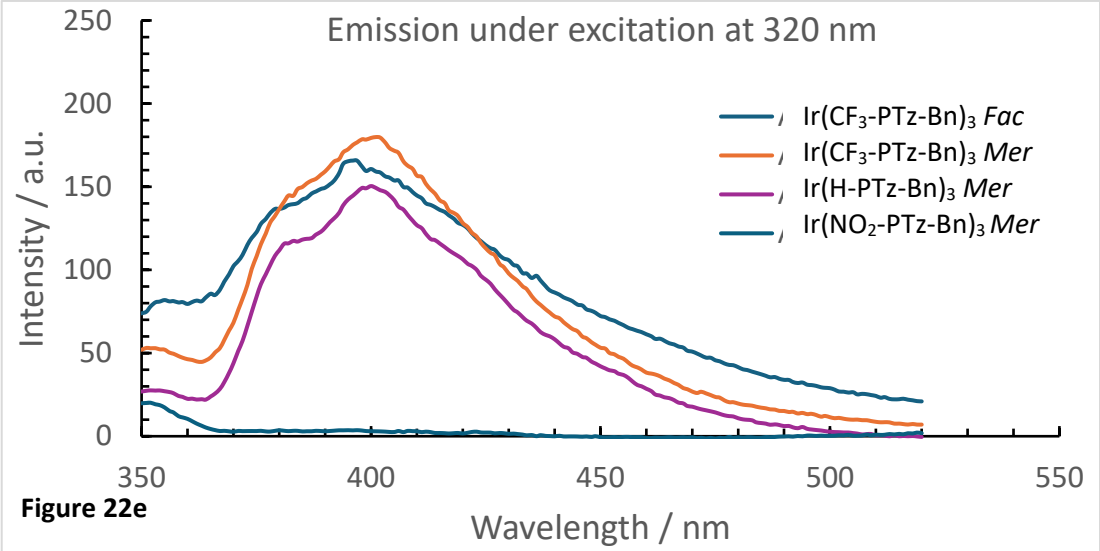

Figure 22e

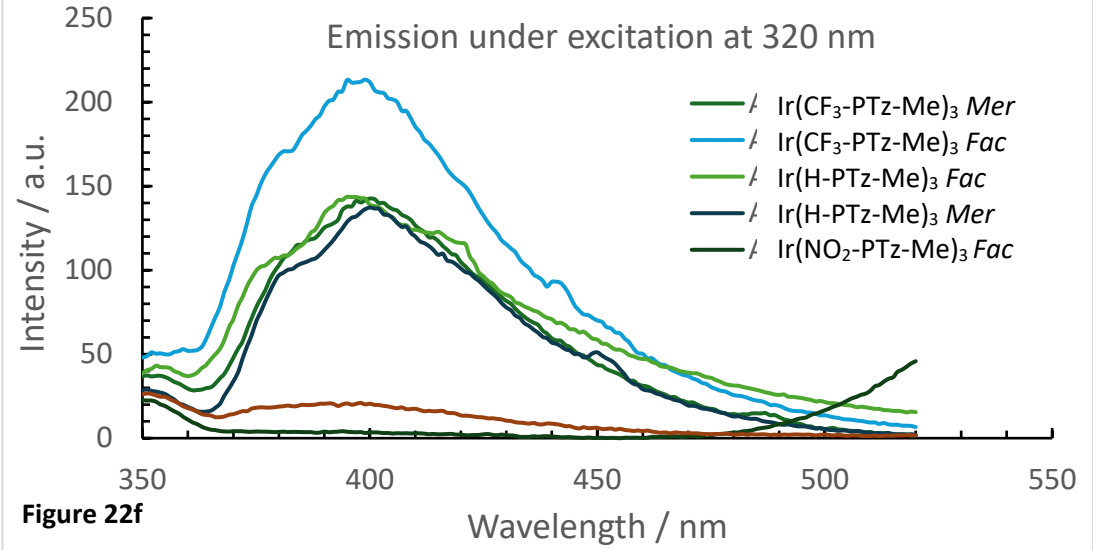

Figure 22f

Figure 22d-f: The Emission spectra of the isolated *mer*/*fac* Ir(III) complexes recorded in a MeCN solution at 320 nm and split into spectra d-f for ease of comparison. Sample concentrations were adjusted to give absorbance values of 0.1 prior to measurement.

2.3.3. Emission under excitation at 320 nm (MLCT Phosphorescence)

The samples were excited at 320 nm and the spectra recorded to in an attempt to minimise ligand fluorescence in order to investigate the emissions caused by the charge-transfer of the Iridium(III) complexes. When exciting at 320 nm all the complexes showed a single emission band of varying intensities which landed somewhere in the region of 390-405nm dependant on the attached substituents. This emission is a phosphorescence caused by decay from the triplet MLCT state. The highest emission intensities come from the CF_3 substituted complexes with the Ir(CF_3-PTz-Me)$_3$ *fac* complex showing the strongest emission at 398 nm with an intensity of 213 a.u. followed by the Ir(CF_3-PTz-Bn)$_3$ *fac* and *mer* isomers who's intensities are markedly lower only reaching to 179 a.u. This trend is readily explained by the strong electron withdrawing behaviour of the CF_3 group which acts to stabilise the ligand π* orbitals making the ligand field stronger and suppressing thermally accessible metal-centred non-radiative decay pathways leading to higher emission intensities.

Conversely the NO_2 substituted complexes, despite emitting at slightly higher energies, show significantly reduced emission intensities due to the substantial emission quenching these complexes experience due to the introduction of low-energy ligand-centred or charge-transfer states that facilitate non-radiative relaxation and reduce emission efficiency. The strongly red-shifted n→π* absorption bands seen in the UV/Vis spectra for the NO_2 substituted complexes indicates the presence of low-lying ligand-centred excited states, which may facilitate non-radiative decay through internal conversion, thereby reducing the intensity of the emission, providing another possible explanation for the excited state quenching as well as the previously discusses re-absorption of light due to the n→π* absorption in the same region as the emission. These increases in non-radiative decay pathways likely compound to produce the extreme amounts of quenching in these compounds.

When comparing the geometric isomers it can be seen that the *fac* isomers generally exhibit emission intensities equal to or higher than their *mer* counterparts, an observation most prevalent in the cases of the Ir(CF_3-PTz-Me)$_3$ and Ir(H-PTz-Me)$_3$ complexes. This trend is supported by the structure of the *fac* isomers which display more symmetrical ligand fields than the *mer* isomers which in turn improves metal-ligand overlap promoting radiative decay. Despite this obvious difference in intensities the emission intensities of both isomers are much less pronounced than those observed when exciting at 280 nm which provides compelling evidence that exciting at 320 nm reduces sensitivity to ligand centred fluorescence and allows the probing of MLCT emission properties. The data provided by exciting at 320 nm highlights that under these conditions, differences in emission wavelength are relatively small between the series of compounds synthesised. This suggests that the energy of the emissive excited state is primarily governed by the electronic effects of the phenyl substituents. In contrast, the substantial variations in emission intensity observed between complexes, particularly between *mer* and *fac* isomers and between methyl and benzyl-substituted complexes, suggests that steric bulk and distortion of the octahedral geometry, predominantly influence the emission efficiency by controlling non-radiative decay pathways rather than altering the excited state energy. This emission behaviour is consistent with the UV/Vis absorption trends seen and supports the discussed structure-photophysics relationships between these complexes. As the emission wavelength changes very little when different substituents are introduced this indicates that the emission of these complexes originates from a triplet MLCT state, where the emission energy is predominantly controlled by the iridium ligand

framework rather than by the attached substituents which reside on the outer parts of the ligand. Despite this these substituents may indirectly influence emission efficiency through steric and non-radiative decay effects.

Building on the understanding gained from the iridium(III) complexes, the scope of this work was expanded to investigate chromium(III) complexes incorporating the same ligand systems. Unlike iridium(III), chromium(III) has a d^3 electronic configuration and emits via spin-forbidden ligand field transitions. meaning that ligand modification is expected to affect emission primarily by influencing ligand-field strength and non-radiative decay processes rather than directly altering HOMO–LUMO energy gaps. With this in mind the work carried out to synthesise the analogous Cr(III) complexes explored whether the "blue-shifting" effect seen in the iridium (III) complexes due to ligand design could be employed to shift the emission of the Cr(III) complexes from the near-infrared region into the red region whilst maintaining a rigid structure in order to suppress non-radiative decay. The following section summarises the synthetic approaches attempted, the outcomes obtained, and the key challenges encountered in the attempted synthesis of the Cr(III) analogues.

2.4. Cr Complexes

2.4.1. Initial attempts using conditions derived from Ir(III) complex reactions

In order to explore whether the same ligand framework design successfully applied to the iridium(III) systems could be translated to chromium(III), initial complexation reactions were conducted using conditions that closely resembled those used for the synthesis of the Ir(III) NHC complexes. A chromium(III) chloride tetrahydrofuran complex ($CrCl_3 \cdot 3THF$) was selected as a precursor inspired by examples seen in the literature such as the research performed by Liu *et al*. who used $CrCl_3 \cdot 3THF$ to synthesise chromium complexes with amidinato-phosphino ligands.[146] The $CrCl_3 \cdot 3THF$ complex was synthesised by heating chromium(III) chloride for 48hrs at 100 ^oC in dry THF under nitrogen, following literature procedures.[146-148] Due to limitations in available equipment, the reaction flask could not be evacuated, and instead was extensively purged with nitrogen prior to heating. After 48 hours, a purple solution was obtained, which gave a purple solid upon evaporation of the solvent. This precursor was then stored under nitrogen and used in subsequent reactions. In these initial experiments, the ligands were refluxed with $CrCl_3.3THF$ in the presence of silver tosylate (AgTos), under an inert nitrogen atmosphere using dry THF as solvent, with the aim of promoting abstraction of the halide and facilitating coordination to the carbene centre similar to what was done for the Ir(III) complexes. Small quantities of zinc were also introduced to facilitate reduction of the chromium and promote ligand substitution, as has been reported in related chromium systems.[147] Zinc was added in stoichiometric quantities as a mild reductant, with the aim of accessing more labile Cr(II) species that were capable of facilitating ligand substitution before reoxidation occurred.

Reactions were typically refluxed at 80–90 °C for 24–48 hours. During these reactions, the formation of white or grey precipitates was consistently noted across all reactions which is attributed to the insoluble silver salts forms during the complexation reaction. Colour changes were often observed, giving solutions that were typically yellow to brown in colour following filtration. After working up these solutions and purifying them on a silica gel chromatography column in DCM, several yellow-coloured fractions were obtained.

However, crystallographic analysis of one isolated fraction revealed it to be a tosylate salt (**Figure 23**) rather than a chromium-ligand complex, suggesting that ligand protonation and tosylate salt formation were competing with metal coordination under these conditions.

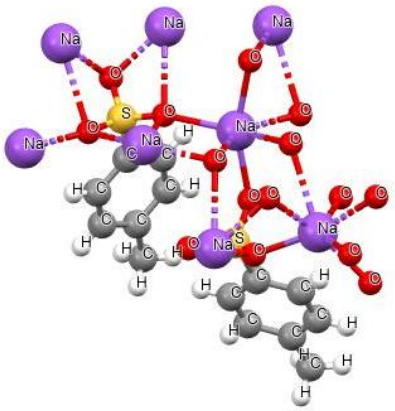

Figure 23: Crystal structure of the tosylate salt isolated

Furthermore, magnetic susceptibility measurements performed on the isolated materials consistently did not indicate the presence of any paramagnetic chromium(III) centre, and UV/Vis spectra lacked diagnostic features usually associated with ligand field transitions of octahedral Cr(III). On these basis, these products were discounted as successful chromium complexes. Although NHC ligands bind very strongly to many late transition metals such as iridium, their σ-donating ability alone is often not sufficient to overcome the low reactivity of Cr(III), especially when the ligand framework does not enforce strong chelation. From the perspective of hard-soft acid-base (HSAB) theory, chromium(III) is classified as a hard Lewis acid, whereas N-heterocyclic carbenes are soft σ-donor ligands. As a result, carbene donors are more favourably matched to softer metal centres such as Ir(III) than to the harder Cr(III) centre. This difference in hard-soft character contributes to the reduced reactivity observed for chromium in these systems and helps to explain the difficulty encountered in achieving stable NHC coordination under the conditions used. These results suggest that, unlike iridium(III), chromium(III) does not readily undergo carbene complexation via AgTos-mediated halide abstraction as this approach is not sufficient enough to promote stable NHC coordination to chromium under the conditions used. This could be explained by the differences in the relative metal-carbene bond strengths, rapid ligand protonation and competitive tosylate binding seen in these complexes.

2.4.2 Modification of reaction conditions and removal of silver salts

Due to the formation of ligand tosylate salts and the lack of evidence of successful chromium coordination in the previous reaction, subsequent reactions were conducted in the absence of silver salts. These experiments aimed to determine whether direct coordination of the ligand to chromium could occur without halide abstraction by AgTos. Ligands were refluxed with the chromium chloride precursor in dry THF under nitrogen. However, these reactions frequently resulted in rapid colour changes from yellow or orange to green, which may indicate oxidation of the chromium centre and/or formation of chromium hydroxide species such as $Cr(OH)_3$. After work-up, the isolated materials were

again found to lack any clear paramagnetic behaviour or spectroscopic features that are expected for Cr(III) coordination.

In some cases such as the chromium reaction with the CF_3 and Me substituted ligand, weak absorption bands were observed in the UV/Vis spectra near 360 nm and 290 nm, and excitation at higher energies produced a ligand-centred fluorescence around 316 nm and a weak emission band near 620 nm. Despite the presence of this band this evidence was deemed inconclusive as the low intensity of the emission band and lack of reproducibility for any further attempts, combined with the material being impure and there being insufficient material for reliable magnetic susceptibility or elemental analysis to back this observation up. Hence a confident assignment of this emission to a chromium-centred excited state could not be made. Consequently, these reactions were also discounted as unsuccessful.

These results highlight a key contrast with the iridium complexes: while Ir(III) readily forms robust cyclometallated carbene complexes under mildly forcing conditions, the chromium(III) systems appear to be significantly more sensitive to the reaction environment, showing a strong tendency towards ligand degradation over complexation.

2.4.3. Selecting an alternate organometallic chromium precursor: $CrPh_3 \cdot 3THF$

Despite successful formation of the $CrPh_3 \cdot 3THF$ precursor, the subsequent reactions with the ligand systems failed to yield isolable chromium complexes. Products obtained after work-up showed poor solubility, instability upon exposure to air and moisture, and tiny yields giving products in quantities too small for magnetic susceptibility measurements. These limitations prevented definitive characterisation and hence it was determined that the direct translation of the Ir(III) synthetic strategy to Cr(III) was unsuccessful therefore alternate chromium precursors were explored.

A more reactive but significantly less stable organochromium precursor, $CrPh_3 \cdot 3THF$ was identified and generated in situ by the reaction of $CrCl_3 \cdot 3THF$ with phenylmagnesium bromide (PhMgBr) at −78 °C, following established literature methods.[149] Addition of the Grignard reagent resulted in a red-brown solution, consistent with formation of an organochromium species. The freshly prepared precursor was transferred under inert conditions and reacted directly with the ligand systems in THF (**Scheme 4**). Upon refluxing at 80-90 ^{o}C, intense yellow or red solutions formed which suggests some degree of ligand interaction in the reaction.

Purification on a silica column in DCM yielded multiple coloured fractions including yellow and green solids; however, none could be conclusively identified as chromium-ligand complexes as the isolated materials were not obtained in sufficient quantities for magnetic susceptibility measurements, and attempts at crystallisation were unsuccessful. Additionally, the high air and moisture sensitivity of the organochromium intermediate, combined with the multi-step handling required for this reaction, likely caused decomposition of the organochromium intermediate or the ligand framework during work-up which would explain the presence of the green fractions present and the lack of evidence for the formation of a stable chromium complex.

Other non-green fractions collected were discounted or found to be inconclusive as no evidence was found to prove complex formation as small-scale reactions and small yields meant no further analysis such as magnetic susceptibility or UV/Vis analysis could be

performed. A future attempt at this reaction to determine the identity of the non-green fractions could involve scaling up the reaction and optimising reaction conditions such as temperature to produce higher yields and thus enough product for further analysis, and analysis via mass spectrometry to determine whether a chromium(III) species is formed in these reactions.

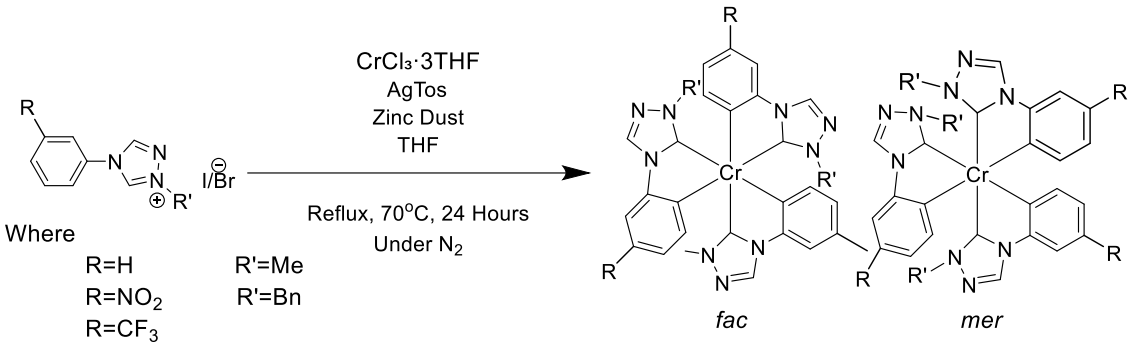

Scheme 4: Attempted chromium(III) complexation reaction which used the chromium precursor $CrPh_3 \cdot 3THF$.

2.4.4. Selecting an alternate chromium precursor: Chromium(II) chloride

Finally, chromium(II) chloride was explored due to it being a more labile and potentially more reactive precursor as seen in literature examples such as the p-Aryl-Substituted Iminopyridine Chromium Complexes synthesised by Zanchin *et al.* in 2024. In these derived reactions, the ligand was stirred for an hour in inert atmosphere under nitrogen in dry THF prior to addition of $CrCl_2$ (**Scheme 5**).[150] This addition resulted in an immediate colour change to yellow which afforded yellow and orange solids after purification. Thin-layer chromatography showed distinct from the free ligand and comparable to those observed for the analogous iridium(III) complex, which would suggest successful interaction with the chromium centre.

Although some fractions showed movement on silica comparable to the Ir(III) analogues, the small amount of product obtained in these reactions meant that no definitive magnetic or spectroscopic characterisation could be completed. In addition, attempts made to isolate crystals were largely unsuccessful, although pale pink crystals were briefly observed for some complexes. These rapidly decomposed to a green sludge upon exposure to ambient atmosphere, suggesting that any chromium containing species formed were highly air and/or moisture sensitive. Consequently, these results were considered inconclusive.

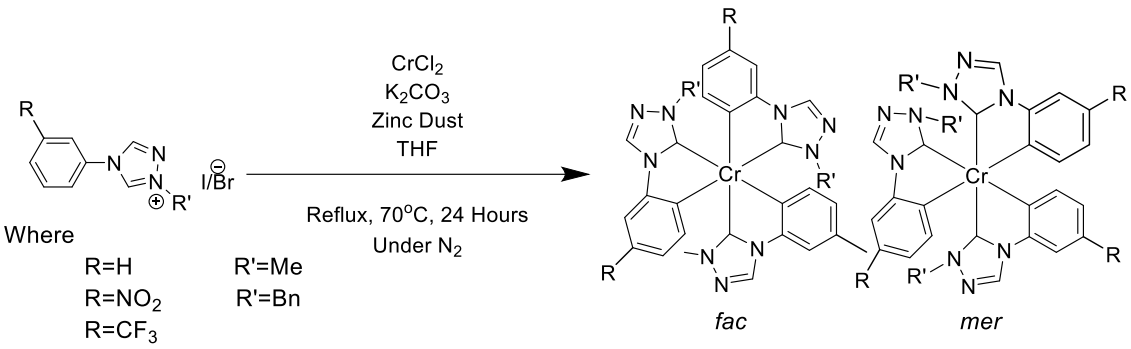

Scheme 5: Attempted chromium(III) complexation reaction which used the chromium precursor $CrCl_2$

2.4.5. Summary and challenges in chromium complex formation

Despite extensive exploration of multiple chromium precursors and reaction conditions, no chromium(III) complexes analogous to the iridium systems could be conclusively isolated or characterised. The main challenges encountered in these attempted syntheses include the high air and moisture sensitivity of the chromium intermediates, the paramagnetic nature of Cr(III) preventing standard NMR characterisation, difficulties in obtaining sufficient material for magnetic susceptibility measurements due to incredibly small yields, and failure to grow single crystals suitable for X-ray diffraction. The inability to obtain sufficient quantities of material for magnetic susceptibility or elemental analysis therefore represents a key limitation of this study.

When compared to iridium(III), chromium(III) appears to display slower ligand substitution kinetics and a stronger preference for hard donor ligands, which could be why the chromium species struggle to form the stable carbene-binding complexes under the conditions explored. Additionally, the tendency for the chromium species to undergo oxidation, combined with the low-lying ligand field excited states of the chromium which cause additional competing non-radiative pathways, both synthesis and photophysical characterisation becomes complicated and nuanced than that of the Ir(III) complexes.

It is suggested that future work in this area should focus on improving the coordination efficiency and kinetic stability of the existing ligand framework for chromium. The results obtained in this study suggest that the main challenge to forming these chromium(III) complexes lies in the difficulty achieving and maintaining robust chelation at the chromium centre under the reaction conditions explored rather than in the electronic suitability of the ligands. In contrast to the iridium(III) complexes, which readily undergo ligand substitution and rearrangement under prolonged reflux conditions, the chromium(III) displays a much higher sensitivity to ligand lability, decomposition, and air/moisture sensitivity during complexation.

One suggested strategy to address this issue would be to use stepwise ligand installation. During this the ligand framework is coordinated to chromium in a controlled, sequential manner rather than under one-pot conditions. This could involve the initial formation of a partially ligated chromium intermediate in which one donor fragment of the ligand binds first, followed by a controlled coordination of the remaining donor site. This would enforce early chelation and could reduce the likelihood of forming a weakly bonded or

monodentate intermediate, as these are particularly prone to ligand dissociation and oxidative degradation in chromium systems. As Cr(III) systems become kinetically inert once a stable coordination sphere has formed, early control over ligand binding could be crucial to forming these complexes.

In addition, future studies could explore the use of chromium precursors which have more labile ancillary ligands, such as THF or acetonitrile, in order to facilitate ligand coordination before oxidation or coordination saturation. The difficulties encountered using the $CrCl_3 \cdot 3THF$ precursor in this work suggests that using strongly bound chloride ligands may prevent efficient ligand chelation and instead promote competing pathways such as hydrolysis or oxidation. By using chromium sources with weaker, more easily displaced ligands could allow the NHC framework to coordinate more rapidly thereby increasing the likelihood of Cr(III) complexes forming.

Reaction conditions themselves could also benefit from further optimisation. The prolonged heating required for iridium complex formation was found to be detrimental when applied to the chromium complexation reactions, with extended reflux periods coinciding with colour changes to green and evidence of decomposition. Future work should therefore focus on exploring the use of lower reaction temperatures, shorter reaction times, and closer monitoring of reaction progress such as by TLC analysis to pinpoint the reaction endpoint before decomposition as the reactions are shown to be being quenched once coordination is achieved rather than being driven to completion by extended heating like in the Ir(III) systems. Reducing reaction temperatures could help protect the fragile chromium-ligand bonds and improve the stability of any chromium-containing species formed during the reaction.

Another major problem in this study is the extreme moisture sensitivity observed for the chromium reactions throughout this work. It is suggested that work going forward may benefit from the use of a glovebox to contain the reaction in a completely inert environment. While Schlenk techniques were sufficient for the needs of the iridium chemistry, even trace exposure to moisture was found to rapidly develop green chromium species, which were then seen to be inactive towards any further coordination hence the use of a glovebox might not only be beneficial but may be essential for the successful synthesis of these chromium complexes.

Collectively, these approaches aim to promote early ligand coordination in order to stabilise the metal-ligand framework before oxidative or dissociative processes can dominate, while also minimising the competing pathways, and improving the reproducibility of the reactions. Crucially, these strategies preserve the original ligand design employed in the iridium systems which allows the same electronic “blue-shifting” effects used in the iridium chemistry to be applied to chromium systems. If successful, this would enable the tuning of Cr(III) emission energies from the near-infrared region into the red region while maintaining the rigid coordination environments required to suppress non-radiative decay.

3. Conclusions

This work set out to investigate how the modification of cyclometallating N-heterocyclic carbene ligands via the introduction of electronic and sterically bulky substituents, influences the geometric structure, isomer distribution, and photophysical behaviour of luminescent iridium(III) complexes. This work then further sought to explore whether the same ligand design framework could be used in chromium(III) systems to tune emission energies from the near-infrared region into the red region.

A series of substituted 1,2,4-triazolium precursor ligands were successfully synthesised using procedures adapted from literature. [134] These were then functionalised to give six cyclometallating NHC ligands bearing a mix of one of three distinct electronic phenyl substituents (H, CF_3, NO_2) and one of two different steric substituents on the triazole (methyl or benzyl). These ligands were shown to be robust and versatile, allowing a systematic investigation of the electronic and steric effects on the ligand framework. Complexation of these ligands with iridium(III) afforded six novel tris-cyclometallated Ir(III) complexes, with isolable *mer* and *fac* geometric isomers obtained for four complexes and pure *mer* isomers obtained for the remaining two. The observed *mer*/*fac* ratios were found to be highly sensitive to ligand substitution. Increasing steric bulk at the triazole fragment via a benzyl substitution, resulted in the reaction strongly favouring *mer* isomer formation under kinetic control. While introducing electron-withdrawing substituents on the cyclometallating aryl ring increased *fac* isomer formation in the less sterically hindered systems. These trends reflect the balance between steric crowding during ligand approach and differences in carbene σ-donor strength, and are consistent with previously reported behaviour in related Ir(III) NHC systems.

Single-crystal X-ray diffraction studies provided direct structural evidence to support these observations. The *fac* isomers consistently displayed more symmetrical octahedral coordination environments with reduced geometric distortion, while the *mer* isomers showed increased variation in bond length and bond angles due to trans carbene-carbene interactions. In the benzyl substituted complexes, strong π-π stacking interactions were observed in the solid state and were found to stabilise the *mer* isomer through more efficient crystal packing, which provides a structural explanation for the increased selectivity for the *mer* isomer in these systems. The influence of electron-withdrawing substituents could also be seen in the differences in crystal packing efficiency and lattice symmetry, as complexes substituted with CF_3 showed greater *fac* stabilisation than their NO_2 analogues.

Photophysical studies allowed clear links to be drawn between the structure and properties of the iridium(III) complexes. UV/Vis absorption spectra showed three characteristic absorption bands corresponding to ligand centred π → π*, MLCT, and n → π* transitions. Strong red shifts of the n → π* absorption bands were observed for NO_2-substituted complexes showing evidence of a reduction in the energy of ligand centred excited states. This trend is consistent with the expected stabilisation of ligand-centred π* orbitals induced by strongly π-withdrawing substituents. In contrast, substitution at the triazole fragment had minimal impact on the absorption energies, confirming that these groups are not directly conjugated to the emissive electronic framework.

The emission data reinforced the conclusion that both electronic substitution of ligands and geometry strongly influence the control over the photophysical behaviour of these complexes. Under high-energy excitation at 280 nm, ligand centred fluorescence dominated the emission spectra, with *fac* isomers generally displaying higher intensities due to their increased rigidity and reduced non-radiative decay. When selectively exciting at 320 nm, this minimised ligand fluorescence and allowed clearer observation of the MLCT phosphorescence. This revealed emission maxima for all the iridium(III) complexes excited, which all appeared close together between 390–405 nm. The observation that emission energies change very little upon substitution on the non-coordinating parts of the ligand, indicates that the emissive state is a triplet MLCT state, whose energy is largely controlled by the iridium-ligand core rather than outer ligand substituents. Emission intensities however, varied significantly with differences in the geometric isomerism and steric bulk of the complexes which highlights the importance of geometric distortion and non-radiative decay pathways in determining the efficiency of emission.
Following on from the conclusions gained from the iridium(III) systems, the synthesis of analogous chromium(III) complexes was attempted using the same ligand frameworks with the aim of using the same "blue-shifting" of emission energy through electronic substitutions to shift Cr(III) emission from the near-infrared region into the red region. Despite extensive exploration of multiple chromium precursors and reaction conditions, no chromium(III) complexes could be conclusively isolated or characterised. The attempted reactions highlighted fundamental challenges associated with chromium chemistry, including slow ligand substitution kinetics, a strong preference for hard donor ligands meaning that there was incompatibility of the soft carbene donors with the hard Cr(III) centre as is predicted by the HSAB theory and the extremely high air and moisture sensitivity these reactions faced which led to rampant oxidation and decomposition. As a result of these differences, it strongly suggests that the synthetic approaches that are successful for late transition metals such as Ir(III) cannot be directly translated to the Cr(III) systems.

Although definitive chromium complexes were not obtained, the systematic exploration undertaken in this work provides a valuable insight into the limitations and challenges of applying NHC-based ligand design strategies to early transition metals. The results of this study suggest that while the electronic framework of the ligands is suitable for tuning excited-state energies, achieving stable coordination to a chromium centre will require much stronger chelation strategies, more labile precursors, and stricter exclusion of oxygen and moisture from the reaction. Importantly, the ligand systems developed here remain promising platforms for future exploration, as they are clearly shown to allow electronic tuning of complexes whilst maintaining the rigid coordination environment necessary for suppressing non-radiative decay pathways.

Overall, this work demonstrates that the fine control over electronic and steric ligand design will enable predictable tuning of the structure, isomer distribution, and photophysical behaviour in cyclometallated iridium(III) complexes and simultaneously highlights the fundamental differences in coordination chemistry that control the behaviour of chromium(III) systems, providing a solid foundation for future attempts to expand NHC-based photophysical design approaches to earth-abundant metal systems.

4. Experimental Procedures

4.1. General information

Unless otherwise stated, all reagents and solvents were used as obtained from commercial suppliers without further purification. Deionised water was used in all cases in which water is referred. When Petroleum ether is used it refers to the Pet ether fractions that boil between 40 °C and 60 °C .

Where column chromatography was performed the stationary phase used was silica gel with a 60 Å particle size unless otherwise stated. TLC was used to monitor the progress of column chromatography, and the plates were examined under a 245 nm UV light.

NMR spectra were recorded on a Bruker AVANCE III 400 spectrometer or a Bruker AVANCE NEO 400 spectrometer at 298 K. Chemical shifts are reported in parts per million and Coupling constants (J) are reported in hertz (Hz). Standard abbreviations of: m = multiplet, q = quartet, t = triplet, d= doublet, s= singlet, br = broad, were used to describe the peak multiplicity seen. All analysis was performed using a selection of COSY, HMBC, HSQC, DEPT135 and NOESY NMR, as required using ACD/NMR Processor Academic Education Product Version 12.01.

Mass spectra were recorded on a Shimadzu LCMS-8040 instrument.
Single crystals were selected and mounted on a Mitegen loop on a SuperNova diffractometer using Cu Kα radiation. The crystal was kept at 100(1) K during data collection. Using Olex2[151], the structure was solved with the SHELXT[152] structure solution program using Intrinsic Phasing and refined with the SHELXL[153] refinement package using Least Squares minimisation.

4.2. Ligand precursor synthesis

Of the three ligand precursors H-PTz and NO_2-PTz have been previously reported[135-137] while CF_3-PTz is yet to be reported in the literature. A poor reaction yield was obtained for H-PTz which was likely due to a handling mishap, whilst NO_2-PTz was not synthesised as it was supplied by Nick Fletcher from previous group work.

Synthesis of H-PTz
Analine (0.91 mL, 0.928 g, 9.97 mmol) was added to diformylhydrazine (0.899 g, 10.21 mmol) and gradually heated to a maintained temperature of 180 °C in a Silicon oil bath. After 6 hours the reaction mixture was cooled to room temperature leaving a brown oil from which the product was isolated via silica column chromatography (eluent = DCM ramped up to 5% methanol) giving an off white/ beige powder (0.276 g, 1.90 mmol, 19%)

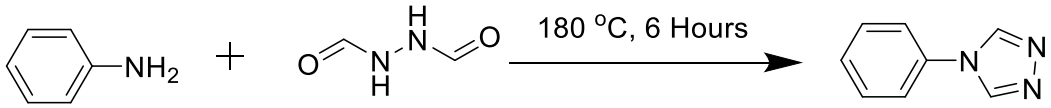

^{1}H NMR (400 MHz, $CDCl_3$-*d*) δ ppm 7.40 - 7.44 (2H, m), 7.51 (1H, tt, *J* = 7.4, 1.3 Hz), 7.57 (2H, tt, *J* = 7.0, 1.6 Hz), 8.50 (2H, s)

Synthesis of CF_3-PTz

3-(Trifluoromethyl)analine (1.23 mL, 1.588g, 9.86 mmol) was added to diformylhydrazine (0.887 g, 10.07 mmol) and gradually heated to a maintained temperature of 180 °C in a Silicon oil bath. After 6 hours the reaction mixture was cooled to room temperature leaving a brown oil from which the product was isolated via silica column chromatography (eluent = DCM ramped up to 5% methanol) giving an off white/ beige powder (1.083 g, 5.08 mmol, 52%)

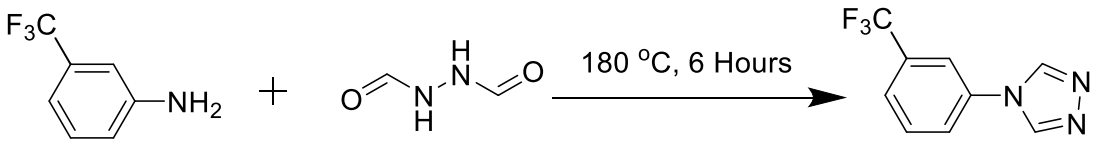

^{1}H NMR (400 MHz, $CDCl_3$-*d*) δ ppm 7.40 - 7.44 (2H, m), 7.51 (1H, tt, *J* = 7.4, 1.3 Hz), 7.57 (2H, tt, *J* = 7.0, 1.6 Hz), 8.50 (2H, s)

4.3. Ligand synthesis

Synthesis of H-PTz-Me

H-PTz (0.507 g, 3.49 mmol), MeI (0.25 mL, 0.570 g, 4.02 mmol) and MeCN (5 mL) was added to a sealed ACE pressure tube and reacted at 110 °C for 24 hours under constant stirring. After reacting the brick red reaction mixture was cooled to room temperature then further cooled in an ice bath forming a white precipitate collected via filtration giving a white powder (0.599 g, 2.09 mmol, 60%)

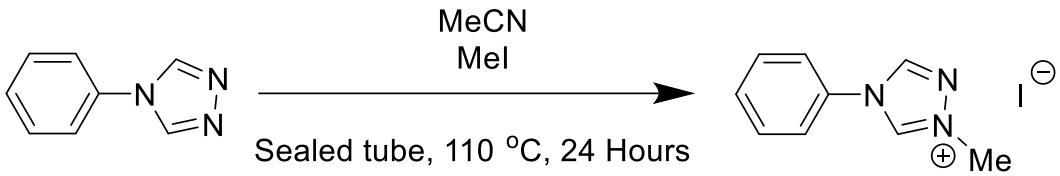

^{1}H NMR (400 MHz, DMSO-d_6) δ ppm 4.16 (3H, d, *J* = 0.4 Hz), 7.66 (1H, tt, *J* = 7.4, 1.3 Hz), 7.69 - 7.75 (2H, m), 7.82 (2H, d, *J* = 7.9 Hz), 9.75 (1H, s), 10.73 (1H, s)
^{13}C NMR (101 MHz, DMSO-d_6) δ ppm 123.00 (1C, s), 130.74 (2C, s), 131.00 (2C, s), 132.57 (1C, s), 142.55 (1C, s), 143.28 (1C, s)

Synthesis of CF_3-PTz-Me

CF_3-PTz (0.449 g, 2.11 mmol), MeI (0.20 mL, 0.456 g, 3.21 mmol) and MeCN (5 mL) was added to a sealed ACE pressure tube and reacted at 110 °C for 24 hours under constant stirring. After reacting the brick red reaction mixture was cooled to room temperature then further cooled in an ice bath forming a yellow precipitate collected via filtration giving a pale yellow powder (0.6603 g, 1.86 mmol, 88%)

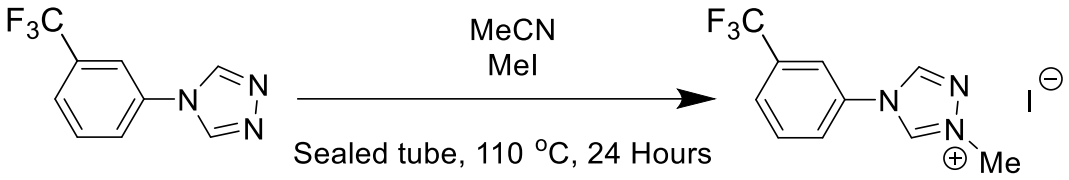

^{1}H NMR (400 MHz, DMSO-d_6) δ ppm 4.18 (3H, d, *J* = 0.5 Hz), 7.98 (1H, t, *J* = 7.9 Hz), 8.06 (1H, dt, *J* = 7.9, 1.0 Hz), 8.15 (1H, dd, *J* = 8.1, 1.00 Hz), 8.30 (1H, s), 9.80 (1H, s), 10.80 (1H, s)

^{13}C NMR (101 MHz, DMSO-d_6) δ ppm 120.55 (1C, s), 122.48 (1C, s), 127.36 (1C, s), 127.61 - 127.65 (1C, m), 127.66 - 127.70 (1C, m), 131.22 (1C, s), 132.08 (1C, s), 133.27 (1C, s), 142.98 (1C, s), 143.55 (1C, s)

Synthesis of NO_2-PTz-Me

H-PTz (0.570 g, 3.93 mmol), MeI (0.30 mL, 0.684 g, 4.82 mmol) and MeCN (5 mL) was added to a sealed ACE pressure tube and reacted at 110 °C for 24 hours under constant stirring. After reacting the brick red reaction mixture was cooled to room temperature then further cooled in an ice bath forming a yellow precipitate collected via filtration giving a pale yellow powder (0.943 g, 2.84 mmol, 72%)

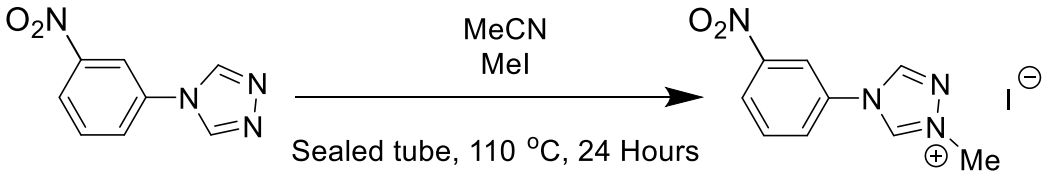

^{1}H NMR (400 MHz, DMSO-d_6) δ ppm 4.19 (3H, s), 8.03 (1H, t, *J* = 8.3 Hz), 8.28 (1H, ddd, *J* = 8.1, 2.1, 0.8 Hz), 8.51 (1H, ddd, *J* = 7.5, 2.1, 1.0 Hz), 8.78 (1H, t, *J* = 2.1 Hz), 9.84 (1H, s), 10.86 (1H, s)

^{13}C NMR (101 MHz, DMSO-d_6) δ ppm 118.78 (1C, s), 125.63 (1C, s), 129.65 (1C, s), 132.27 (1C, s), 133.37 (1C, s), 143.14 (1C, s), 143.61 (1C, s), 148.76 (1C, s)

Synthesis of NO_2-PTz-Bn

Benzyl bromide (0.50 mL, 0.720g, 4.21 mmol), NO_2-PTz (0.324 g, 1.70 mmol) and 50 mL MeCN were added to a reaction flask and refluxed under N_2 and constant stirring for 24 hours leaving a pale yellow solution. Excess MeCN evaporated until 5 mL remained followed by adding excess diethyl ether forming a white precipitate collected via filtration under vacuum and washed with diethyl ether giving a white solid powder (0.508 g, 1.41 mmol, 82%)

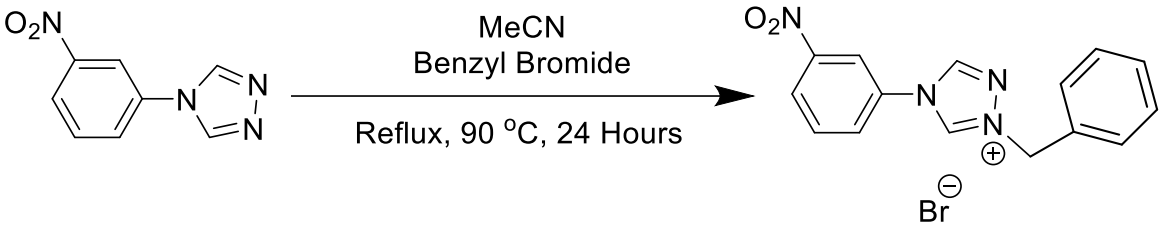

^{1}H NMR (400 MHz, DMSO-d_6) δ ppm 5.74 (2H, s), 7.42 - 7.50 (3H, m), 7.53 - 7.58 (2H, m), 8.03 (1H, t, *J* = 8.3 Hz), 8.31 (1H, ddd, *J* = 8.1, 2.2, 0.9 Hz), 8.50 (1H, ddd, *J* = 8.3, 2.2, 0.9 Hz), 8.83 (1H, t, *J* = 2.1 Hz), 9.88 (1H, s), 11.04 (1H, s)

^{13}C NMR (101 MHz, DMSO-d_6) δ ppm 58.26 (1C, s), 118.93 (1C, s), 125.60 (1C, s), 129.33 (1C, s), 129.46 - 129.58 (1C, m), 129.81 (1C, s), 132.13 (1C, s), 133.27 (1C, s), 133.48 (1C, s), 142.97 (1C, s), 144.15 (1C, s), 148.69 (1C, s)

Synthesis of H-PTz-Bn

Benzyl bromide (0.50 mL, 0.720 g, 4.21 mmol), H-PTz (0.260 g, 1.79 mmol) and 50 mL MeCN were added to a reaction flask and refluxed under N_2 and constant stirring for 24 hours leaving a pale yellow solution. Excess MeCN evaporated until 5 mL remained followed by adding excess diethyl ether forming a white precipitate collected via filtration under vacuum and washed with diethyl ether giving a white solid powder (0.503 g, 1.59 mmol, 89 %)

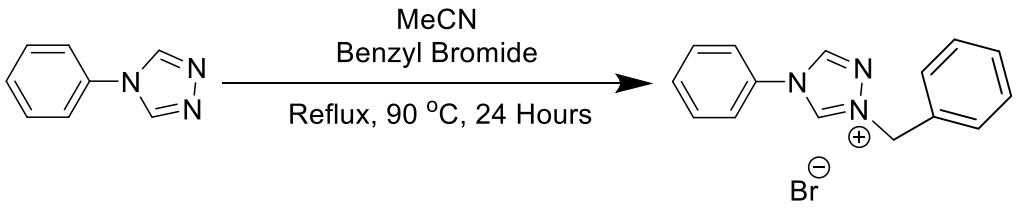

^{1}H NMR (400 MHz, DMSO-d_6) δ ppm 5.71 (2H, s), 7.40 - 7.49 (3H, m), 7.55 (2H, d, *J* = 7.4 Hz), 7.65 (1H, tt, *J* = 6.3, 1.3 Hz), 7.72 (2H, tt, *J* = 7.0, 1.5 Hz), 7.81 - 7.91 (2H, m), 9.79 (1H, d, *J* = 3.5 Hz), 10.90 - 11.03 (1H, m)

^{13}C NMR (101 MHz, DMSO-d_6) δ ppm 55.51 (1C, s), 123.06 (1C, s), 129.30 (1C, s), 129.44 (1C, s), 129.52 (1C, s), 130.63 (1C, s), 130.97 (1C, s), 132.66 (1C, s), 133.41 (1C, s), 142.35 (1C, s), 143.84 (1C, s)

Synthesis of CF_3-PTz-Bn

Benzyl bromide (0.40 mL, 0.576 g, 3.37 mmol), CF_3-PTz (0.224 g, 1.05 mmol) and 50 mL MeCN were added to a reaction flask and refluxed under N_2 and constant stirring for 24 hours leaving a pale yellow solution. Excess MeCN evaporated until 5 mL remained followed by adding excess diethyl ether forming a white precipitate collected via filtration under vacuum and washed with diethyl ether giving a white solid powder (0.336 g, 0.88 mmol, 83%)

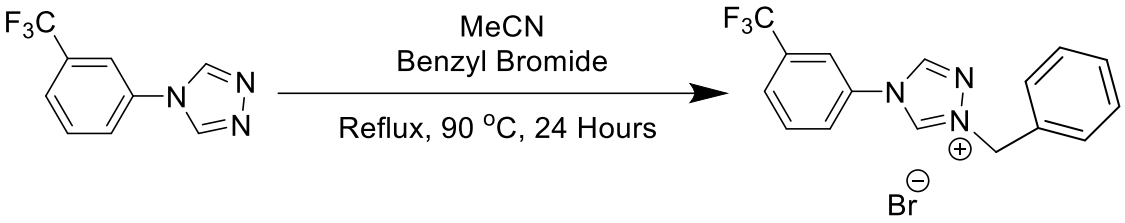

^{1}H NMR (400 MHz, DMSO-d_6) δ ppm 5.74 (2H, s), 7.38 - 7.51 (3H, m), 7.52 - 7.59 (2H, m), 7.97 (1H, t, *J* = 8.0 Hz), 8.02 - 8.08 (1H, m), 8.16 - 8.23 (1H, m), 8.35 (1H, d, *J* = 0.4 Hz), 9.86 (1H, s), 11.07 (1H, s)

^{13}C NMR (101 MHz, DMSO-d_6) δ ppm 55.56 (1C, s), 120.69 (1C, s), 122.51 (1C, s), 125.17 - 125.29 (1C, m), 127.50 (1C, s), 129.31 (1C, s), 129.48 (1C, s), 129.56 (1C, s), 130.78 (1C, s), 131.11 (1C, s), 131.94 (1C, s), 133.32 (1C, s), 142.82 (1C, s), 144.05 (1C, s)

4.4. Synthesis of iridium complexes

Assignment of individual NMR resonances for several complexes proved challenging due to the complexity of the spectra and therefore some signals are reported as multiplet ranges rather than fully resolved assignments. In particular, the benzyl-substituted complexes displayed additional spectral complexity due to geminal coupling of the CH_2 protons. In some cases, residual solvent peaks partially obscured product resonances, most notably the $CDCl_3$ signal at 7.28 ppm in the *mer*-Ir(H-PTz-Bn)$_3$ complex. Isolated yields for certain complexes exceeded 100 %, which is attributed to residual solvent and/or moisture retained within the samples. Due to time constraints, further drying and reweighing was not performed and therefore these yields should be considered approximate. Additionally, the *fac*-Ir(NO_2-PTz-Me)$_3$ sample contained trace amounts of the *mer* isomer, while the low isolated yield of the *mer*-Ir(NO_2-PTz-Bn)$_3$ complex is likely attributable to product loss during repeated column chromatography and potentially increased steric strain or reduced stability of the *mer* isomer.

Synthesis of Ir(H-PTz-Me)$_3$

AgTos (0.142 g, 0.51 mmol, 4.3 eq.), H-PTz-Me (0.130 g, 0.45 mmol, 3.8 eq.), $IrCl_3 \cdot 3H_2O$ (0.044 g, 0.12 mmol, 1.0 eq.) K_2CO_3 (0.077 g, 0.56 mmol, 4.7 eq.) and ethylene glycol (10 mL, 11.1 g, 0.18 mol) was added to a reaction flask protected from light with aluminium foil and refluxed under N_2 and constant stirring at 120 ^oC for 24 hours. After cooling to room temperature 40 mL water was added to the brown/grey reaction mixture and the resulting solution filtered through celite with DCM to remove the silver salts giving an off-white solid powder. Crude product purified and isolated into the *mer* and *fac* isomers via silica column chromatography (eluent 50 : 50 Pet ether : ethyl acetate ramped up to 20% acetone) giving 2 white solids which were *mer*- Ir(H-PTz-Me)$_3$ (0.0471 g, 0.071 mmol, 57%) and *fac*- Ir(H-PTz-Me)$_3$ (0.00690 g, 0.010 mmol, 8%)

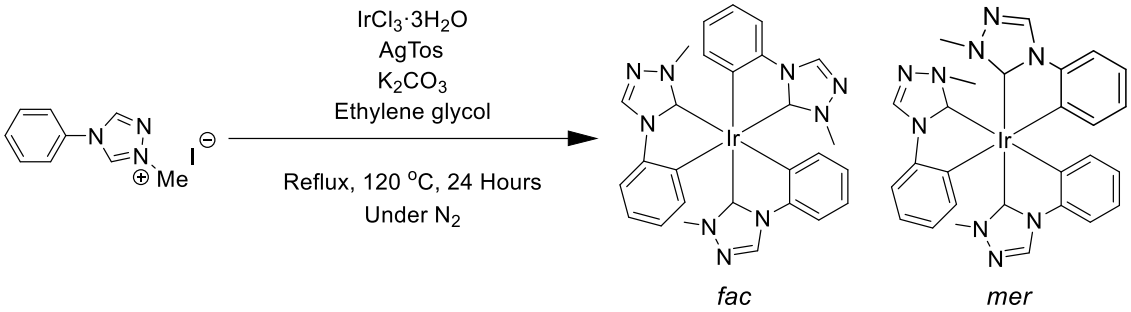

Ir(H-PTz-Me)$_3$ *fac*

^{1}H NMR (400 MHz, $CDCl_3$-*d*) δ ppm 3.40 - 3.43 (9H, m), 6.58 (3H, dd, *J* = 7.4, 1.3 Hz), 6.78 (3H, td, *J* = 7.4, 1.0 Hz), 6.99 (3H, td, *J* = 7.4, 1.34 Hz), 7.28 (1H, s), 8.39 (3H, s)

Ir(H-PTz-Me)$_3$ *mer*

^{1}H NMR (400 MHz, $CDCl_3$-*d*) δ ppm 3.24 - 3.25 (3H, m), 3.31 (3H, s), 3.41 (3H, s), 6.62 - 6.78 (3H, m), 6.79 - 6.88 (3H, m), 6.88 - 6.98 (3H, m), 7.23 - 7.28 (3H, m), 8.33 - 8.34 (1H, m), 8.40 - 8.41 (1H, m), 8.46 - 8.46 (1H, m)

Synthesis of Ir(CF_3-PTz-Me)$_3$

AgTos (0.170 g, 0.61 mmol,4.4 eq.), CF_3-PTz-Me (0.133 g, 0.38 mmol, 2.7 eq.), $IrCl_3 \cdot 3H_2O$ (0.0476 g, 0.14 mmol, 1.0 eq.) K_2CO_3 (0.0778 g, 0.56 mmol, 4.0 eq.) and ethylene glycol (10 mL, 11.1 g, 0.18 mol) was added to a reaction flask protected from light with aluminium foil and refluxed under N_2 and constant stirring at 120 ^oC for 24 hours. After cooling to room temperature 40 mL water was added to the brown/grey reaction mixture and the resulting solution filtered through celite with DCM to remove the silver salts giving an off-white solid powder. Crude product purified and isolated into the *mer* and *fac* isomers via silica column chromatography (eluent 50 : 50 Pet ether : ethyl acetate ramped up to 20% acetone) giving 2 white solids which were *mer*- Ir(CF_3-PTz-Me)$_3$ (0.09 g, 0.10 mmol, 76%) and *fac*- Ir(CF_3-PTz-Me)$_3$ (0.01 g, 0.012 mmol, 8%)

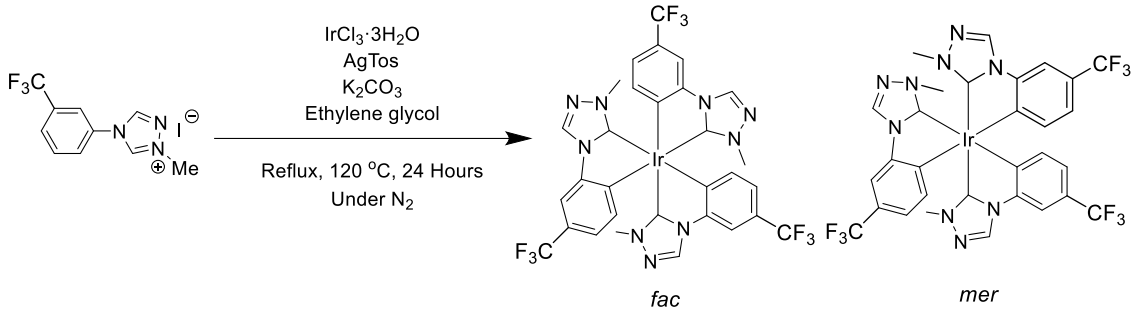

Ir(CF_3-PTz-Me)$_3$ *fac*:

^{1}H NMR (400 MHz, $CDCl_3$-*d*) δ ppm 3.45 (9H, s), 6.65 (3H, d, *J* = 7.6 Hz), 7.28 (3H, s), 7.52 (3H, d, *J* = 0.6 Hz), 8.49 (3H, s)

Ir(CF_3-PTz-Me)$_3$ *mer*:

^{1}H NMR (400 MHz, $CDCl_3$-*d*) δ ppm 3.26 (s, 3H) 3.33 (s, 3H) 3.41 (s, 3H) 6.69 (d, *J* = 7.6 Hz, 1H) 6.90 (d, *J* = 7.6 Hz, 1H) 6.97 (d, *J* = 7.5 Hz, 1H) 7.02 (dddd, *J* = 23.2, 15.6, 7.6, 0.9 Hz, 3H) 7.49 (d, *J* = 10.4 Hz, 3H) 8.44 (s, 1H) 8.52 (s, 1H) 8.56 (s, 1H)

Synthesis of Ir(CF_3-PTz-Bn)$_3$

AgTos (0.155 g, 0.52 mmol, 3.7 eq.), CF_3-PTz-Bn (0.193 g, 0.50 mmol, 3.6 eq.), $IrCl_3 \cdot 3H_2O$ (0.0498 g, 0.14 mmol, 1.0 eq.) K_2CO_3 (0.0772 g, 0.56 mmol, 4.0 eq.) and ethylene glycol (10 mL, 1.11g 0.18 mol) was added to a reaction flask protected from light with aluminium foil and refluxed under N_2 and constant stirring at 120 °C for 24 hours. After cooling to room temperature 40 mL water was added to the brown/grey reaction mixture and the resulting solution filtered through celite with DCM to remove the silver salts giving an off-white solid powder. Crude product purified and isolated into the *mer* and *fac* isomers via silica column chromatography (eluent 50 : 50 Pet ether : ethyl acetate ramped up to 20% acetone) giving 2 white solids which were *mer*- Ir(CF_3-PTz-Bn)$_3$ (0.154 g, 0.14 mmol, 99%) and *fac*- Ir(CF_3-PTz-Bn)$_3$ (0.0167 g, 0.015 mmol, 11%)

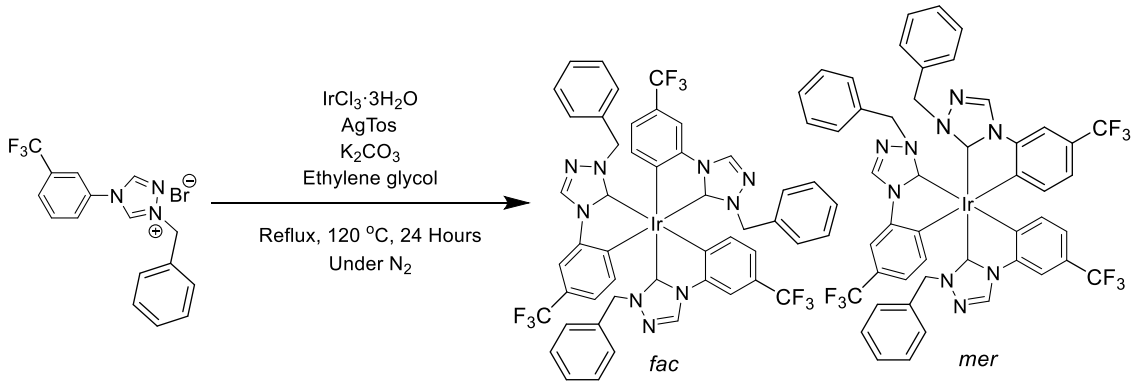

Ir(CF_3-PTz-Bn)$_3$ *fac*

^{1}H NMR (400 MHz, $CDCl_3$-*d*) δ ppm 4.89 (d, *J* = 16.0 Hz, 3H) 5.04 (d, *J* = 15.89 Hz, 3H) 6.33 (d, *J* = 7.3 Hz, 6H) 6.57 (d, *J* = 7.6 Hz, 3H) 6.98 (dd, *J* = 7.8, 1.0 Hz, 3H) 7.05 (t, *J* = 7.9 Hz, 6H) 7.10 (s, 3H) 7.21 (t, *J* = 7.4 Hz, 3H) 8.07 (s, 3H)

Ir(CF_3-PTz-Bn)$_3$ *mer*

^{1}H NMR (400 MHz, $CDCl_3$-*d*) δ ppm 4.78 - 4.97 (m, 4H) 4.98 - 5.05 (m, 1H) 5.13 - 5.20 (m, 1H) 6.20 - 6.26 (m, 4H) 6.30 - 6.35 (m, 2H) 6.56 - 6.59 (m, 1H) 6.69 - 6.73 (m, 1H) 6.79 - 6.83 (m, 1H) 7.06 (s, 15H) 7.50 (s, 1H) 8.13 (s, 1H) 8.53 - 8.58 (m, 1H)

Synthesis of Ir(NO_2-PTz-Me)$_3$

AgTos (0.142 g, 0.51 mmol, 3.9 eq.), NO_2-PTz-Me (0.170 g, 0.51 mmol, 3.9 eq.), $IrCl_3 \cdot 3H_2O$ (0.0453 g, 0.13 mmol, 1.0 eq.) K_2CO_3 (0.0677 g, 0.49 mmol, 3.7 eq.) and ethylene glycol (10 mL, 1.11 g, 0.18 mol) was added to a reaction flask protected from light with aluminium foil and refluxed under N_2 and constant stirring at 120 ^oC for 24 hours. After cooling to room temperature 40 mL water was added to the brown/grey reaction mixture and the resulting solution filtered through celite with DCM to remove the silver salts giving an off-white solid powder. Crude product purified and isolated into the *mer* and *fac* isomers via silica column chromatography (eluent 50 : 50 Pet ether : ethyl acetate ramped up to 20% acetone) giving 2 white solids which were *mer*- Ir(NO_2-PTz-Me)$_3$ (0.0707 g, 0.082 mmol, 69%) and *fac*- Ir(NO_2-PTz-Me)$_3$ 0.0221 g, 0.028 mmol, 21%)

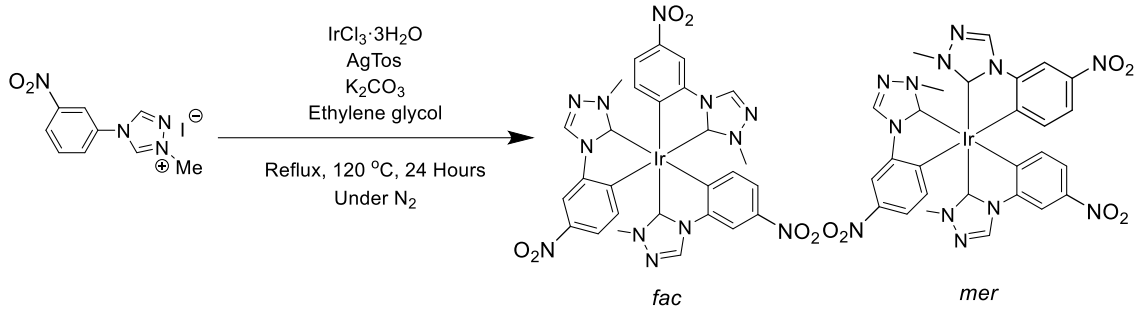

Ir(NO_2-PTz-Me)$_3$ *fac*

^{1}H NMR (400 MHz, $CDCl_3$-*d*) δ ppm 3.46 (s, 9H) 6.71 (d, *J* = 8.3 Hz, 3H) 7.67 (dd, *J* = 8.2, 2.2 Hz, 3H) 8.21 (d, *J* = 2.1 Hz, 3H) 8.61 (s, 3H)

Ir(NO_2-PTz-Me)$_3$ *mer*:

^{1}H NMR (400 MHz, $CDCl_3$-*d*) δ ppm 3.30 (s, 3H) 3.36 (s, 3H) 3.43 (s, 3H) 6.56 (d, *J* = 7.8 Hz, 2H) 6.73 (d, *J* = 8.1 Hz, 1H) 7.67 (td, *J* = 8.4, 2.1 Hz, 2H) 7.72 (dd, *J* = 8.1, 2.1 Hz, 1H) 8.17 (t, *J* = 1.9 Hz, 2H) 8.20 (d, *J* = 2.0 Hz, 1H) 8.56 (s, 1H) 8.57 (s, 1H) 8.64 (s, 1H) 8.68 (s, 1H)

Synthesis of Ir(H-PTz-Bn)$_3$

AgTos (0.142 g, 0.51 mmol, 4.6 eq.), H-PTz-Bn (0.149 g, 0.47 mmol, 4.2 eq.), $IrCl_3 \cdot 3H_2O$ (0.0401 g, 0.11 mmol, 1.0 eq.) K_2CO_3 (0.0885 g, 0.64 mmol, 5.8 eq.) and ethylene glycol (10 mL, 1.11 g, 0.18 mol) was added to a reaction flask protected from light with aluminium foil and refluxed under N_2 and constant stirring at 120 ^oC for 24 hours. After cooling to room temperature 40 mL water was added to the brown/grey reaction mixture and the resulting solution filtered through celite with DCM to remove the silver salts giving an off-white solid powder. Crude product purified and isolated into the *mer* and *fac* isomers via silica column chromatography (eluent 50 : 50 Pet ether : ethyl acetate ramped up to 20% acetone) giving a white solid which was *mer*- Ir(H-PTz-Bn)$_3$ (0.0597 g, 0.067 mmol, 59%)

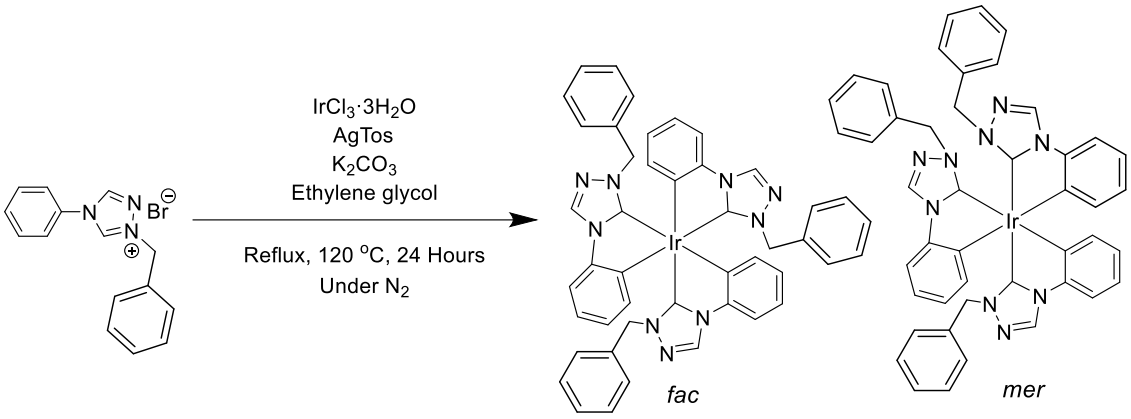

Ir(H-PTz-Bn)$_3$ *mer*

^{1}H NMR (400 MHz, $CDCl_3$-*d*) δ ppm 4.77 (t, *J* = 15.1 Hz, 1H) 4.89 (d, *J* = 7.3 Hz, 3H) 4.93 (d, *J* = 3.4 Hz, 1H) 5.00 (d, *J* = 15.9 Hz, 1H) 6.40 (qd, *J* = 8.8, 1.1 Hz, 4H) 6.47 (dd, *J* = 7.6, 0.5 Hz, 2H) 6.77 - 6.90 (m, 6H) 6.94 - 7.03 (m, 6H) 7.04 - 7.21 (m, 6H) 7.28 (td, *J* = 3.5, 0.8 Hz, 3H) 7.57 (s, 1H) 8.15 (s, 1H) 8.41 (s, 1H)

Synthesis of Ir(NO_2-PTz-Bn)$_3$

AgTos (0.146 g, 0.52 mmol, 2.9 eq.), NO_2-PTz-Bn (0.203 g, 0.56 mmol, 3.1 eq.), $IrCl_3 \cdot 3H_2O$ (0.0644 g, 0.18 mmol, 1.0 eq.) K_2CO_3 (0.0730 g, 0.53 mmol, 2.9 eq.) and ethylene glycol (10 mL, 1.11 g, 0.18 mol) was added to a reaction flask protected from light with aluminium foil and refluxed under N_2 and constant stirring at 120 ^oC for 24 hours. After cooling to room temperature 40 mL water was added to the brown/grey reaction mixture and the resulting solution filtered through celite with DCM to remove the silver salts giving an off-white solid powder. Crude product purified and isolated into the *mer* and *fac* isomers via silica column chromatography (eluent 50 : 50 Pet ether : ethyl acetate ramped up to 20% acetone) giving a white solid which was *mer*- Ir(NO_2-PTz-Bn)$_3$ (0.0441 g, 0.043 mmol, 23%) Low product yield likely due to product loss during repeated columns but may also be lower due to increased steric strain and instability of the *mer* isomer

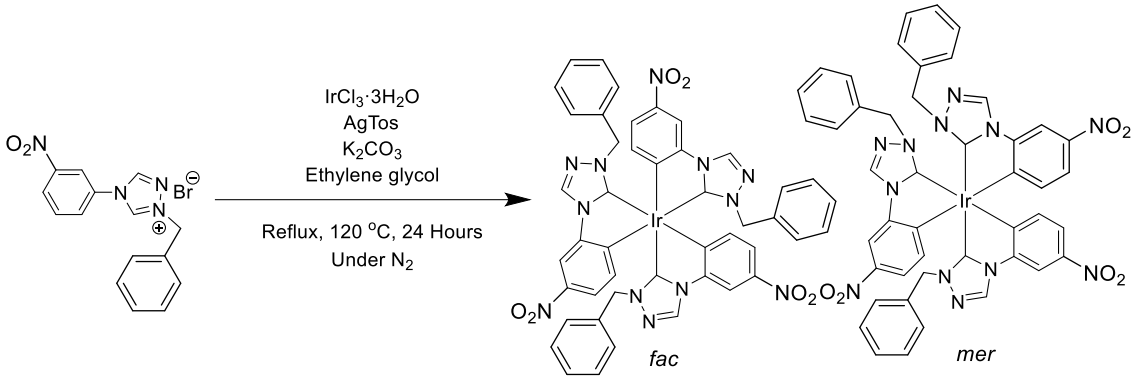

Ir(NO_2-PTz-Bn)$_3$ *mer*

^{1}H NMR (400 MHz, $CDCl_3$-*d*) δ ppm 4.67 - 4.85 (m, 3H) 4.95 (d, *J* = 15.6 Hz, 1H) 5.02 (d, *J* = 15.8 Hz, 1H) 5.18 (d, *J* = 16.4 Hz, 1H) 6.25 (t, *J* = 6.8, 7.0 Hz 2H) (d, *J* = 7.6 Hz, 1H) 7.01 (d, *J* = 6.6 Hz, 1H) 7.05 (d, *J* = 7.9 Hz, 3H) 7.10 - 7.16 (m, 3H) 7.16 - 7.22 (m, 3H) 7.62 (dd, *J* = 8.1, 2.1 Hz, 1H) 7.65 (s, 1H) 7.69 (ddd, *J* = 8.1, 4.9, 2.2 Hz, 2H) 7.74 (d, *J* = 2.1 Hz, 1H) 8.21 (d, *J* = 2.1 Hz, 1H) 8.26 (s, 1H) 8.68 - 8.70 (m, 1H)

5. Appendix

5.1. Ligand Precursors

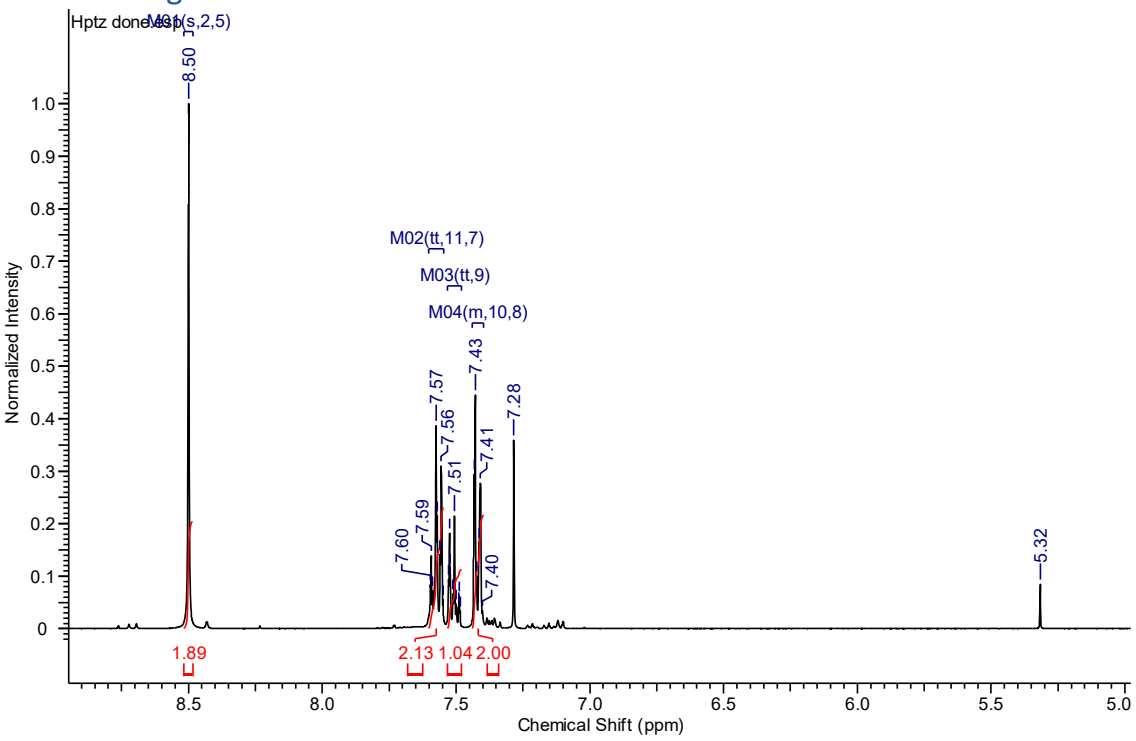

A1: ^{1}H NMR spectrum analysis for H-PTz

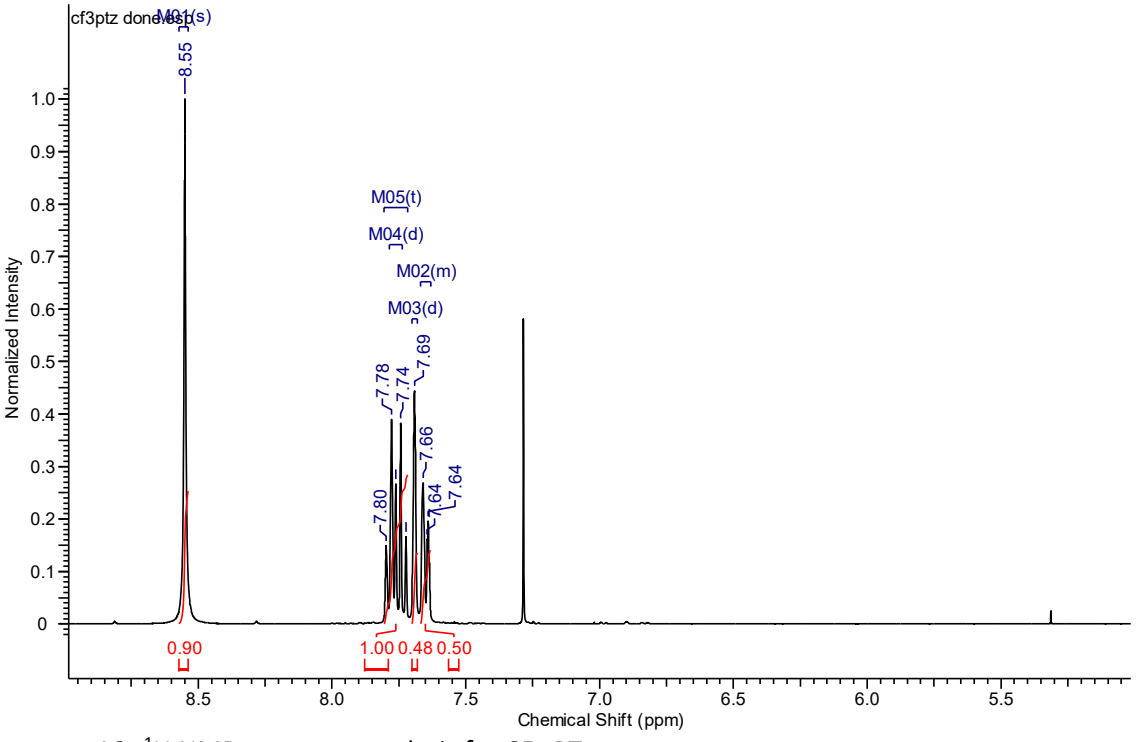

A2: ^{1}H NMR spectrum analysis for CF_3-PTz

5.2. Me-trz ligands

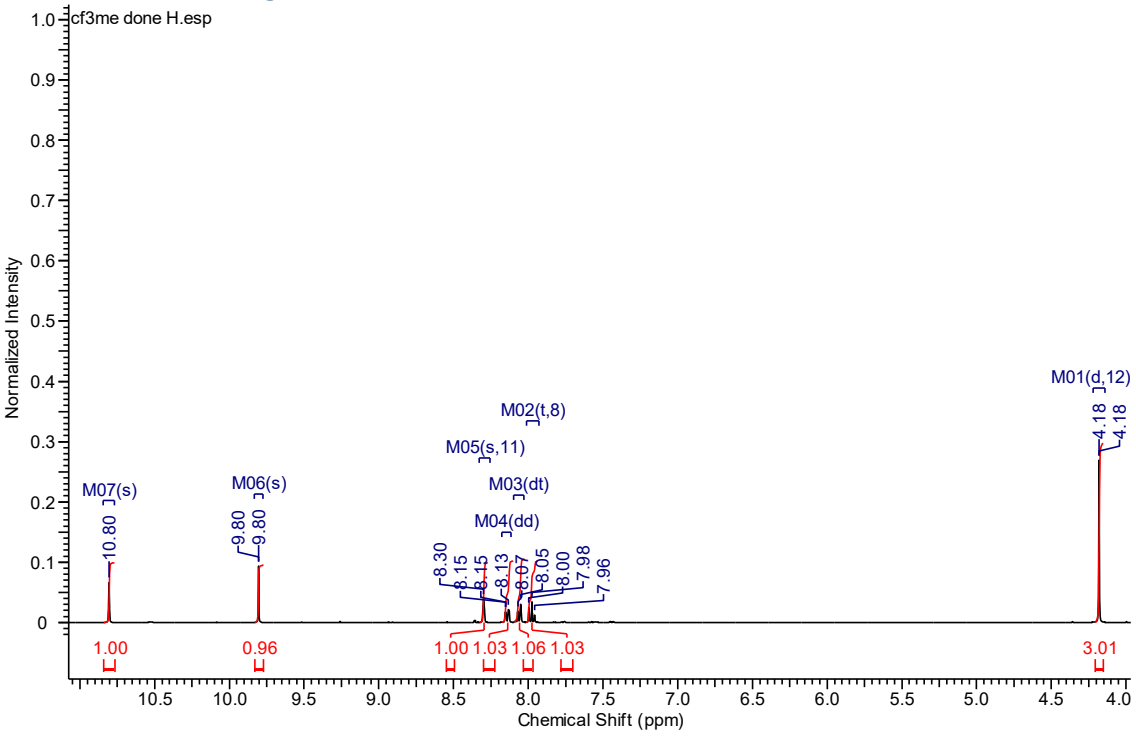

A3: ^{1}H NMR spectrum analysis for CF_3-PTz-Me

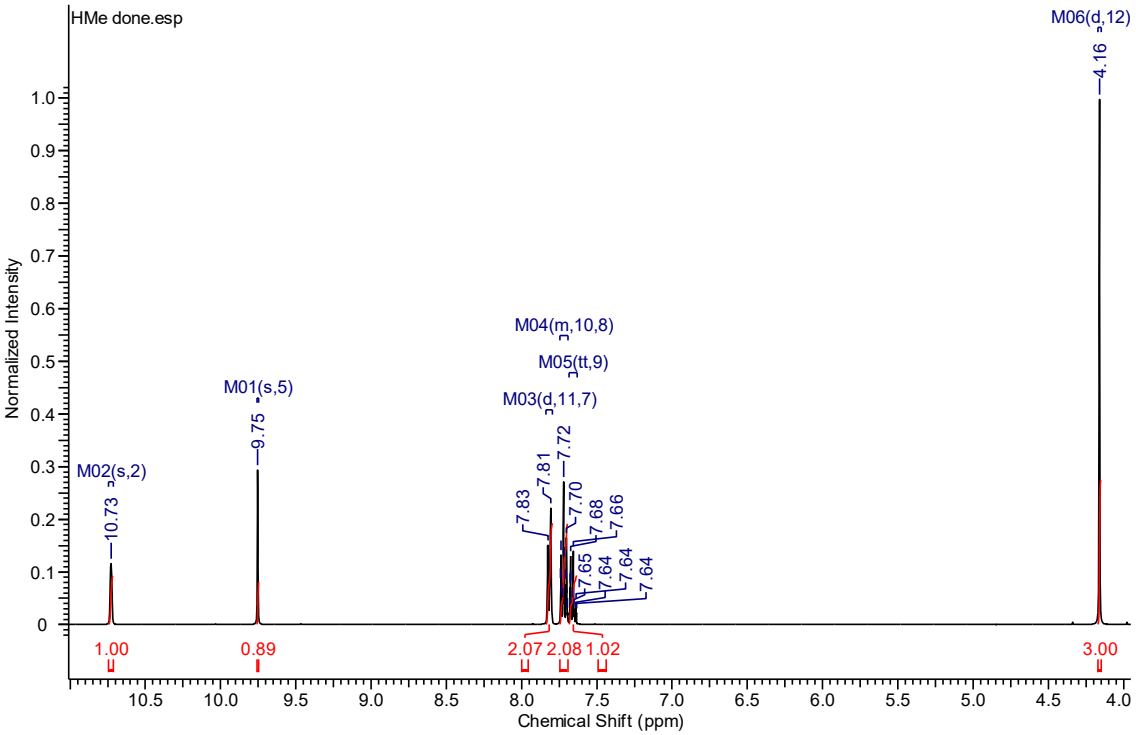

A4: ^{1}H NMR spectrum analysis for H-PTz-Me

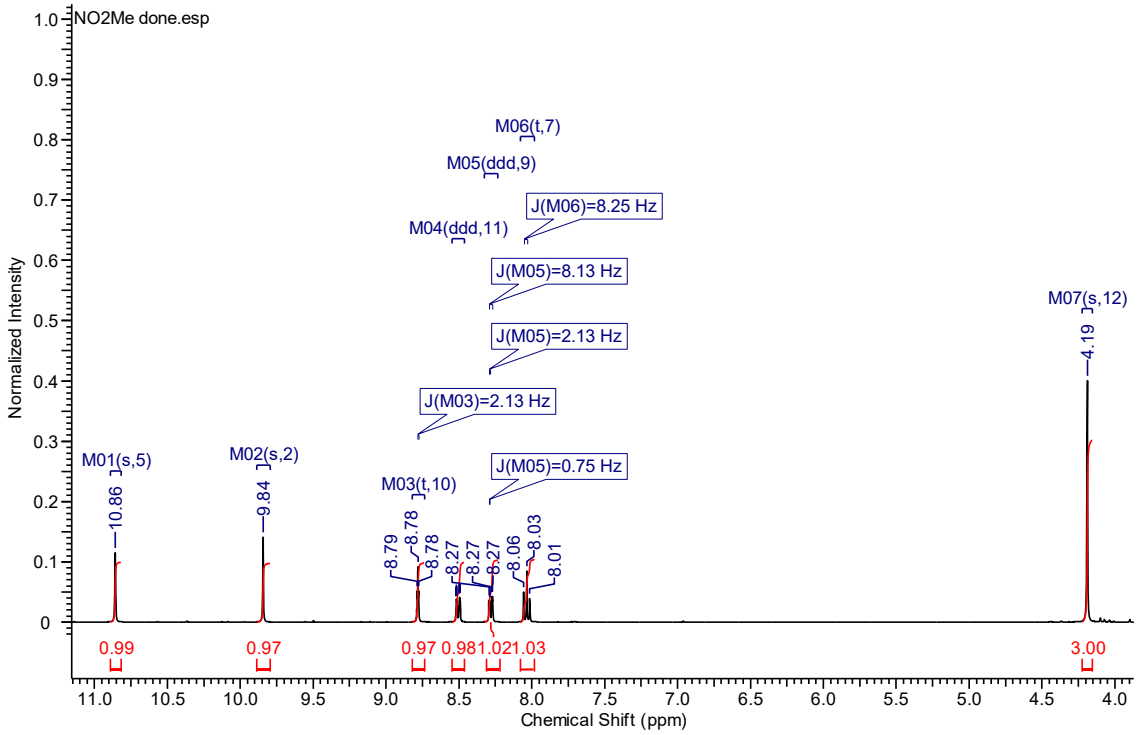

A5: ^{1}H NMR spectrum analysis for NO_2-PTz-Me

5.3. Bn-trz ligands

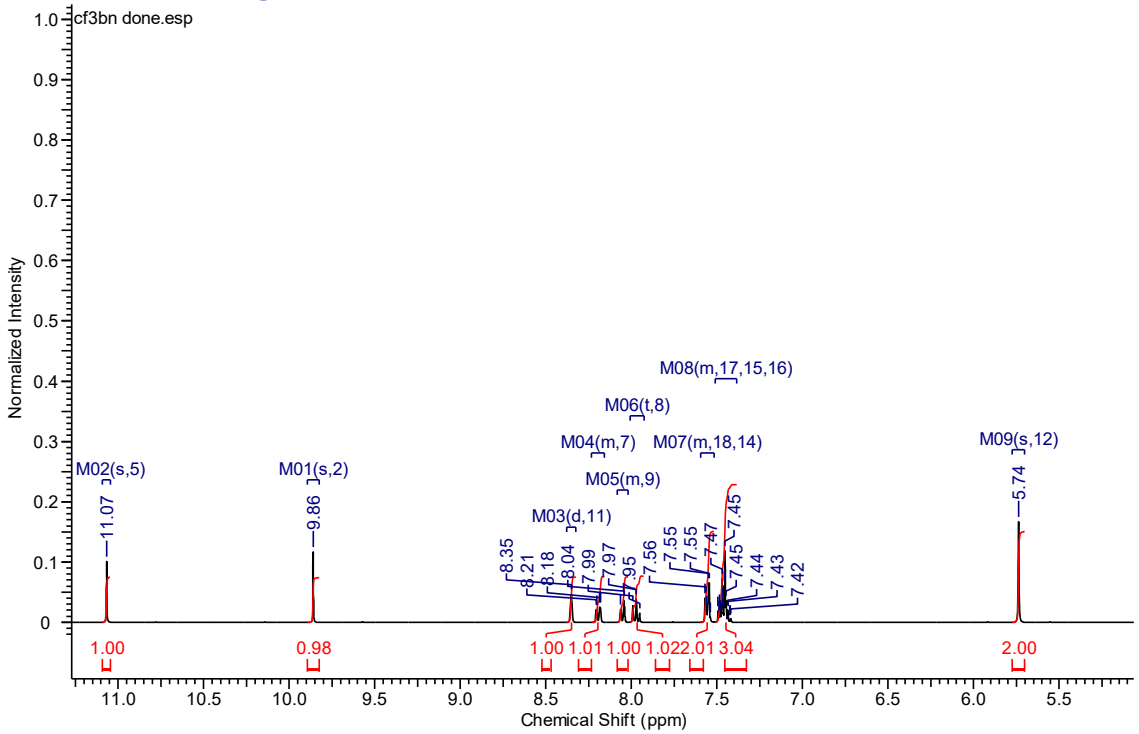

A6: ^{1}H NMR spectrum analysis for CF_3-PTz-Bn

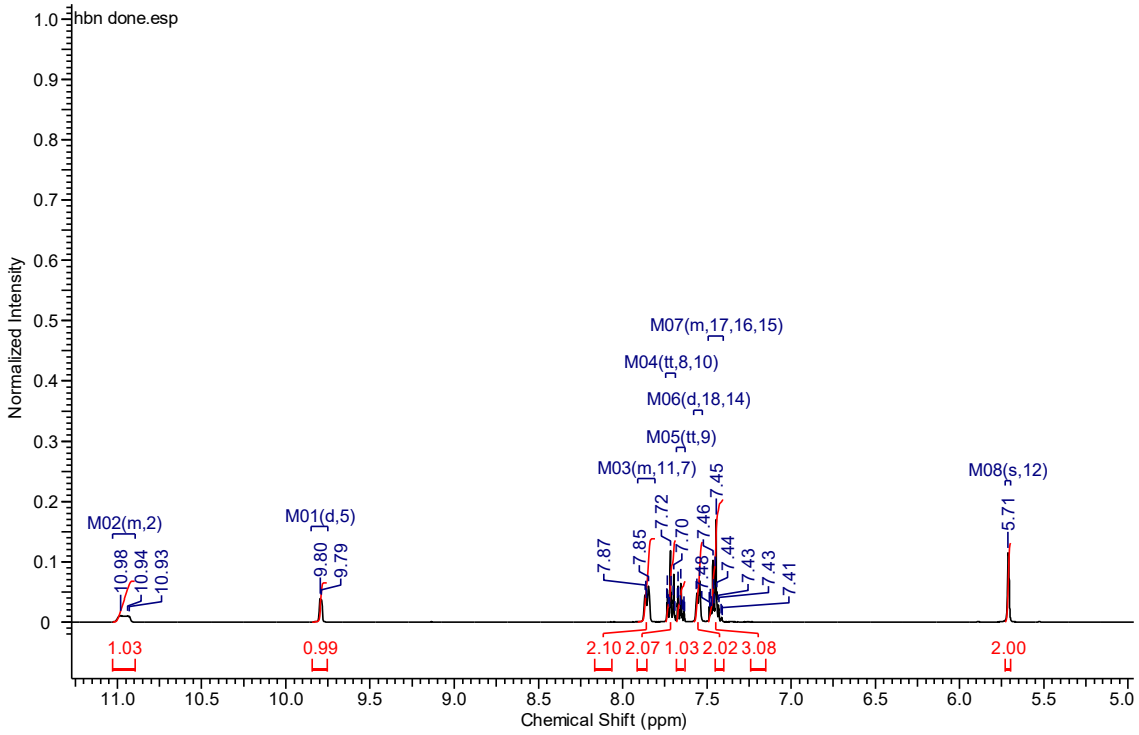

A7: ^{1}H NMR spectrum analysis for H-PTz-Bn

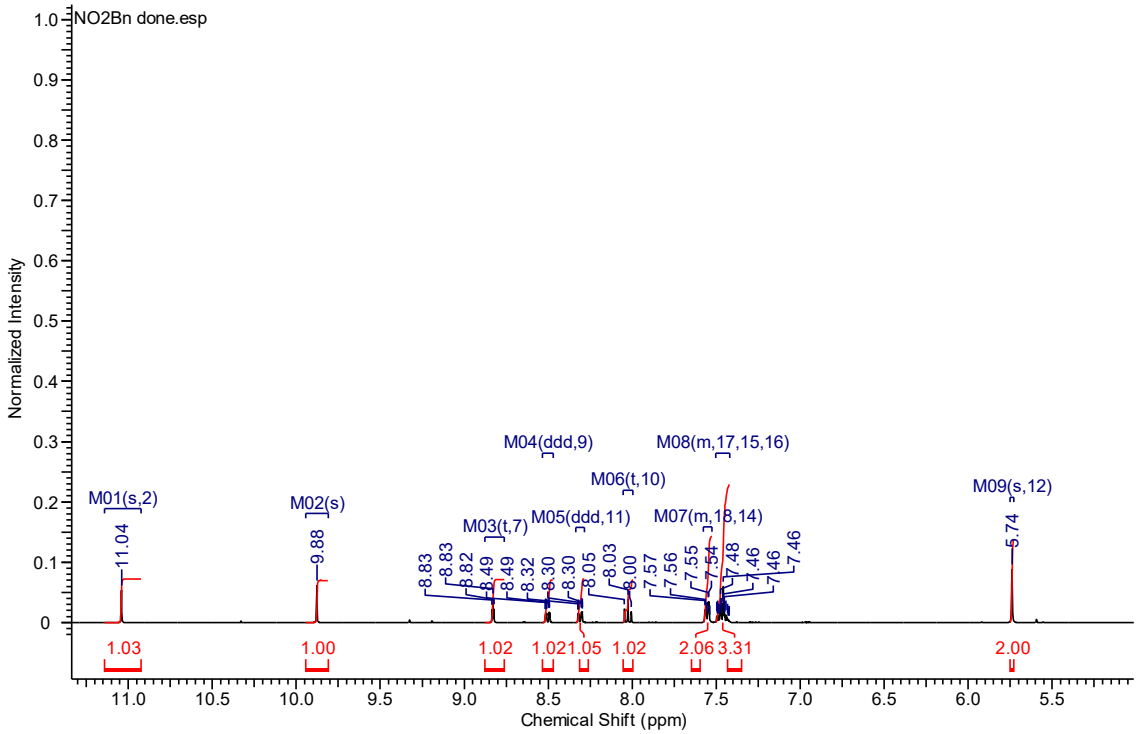

A8: ^{1}H NMR spectrum analysis for NO_2-PTz-Bn

5.4. Iridium complexes

5.4.1. *Mer* isomers

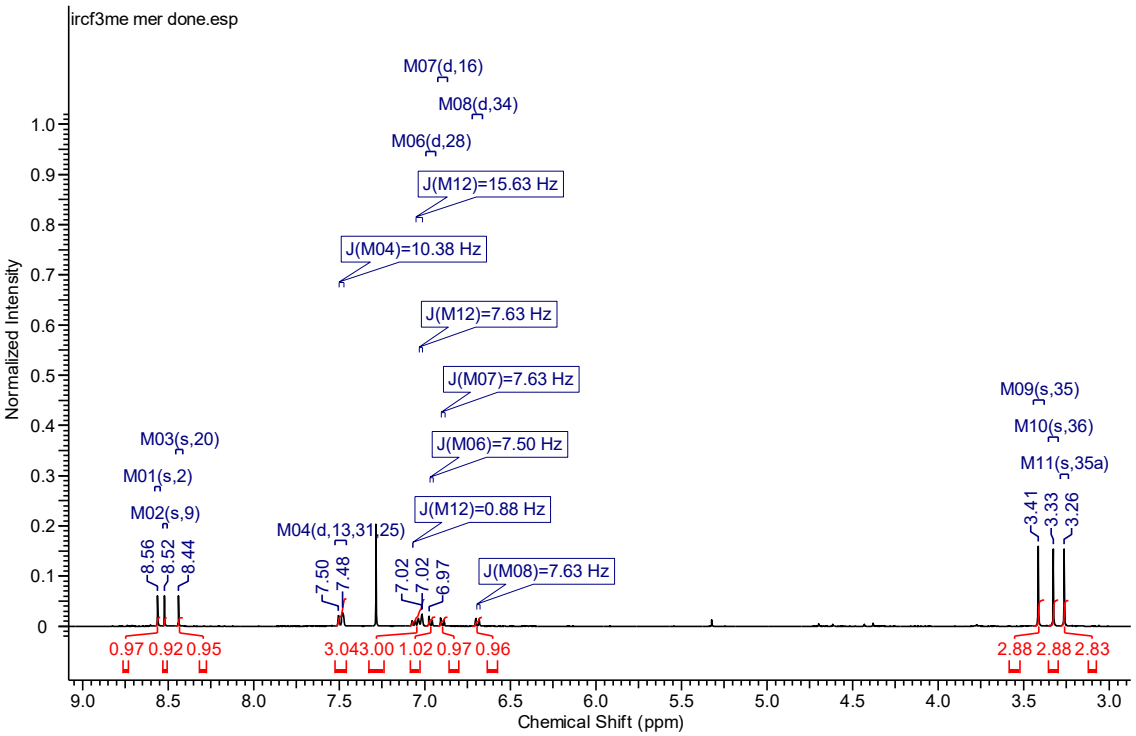

A9: ^{1}H NMR spectrum analysis for the *mer* isomer of Ir(CF_3-PTz-Me)$_3$

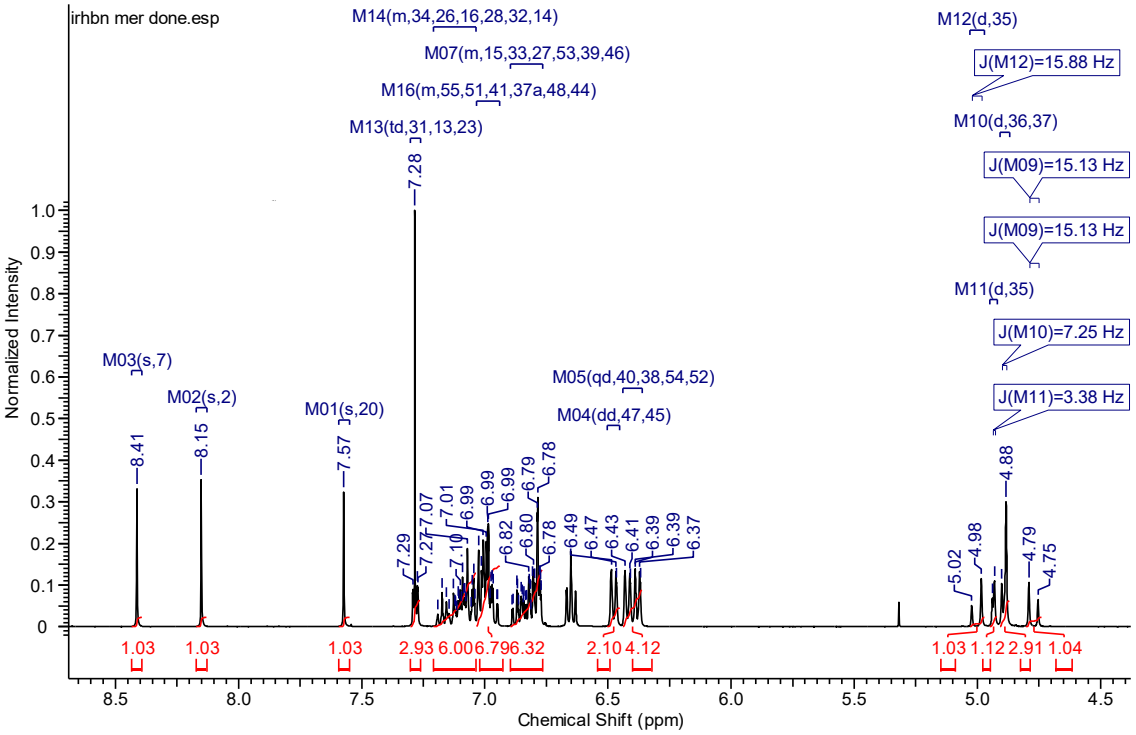

A10: ^{1}H NMR spectrum analysis for the *mer* isomer of Ir(H-PTz-Bn)$_3$

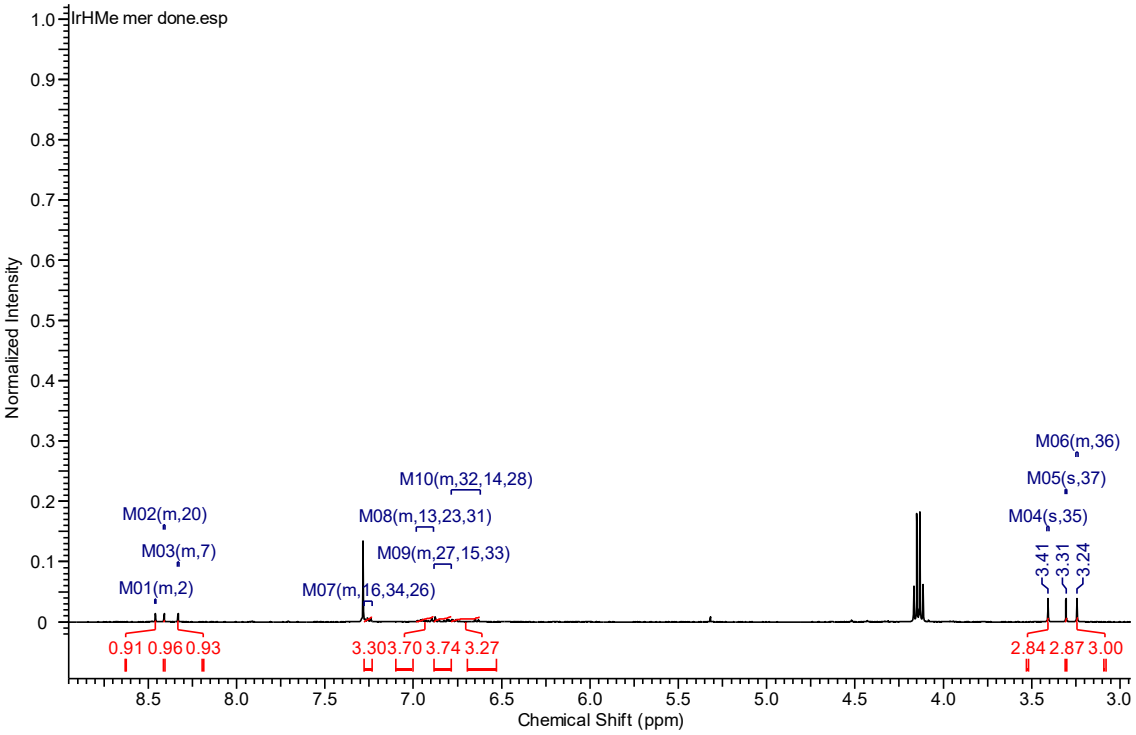

A11: ^{1}H NMR spectrum analysis for the *mer* isomer of Ir(H-PTz-Me)$_3$

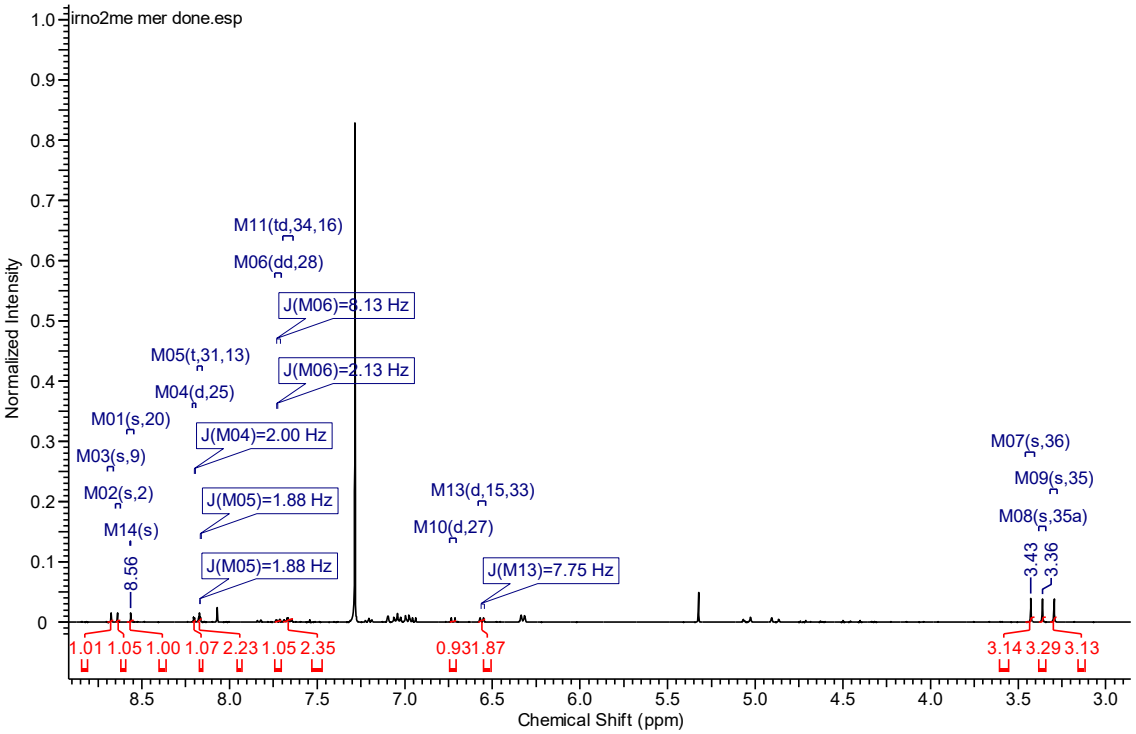

A12: ^{1}H NMR spectrum analysis for the *mer* isomer of Ir(NO_2-PTz-Me)$_3$

5.4.2. *Fac* isomers

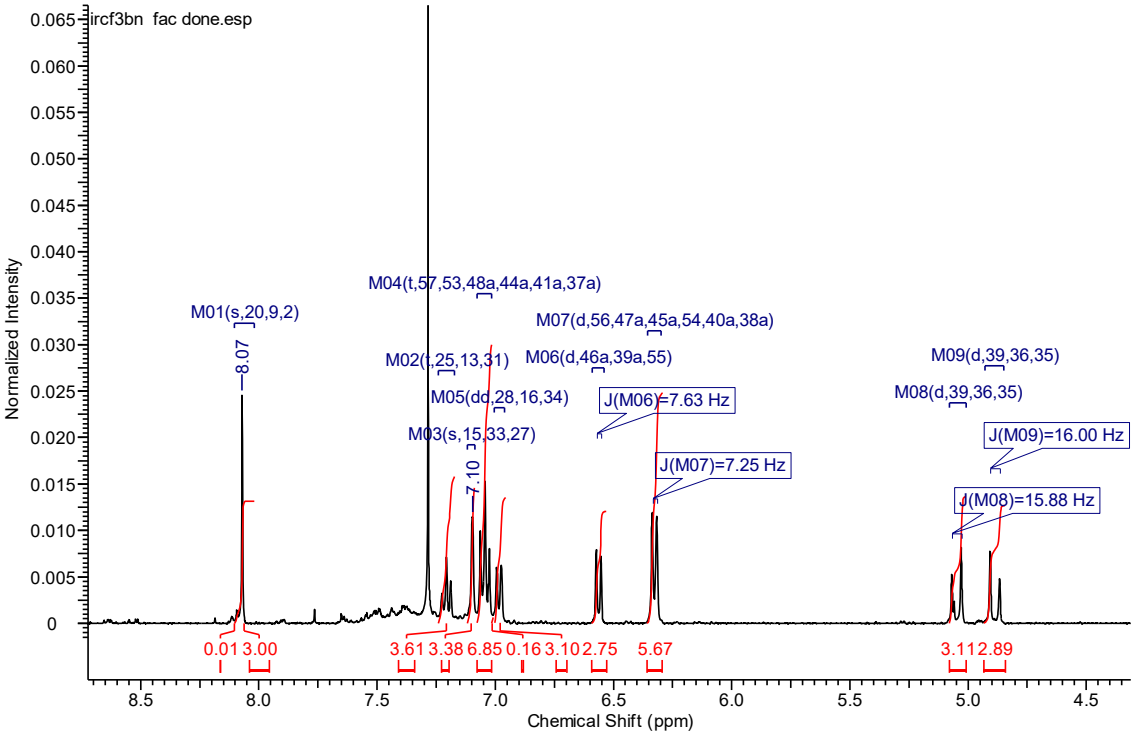

A13: ^{1}H NMR spectrum analysis for the *fac* isomer of Ir(CF_3-PTz-Bn)$_3$

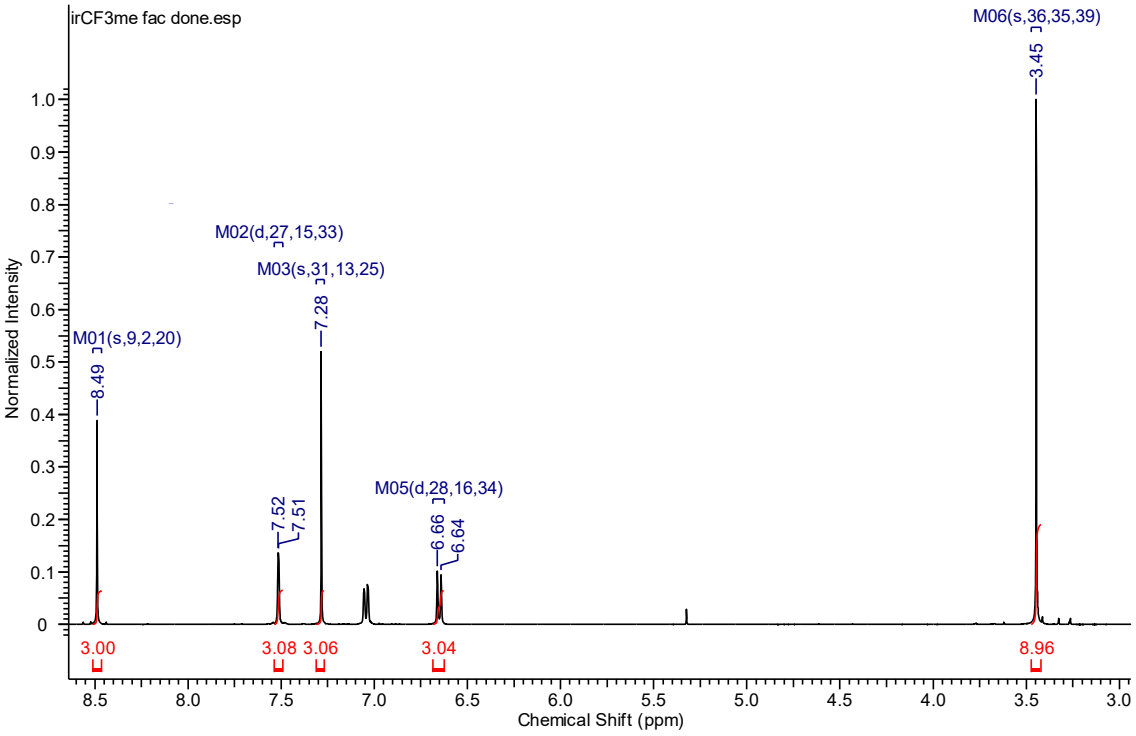

A14: ^{1}H NMR spectrum analysis for the *fac* isomer of Ir(CF_3-PTz-Me)$_3$

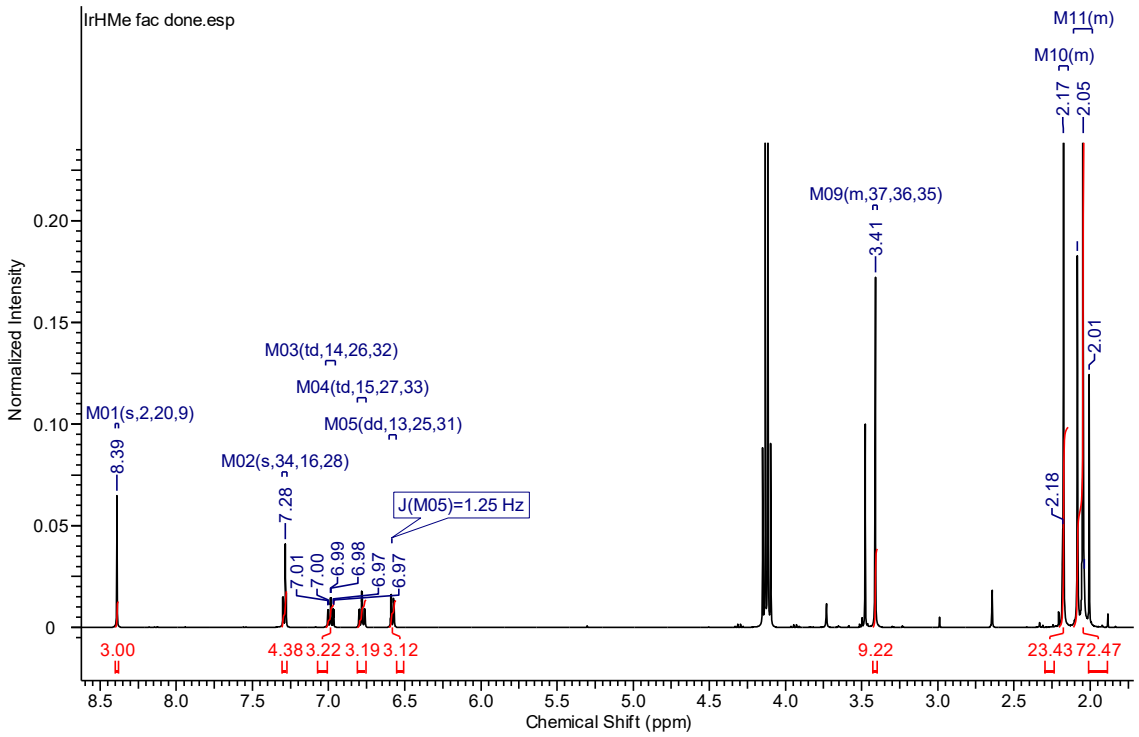

A15: ^{1}H NMR spectrum analysis for the *fac* isomer of Ir(H-PTz-Me)$_3$

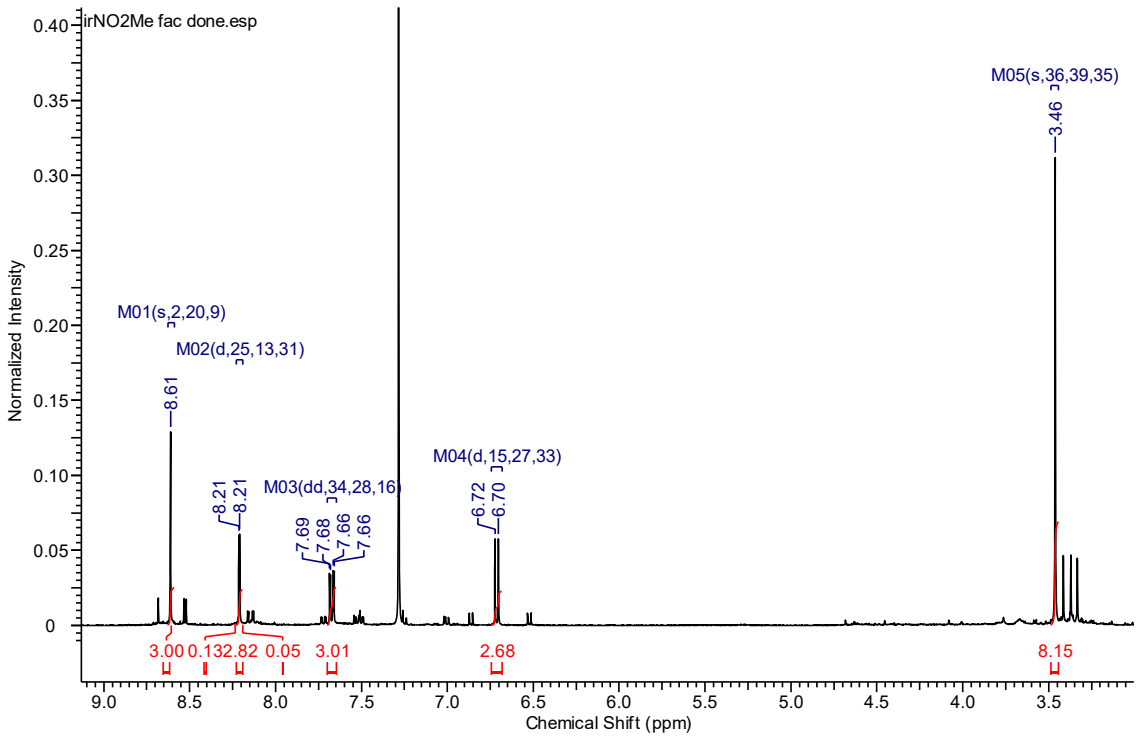

A16: ^{1}H NMR spectrum analysis for the *fac* isomer of Ir(NO$_2$-PTz-Me)$_3$

6. References

1. Q. Zhao, F. Li and C. Huang, *Chem.Soc.Rev.*, 2010, **39**, 3007-3030.
2. Y. Wu, Z. Zhao, S. Jiao, T. Song, C. Du, B. Fan, Y. Pang, H. Yuan and H. Ou, *Biomed.Technol.*, 2025, **11**, 100098.
3. Z. Ruan, J. Yang, Y. Li and K. Y. Zhang, *ChemBioChem*, 2024, **25**, e202400094.
4. S. Kappaun, C. Slugovc and E. J. W. List, *Int. J. Mol. Sci.*, 2008, **9**, 1527-1547.
5. S. Jing, X. Wu, D. Niu, J. Wang, C.-H. Leung and W. Wang, *Molecules*, 2024, **29**.
6. A. Lena, M. Marino, M. Manzano, C. Comuzzi and M. Maifreni, *Food Eng. Rev.*, 2024, **16**, 59-84.
7. M. Sarma and K.-T. Wong, *Chem. Rec.,* 2019, **19**, 1667-1692.
8. S. Schmidbauer, A. Hohenleutner and B. König, *Beilstein J. Org. Chem.*, 2013, **9**, 2088-2096.
9. E. Tankelevičiūtė, I. D. W. Samuel and E. Zysman-Colman, *J. Phys. Chem. Lett.*, 2024, **15**, 1034-1047.
10. I. Siddiqui, S. Kumar, Y.-F. Tsai, P. Gautam, Shahnawaz, K. Kesavan, J.-T. Lin, L. Khai, K.-H. Chou, A. Choudhury, S. Grigalevicius and J.-H. Jou, *Nanomaterials*, 2023, **13**, 2521.
11. A. Monkman, *ACS Applied Materials & Interfaces*, 2022, **14**, 20463-20467.
12. Y. Zhang, J. Lee and S. R. Forrest, *Nat.Commun.*, 2014, **5**, 5008.
13. M. Idris, S. C. Kapper, A. C. Tadle, T. Batagoda, D. S. Muthiah Ravinson, O. Abimbola, P. I. Djurovich, J. Kim, C. Coburn, S. R. Forrest and M. E. Thompson, *Adv. Opt. Mater.*, 2021, **9**, 2001994.
14. X. Yang, X. Zhou, Y.-X. Zhang, D. Li, C. Li, C. You, T.-C. Chou, S.-J. Su, P.-T. Chou and Y. Chi, *Adv.Sci.*, 2022, **9**, 2201150.
15. Z. Zhang, L. Sun, B. Devakumar, J. Liang, S. Wang, Q. Sun, S. J. Dhoble and X. Huang, *J.Lumin.*, 2020, **221**, 117105.
16. S. Ling, J. Liang, Y. Yan, C. Luo, S. Liao and Y. Huang, *J.Solid State Chem.*, 2022, **311**, 123099.
17. F. Lian, C. Sun, K. Xu and C. Zeng, *Org.Lett.*, 2019, **21**, 156-159.
18. Z. Li, H. Wang, Z. Su, R. Kang, T. Seto and Y. Wang, *Angew. Chem., Int. Ed.*, 2024, e202419910.
19. P. Anastas and N. Eghbali, *Chem.Soc.Rev.*, 2010, **39**, 301-312.
20. T. E. Graedel and B. K. Reck, *J.Ind.Ecol.*, 2016, **20**, 692-699.
21. J.-C. G. Bünzli and C. Piguet, *Chem.Soc.Rev.*, 2005, **34**, 1048-1077.
22. M. Srinivas, G. R. Vijayakumar, K. M. Mahadevan, H. Nagabhushana and H. S. Bhojya Naik, *J. Sci.: Adv. Mater. Devices.*, 2017, **2**, 156-164.
23. Q. Zhao, C. Huang and F. Li, *Chem.Soc.Rev.*, 2011, **40**, 2508-2524.
24. V. A. Krylova, P. I. Djurovich, M. T. Whited and M. E. Thompson, *Chem.Commun.,*2010, **46**, 6696-6698.
25. T. Moitra, P. Karak, S. Chakraborty, K. Ruud and S. Chakrabarti, *Phys. Chem. Chem. Phys.*, 2021, **23**, 59-81.
26. R. Hamze, M. Idris, D. S. Muthiah Ravinson, M. C. Jung, R. Haiges, P. I. Djurovich and M. E. Thompson, *Front.Chem.*, 2020, **8**.
27. H. Amouri, *Chem.Rev.*, 2023, **123**, 230-270.
28. S. N. T. Phan, N. B. Nguyen and T. S. Teets, *Chem.Commun.*, 2025, **61**, 17544-17558.
29. J. Jayabharathi, V. Thanikachalam and S. Thilagavathy, *Coord. Chem. Rev.*, 2023, **483**, 215100.
30. C. B. Fialho, T. F. C. Cruz, A. I. Rodrigues, M. J. Calhorda, L. F. Vieira Ferreira, P. Pander, F. B. Dias, J. Morgado, A. L. Maçanita and P. T. Gomes, *Dalton.Trans.*, 2023, **52**, 4933-4953.
31. A. R. G. Smith, P. L. Burn and B. J. Powell, *ChemPhysChem*, 2011, **12**, 2429-2438.

32. M. Stanitska, D. Volyniuk, B. Minaev, H. Agren and J. V. Grazulevicius, *J. Mater. Chem. C.*, 2024, **12**, 2662-2698.
33. P. Pander, A. V. Zaytsev, A. Sil, G. V. Baryshnikov, F. Siddique, J. A. G. Williams, F. B. Dias and V. N. Kozhevnikov, *Chem.Sci.*, 2023, **14**, 13934-13943.
34. Q. Chang, K. Zhang, C. Yan, L. Xie, Y. Yi, W. Su and W. Liu, *Molecules,* 2025, **30**, 861.
35. W. Jiang, W. Hou, C. Yan, Z. Nie, Q. Chang, X. Li and W. Liu, *Molecules,* 2024, **29**, 3183.
36. S. Lamansky, P. Djurovich, D. Murphy, F. Abdel-Razzaq, H.-E. Lee, C. Adachi, P. E. Burrows, S. R. Forrest and M. E. Thompson, *J. Am. Chem. Soc*., 2001, **123**, 4304-4312.
37. B. Liu, M. A. Jabed, J. Guo, W. Xu, S. L. Brown, A. Ugrinov, E. K. Hobbie, S. Kilina, A. Qin and W. Sun, *Inorg.Chem.*, 2019, **58**, 14377-14388.
38. B. D. Stringer, L. M. Quan, P. J. Barnard, D. J. D. Wilson and C. F. Hogan, *Organometallics*, 2014, **33**, 4860-4872.
39. A. Haque, L. Xu, R. A. Al-Balushi, M. K. Al-Suti, R. Ilmi, Z. Guo, M. S. Khan, W.-Y. Wong and P. R. Raithby, *Chem.Soc.Rev.*, 2019, **48**, 5547-5563.
40. C. Cebrián and M. Mauro, *Beilstein J. Org. Chem.*, 2018, **14**, 1459-1481.
41. M. Ibrahim-Ouali and F. Dumur, *Molecules*, 2019, **24**, 1412.
42. C. E. Housecroft and E. C. Constable, *Coord. Chem. Rev.*, 2017, **350**, 155-177.
43. Z. Liu, S.-W. Zhang, M. Zhang, C. Wu, W. Li, Y. Wu, C. Yang, F. Kang, H. Meng and G. Wei, *Front.Chem.*, 2021, **Volume 9 - 2021**.
44. T.-Y. Li, J. Wu, Z.-G. Wu, Y.-X. Zheng, J.-L. Zuo and Y. Pan, *Coord. Chem. Rev.*, 2018, **374**, 55-92.
45. A. R. McDonald, M. Lutz, L. S. von Chrzanowski, G. P. M. van Klink, A. L. Spek and G. van Koten, *Inorg.Chem.*, 2008, **47**, 6681-6691.
46. P. Jolliet, M. Gianini, A. von Zelewsky, G. Bernardinelli and H. Stoeckli-Evans, *Inorg.Chem.*, 1996, **35**, 4883-4888.
47. D. Dalmau and E. P. Urriolabeitia, *Molecules*, 2023, **28**, 2663.
48. Y. Zhang and J. Qiao, *iScience*, 2021, **24**, 102858.
49. J. Föller, D. H. Friese, S. Riese, J. M. Kaminski, S. Metz, D. Schmidt, F. Würthner, C. Lambert and C. M. Marian, *Phys. Chem. Chem. Phys.*, 2020, **22**, 3217-3233.
50. P. Pander, R. Daniels, A. V. Zaytsev, A. Horn, A. Sil, T. J. Penfold, J. A. G. Williams, V. N. Kozhevnikov and F. B. Dias, *Chem.Sci.*, 2021, **12**, 6172-6180.
51. T. Sajoto, P. I. Djurovich, A. Tamayo, M. Yousufuddin, R. Bau, M. E. Thompson, R. J. Holmes and S. R. Forrest, *Inorg.Chem.*, 2005, **44**, 7992-8003.
52. J. Li, P. I. Djurovich, B. D. Alleyne, M. Yousufuddin, N. N. Ho, J. C. Thomas, J. C. Peters, R. Bau and M. E. Thompson, *Inorg.Chem.*, 2005, **44**, 1713-1727.
53. A. Sebris, M. Guzauskas, M. Mahmoudi, D. Volyniuk, J. V. Grazulevicius, A. Mishnev, I. Novosjolova, M. Turks, G. Jonusauskas and K. Traskovskis, *J. Mater. Chem. C.*, 2023, **11**, 14608-14620.
54. Z.-l. Z. Hsin-Hung Kuo, Chun-Sing Lee, Yi-Kuang Chen, Shih-Hung Liu, Pi-Tai Chou, Alex K.-Y. Jen, and Yun Chi, *Adv. Sci.*, 2018, **5**, 1-7.
55. Z. Z. Jibiao Jin, Jie Yan, Xiuwen Zhou, Chen Cao, Pi-Tai Chou, Ye-Xin Zhang, Zhong Zheng, Chun-Sing Lee, and Yun Chi, *Adv. Photonics Res.*, 2022, **3**, 1-11.
56. A. B. Tamayo, B. D. Alleyne, P. I. Djurovich, S. Lamansky, I. Tsyba, N. N. Ho, R. Bau and M. E. Thompson, *J. Am. Chem. Soc.*, 2003, **125**, 7377-7387.
57. Y. Lan, D. Liu, J. Li, Y. Mei and H. Tian, *J. Mater. Chem. C.*, 2022, **10**, 17965-17973.
58. H. Li, L. Huang, Z. Huang, L. Zhang, Y. Tang, X. Wang, Y. He and Z. Liu, *Phys. Chem. Chem. Phys.*, 2022, **24**, 9543-9550.
59. H. W. Ham and Y. S. Kim, *Mol. Cryst. Liq. Cryst.*, 2010, **520**, 97/[373]-107/[383].
60. S.-C. Lo, R. E. Harding, C. P. Shipley, S. G. Stevenson, P. L. Burn and I. D. W. Samuel, *J. Am. Chem. Soc.*, 2009, **131**, 16681-16688.
61. M. A. Baldo, C. Adachi and S. R. Forrest, *Phys.Rev. B*, 2000, **62**, 10967-10977.

62. S. B. Meier, W. Sarfert, J. M. Junquera-Hernández, M. Delgado, D. Tordera, E. Ortí, H. J. Bolink, F. Kessler, R. Scopelliti, M. Grätzel, M. K. Nazeeruddin and E. Baranoff, *J. Mater. Chem. C.*, 2013, **1**, 58-68.
63. C. Yang, F. Mehmood, T. L. Lam, S. L.-F. Chan, Y. Wu, C.-S. Yeung, X. Guan, K. Li, C. Y.-S. Chung, C.-Y. Zhou, T. Zou and C.-M. Che, *Chem.Sci.*, 2016, **7**, 3123-3136.
64. L. A. Büldt and O. S. Wenger, *Chem.Sci.*, 2017, **8**, 7359-7367.
65. F. Reichenauer, C. Wang, C. Förster, P. Boden, N. Ugur, R. Báez-Cruz, J. Kalmbach, L. M. Carrella, E. Rentschler, C. Ramanan, G. Niedner-Schatteburg, M. Gerhards, M. Seitz, U. Resch-Genger and K. Heinze, *J. Am. Chem. Soc.*, 2021, **143**, 11843-11855.
66. S. Yoon and T. S. Teets, *Chem.Commun.*, 2021, **57**, 1975-1988.
67. M. J. Walter and J. M. Lupton, in *Highly Efficient OLEDs with Phosphorescent Materials*, 2007, DOI: https://doi.org/10.1002/9783527621309.ch2, pp. 99-129.
68. G. Shao, H. Yu, N. Zhang, Y. He, K. Feng, X. Yang, R. Cao and M. Gong, *Phys. Chem. Chem. Phys.*, 2014, **16**, 695-702.
69. I. Ayoub, U. Mushtaq, K. Verma, V. Sharma, H. C. Swart and V. Kumar, *Next Mater.*, 2025, **9**, 101177.
70. T. Guner, A. Kus, M. Ozcan, A. Genc, H. Sahin and M. M. Demir, *Beilstein J.Nanotechnol.*, 2019, **10**, 1200-1210.
71. V. T. Jayaraman Jayabharathi, Shanmugam Thilagavathy, *Coord. Chem. Rev.*, 2023, **483**, 1-65.
72. W. R. Kitzmann and K. Heinze, *Angew. Chem., Int. Ed.*, 2023, **62**, e202213207.
73. P. L. dos Santos, P. Stachelek, Y. Takeda and P. Pander, *Mater.Chem.Front.*, 2024, **8**, 1731-1766.
74. K. L. Smitten, P. A. Scattergood, C. Kiker, J. A. Thomas and P. I. P. Elliott, *Chem.Sci.*, 2020, **11**, 8928-8935.
75. J.-L. Liao, Y. Chi, C.-C. Yeh, H.-C. Kao, C.-H. Chang, M. A. Fox, P. J. Low and G.-H. Lee, *J. Mater. Chem. C.*, 2015, **3**, 4910-4920.
76. W. Li, A. Wu, T. Fu, X. Gao, Y. Wang, D. Xu, C. Zhang, Z. Sun, Y. Lu, D. J. Young, H. Li and X.-C. Hang, *J. Phys. Chem. Lett.*, 2022, **13**, 1494-1499.
77. Y. Zhang, D. Zhang, T. Huang, A. J. Gillett, Y. Liu, D. Hu, L. Cui, Z. Bin, G. Li, J. Wei and L. Duan, *Angew. Chem., Int. Ed.*, 2021, **60**, 20498-20503.
78. D. Escudero, *Chem.Sci.*, 2016, **7**, 1262-1267.
79. X. Zhou and B. J. Powell, *Phys. Chem. Chem. Phys.*, 2020, **22**, 27348-27356.
80. X.-y. Wang, A. Del Guerzo and R. H. Schmehl, *J. Photochem. Photobiol., C* , 2004, **5**, 55-77.
81. G.-J. Kang, Y.-F. Wu, X.-F. Ren, J.-Q. Mei, S.-J. Lu and X. Zeng, *Phys. Chem. Chem. Phys.*, 2024, **26**, 23910-23919.
82. F. Monti, A. Baschieri, L. Sambri and N. Armaroli, *Acc.Chem.Res.*, 2021, **54**, 1492-1505.
83. M. Pompei, F. Monti, L. Sambri, N. Armaroli and A. Baschieri, *Dalton.Trans.*, 2025, **54**, 1633-1645.
84. Q. Sun, S. Mosquera-Vazquez, Y. Suffren, J. Hankache, N. Amstutz, L. M. Lawson Daku, E. Vauthey and A. Hauser, *Coord. Chem. Rev.*, 2015, **282-283**, 87-99.
85. J. Moll, C. Wang, A. Päpcke, C. Förster, U. Resch-Genger, S. Lochbrunner and K. Heinze, *Chem.–Eur. J.* , 2020, **26**, 6820-6832.
86. C. Kreitner and K. Heinze, *Dalton.Trans.,* 2016, **45**, 13631-13647.
87. Y. Wei, H. Yang, Z. Gao, Y. Liu, G. Xing, P. Dang, A. A. A. Kheraif, G. Li, J. Lin and R.-S. Liu, *Adv.Sci.*, 2020, **7**, 1903060.
88. S. M. Borisov, A. Alemayehu and A. Ghosh, *J. Mater. Chem. C.*, 2016, **4**, 5822-5828.
89. J. A. Roque, P. C. Barrett, H. D. Cole, Liubov M. Lifshits, G. Shi, S. Monro, D. von Dohlen, S. Kim, N. Russo, G. Deep, C. G. Cameron, M. E. Alberto and S. A. McFarland, *Chem.Sci.*, 2020, **11**, 9784-9806.
90. L. Zhang, Y. Xu, X. Wu, S. Yin and H. You, *Mater.Adv.*, 2022, **3**, 2591-2597.

91. F. Chen, M. N. Akram and X. Chen, *Molecules*, 2023, **28**, 4624.
92. J. Liang, L. Sun, G. Annadurai, B. Devakumar, S. Wang, Q. Sun, J. Qiao, H. Guo, B. Li and X. Huang, *RSC Adv.*, 2018, **8**, 32111-32118.
93. J. Ming, C. Luo, S. Ling, C. Chen, Y. Wang, S. Liao, Y. Huang and J. Liang, *RSC Adv.*, 2022, **12**, 31546-31554.
94. R.-J. Xie, N. Hirosaki, Y. Li and T. Takeda, *J. Mater. Chem.*, 2010, **3**, 3777-3793.
95. S. Otto, M. Grabolle, C. Förster, C. Kreitner, U. Resch-Genger and K. Heinze, *Angew. Chem., Int. Ed.*, 2015, **54**, 11572-11576.
96. S. Otto, M. Dorn, C. Förster, M. Bauer, M. Seitz and K. Heinze, *Coord. Chem. Rev.*, 2018, **359**, 102-111.
97. S. Otto, C. Förster, C. Wang, U. Resch-Genger and K. Heinze, *Chem.–Eur. J.*, 2018, **24**, 12555-12563.
98. J.-R. Jiménez, B. Doistau, M. Poncet and C. Piguet, *Coord. Chem. Rev.*, 2021, **434**, 213750.
99. P. Boden, P. Di Martino-Fumo, G. Niedner-Schatteburg, W. Seidel, K. Heinze and M. Gerhards, *Phys. Chem. Chem. Phys.*, 2021, **23**, 13808-13818.
100. A. D. Kirk and G. B. Porter, *J. Phys. Chem.*, 1980, **84**, 887-891.
101. W. R. Kitzmann, J. Moll and K. Heinze, *Photochem. Photobiol. Sci.*, 2022, **21**, 1309-1331.
102. F. Reichenauer, R. Naumann, C. Förster, W. R. Kitzmann, A.-P. M. Reponen, S. Feldmann and K. Heinze, *Chem.Sci.*, 2024, **15**, 20251-20262.
103. Y. Ye, M. Poncet, P. Yaltseva, P. Salcedo-Abraira, A. Rodríguez-Diéguez, J. H. Martín, L. Cuevas-Contreras, C. M. Cruz, B. Doistau, C. Piguet, O. S. Wenger, J. M. Herrera and J.-R. Jiménez, *Chem.Sci.*, 2025, **16**, 5205-5213.
104. S. Treiling, C. Wang, C. Förster, F. Reichenauer, J. Kalmbach, P. Boden, J. P. Harris, L. M. Carrella, E. Rentschler, U. Resch-Genger, C. Reber, M. Seitz, M. Gerhards and K. Heinze, *Angew. Chem., Int. Ed.*, 2019, **58**, 18075-18085.
105. J. P. Zobel, H. Radatz and L. González, *Molecules*, 2023, **28**, 1668.
106. J. Chong, C. Besnard, C. M. Cruz, C. Piguet and J.-R. Jiménez, *Dalton.Trans.*, 2022, **51**, 4297-4309.
107. J.-R. Jiménez, B. Doistau, C. Besnard and C. Piguet, *Chem.Commun.*, 2018, **54**, 13228-13231.
108. B. Doistau, G. Collet, E. A. Bolomey, V. Sadat-Noorbakhsh, C. Besnard and C. Piguet, *Inorg.Chem.*, 2018, **57**, 14362-14373.
109. B. Doistau, J.-R. Jiménez, S. Guerra, C. Besnard and C. Piguet, *Inorg.Chem.*, 2020, **59**, 1424-1435.
110. B. Doistau, J.-R. Jiménez, L. M. Lawson Daku and C. Piguet, *Inorg.Chem.*, 2022, **61**, 11023-11031.
111. K. Hasan, A. K. Bansal, I. D. W. Samuel, C. Roldán-Carmona, H. J. Bolink and E. Zysman-Colman, *Sci.Rep.*, 2015, **5**, 12325.
112. J.-R. Jiménez, M. Poncet, S. Míguez-Lago, S. Grass, J. Lacour, C. Besnard, J. M. Cuerva, A. G. Campaña and C. Piguet, *Angew. Chem., Int. Ed.*, 2021, **60**, 10095-10102.
113. S. Trippmacher, S. Demeshko, A. Prescimone, F. Meyer, O. S. Wenger and C. Wang, *Chem.–Eur. J.*, 2024, **30**, e202400856.
114. C. Wang, W. R. Kitzmann, F. Weigert, C. Förster, X. Wang, K. Heinze and U. Resch-Genger, *ChemPhotoChem*, 2022, **6**, e202100296.
115. N. Ghodrati, S. Eckert, M. Fondell, A. Scherz, A. Föhlisch and B. E. Van Kuiken, *Chem.Sci.*, 2025, **16**, 6307-6316.
116. M. D. Böhme, T. Eder, M. B. Röthel, P. D. Dutschke, L. F. B. Wilm, F. E. Hahn and F. Dielmann, *Angew. Chem., Int. Ed.*, 2022, **61**, e202202190.
117. P. Mathew, A. Neels and M. Albrecht, *J. Am. Chem. Soc.*, 2008, **130**, 13534-13535.
118. T. Tsubomura, H. Murota and K. Takao, *Inorg.Chem.Commun.*, 2013, **35**, 110-112.

119. D. M. n. E. Marcel Brill, Frank Rominger, Peter Hofmann, *J.Organomet.Chem.*, 2015, **775**, 137-151.
120. W. A. Herrmann and C. Köcher, *Angew. Chem., Int. Ed.*, 1997, **36**, 2162-2187.
121. W. A. Herrmann, *Angew. Chem., Int. Ed.*, 2002, **41**, 1290-1309.
122. S. Díez-González, N. Marion and S. P. Nolan, *Chem.Rev.*, 2009, **109**, 3612-3676.
123. D. Bourissou, O. Guerret, F. P. Gabbaï and G. Bertrand, *Chem.Rev.*, 2000, **100**, 39-92.
124. C. F. R. Mackenzie, L. Zhang, D. B. Cordes, A. M. Z. Slawin, I. D. W. Samuel and E. Zysman-Colman, *Adv. Opt. Mater.*, 2023, **11**, 2201495.
125. H. Na, Louise M. Cañada, Z. Wen, J. I-Chia Wu and T. S. Teets, *Chem.Sci.*, 2019, **10**, 6254-6260.
126. S. Leuthäußer, D. Schwarz and H. Plenio, *Chem.–Eur. J.*, 2007, **13**, 7195-7203.
127. P. L. Arnold and S. Pearson, *Coord. Chem. Rev.*, 2007, **251**, 596-609.
128. J. G. Osiak, T. Setzer, P. G. Jones, C. Lennartz, A. Dreuw, W. Kowalsky and H.-H. Johannes, *Chem.Commun.*, 2017, **53**, 3295-3298.
129. K. A. McGee and K. R. Mann, *Inorg.Chem.*, 2007, **46**, 7800-7809.
130. M. K. Denk, A. Thadani, K. Hatano and A. J. Lough, *Angew. Chem., Int. Ed.*, 1997, **36**, 2607-2609.
131. M. A. Kinzhalov, E. V. Grachova and K. V. Luzyanin, *Inorg. Chem. Front.*, 2022, **9**, 417-439.
132. C. Wu, Y. Wu, K.-N. Tong, M. Kuhn, S.-M. Yiu, Y.-C. Kung, W.-Y. Hung, J. Yan, X. Zhou, G. Wei and Y. Chi, *J. Mater. Chem. C.*, 2025, **13**, 12663-12674.
133. A. Y. Gitlina, F. Fadaei-Tirani and K. Severin, *Dalton.Trans.,* 2023, **52**, 2833-2837.
134. H. G. O. Becker, G. Hoffmann, K. M. Gwan and L. Knüpfer, *J.Prakt.Chem.*, 1988, **330**, 325-337.
135. N. Singh, G. H. Noh, H. Mubarok, C. W. Kim, M. H. Lee and J. Lee, *Polyhedron*, 2022, **227**, 116096.
136. R. H. Wiley and A. J. Hart, *J.Org.Chem.*, 1953, **18**, 1368-1371.
137. *United States Pat.,* 3647810, 1972.
138. R. Visbal and M. C. Gimeno, *Chem.Soc.Rev.*, 2014, **43**, 3551-3574.
139. F. Hao and N. Nishiwaki, *Molecules*, 2020, **25**, 673.
140. M.-C. Chen, D.-G. Chen and P.-T. Chou, *ChemPlusChem*, 2021, **86**, 11-27.
141. Y. Chi and P.-T. Chou, *Chem.Soc.Rev.*, 2010, **39**, 638-655.
142. A. K. Pal, A. F. Henwood, D. B. Cordes, A. M. Z. Slawin, I. D. W. Samuel and E. Zysman-Colman, *Inorg.Chem.*, 2017, **56**, 7533-7544.
143. X. Shang, D. Han, M. Liu and G. Zhang, *RSC Adv.*, 2017, **7**, 5055-5062.
144. A. F. Henwood, A. K. Bansal, D. B. Cordes, A. M. Z. Slawin, I. D. W. Samuel and E. Zysman-Colman, *J. Mater. Chem. C.*, 2016, **4**, 3726-3737.
145. L. Kearney, M. P. Brandon, A. Coleman, A. M. Chippindale, F. Hartl, R. Lalrempuia, M. Pižl and M. T. Pryce, *Molecules*, 2023, **28**, 4149.
146. R. Liu, K. Zhu, X. Zhong, J. Li, Z. Liu, S. Chen and H. Zhu, *Dalton.Trans.,* 2016, **45**, 17020-17029.
147. D. G. Lee, J. W. Baek, J. H. Lee, H. J. Lee, Y. H. Seo, J. Lee, C. G. Lee and B. Y. Lee, *Molecules*, 2021, **26**, 1167.
148. J. Y. Jeon, J. H. Park, D. S. Park, S. Y. Park, C. S. Lee, M. J. Go, J. Lee and B. Y. Lee, *Inorg.Chem.Commun.*, 2014, **44**, 148-150.
149. W. Herwig and H. Zeiss, *J.Org.Chem.*, 1958, **23**, 1404-1404.
150. G. Zanchin, A. Amodio, A. Piovano, V. Guiotto, G. Leone, L. Falivene and E. Groppo, *Organometallics*, 2024, **43**, 2537-2547.
151. O. V. Dolomanov, L. J. Bourhis, R. J. Gildea, J. A. K. Howard and H. Puschmann, *J.Appl.Crystallogr.*, 2009, **42**, 339-341.
152. G. Sheldrick, *Acta Crystallographica Section A*, 2015, **71**, 3-8.
153. G. Sheldrick, *Acta Crystallographica Section C*, 2015, **71**, 3-8.

7. Supplemental Data

7.1. UV/Vis and Emission Spectra

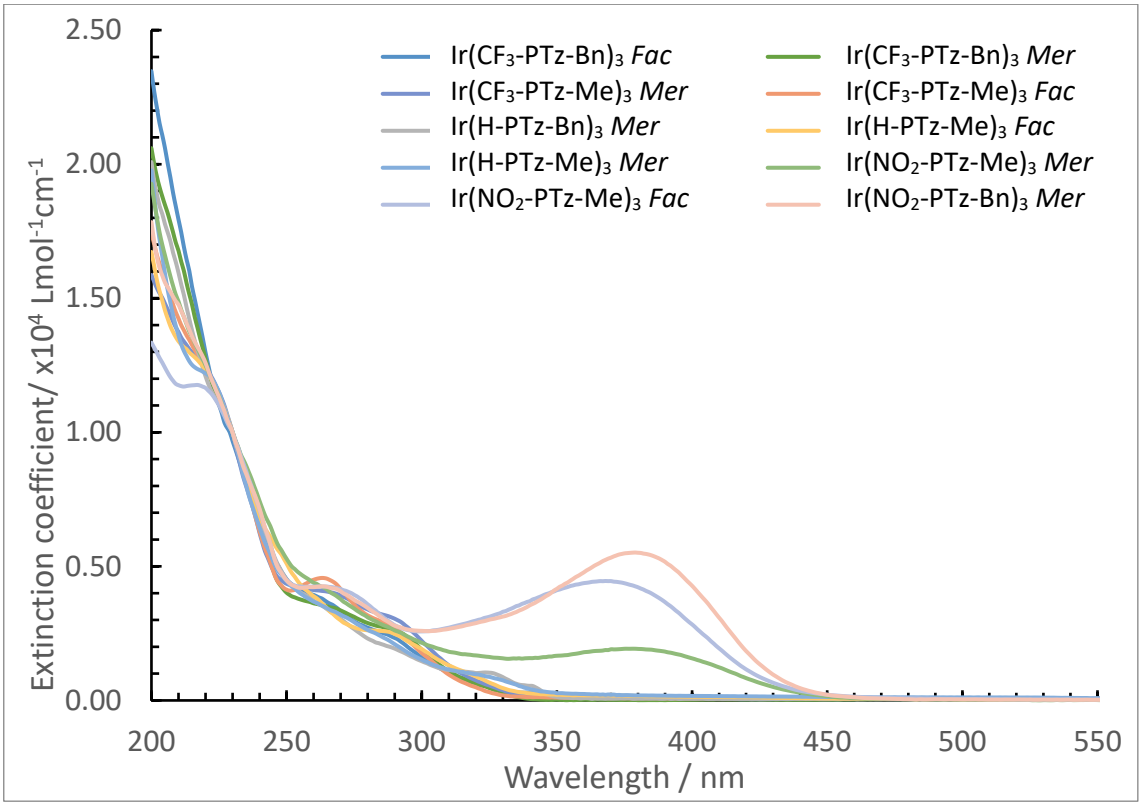

Figure S1: The UV/Vis absorption spectra of the isolated Ir(III) complexes.

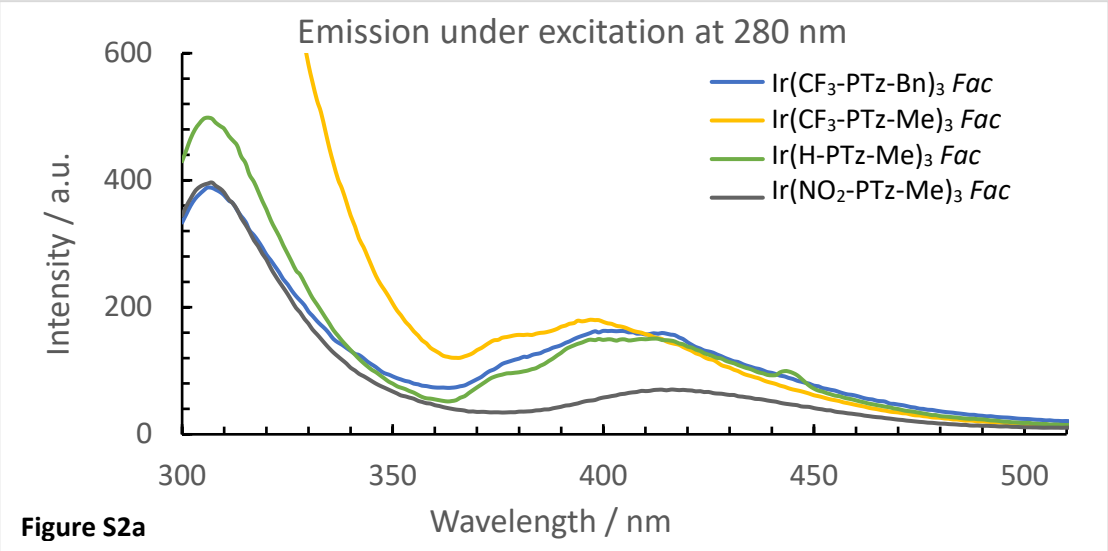

Figure S2a

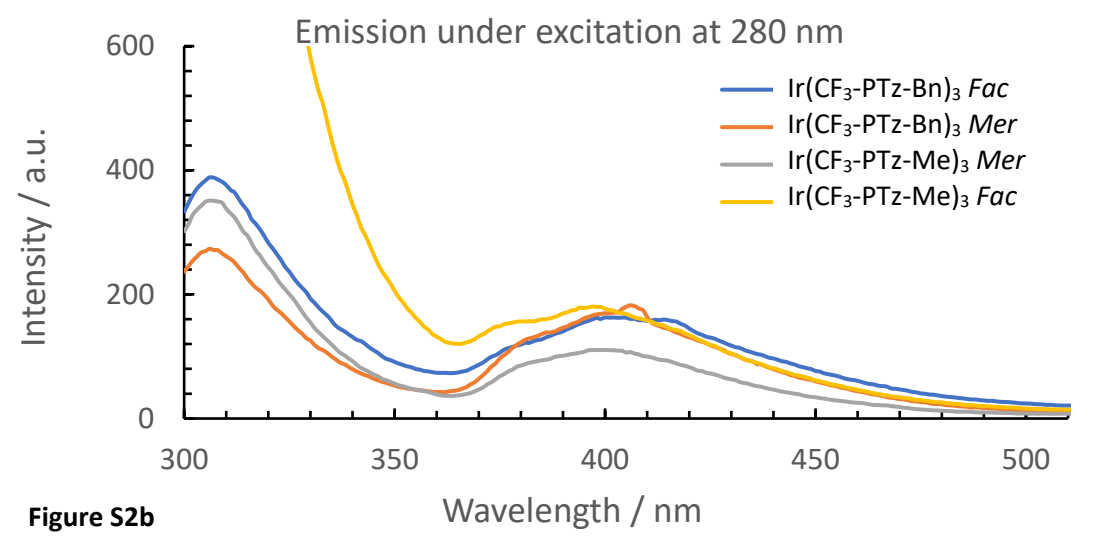

Figure S2b

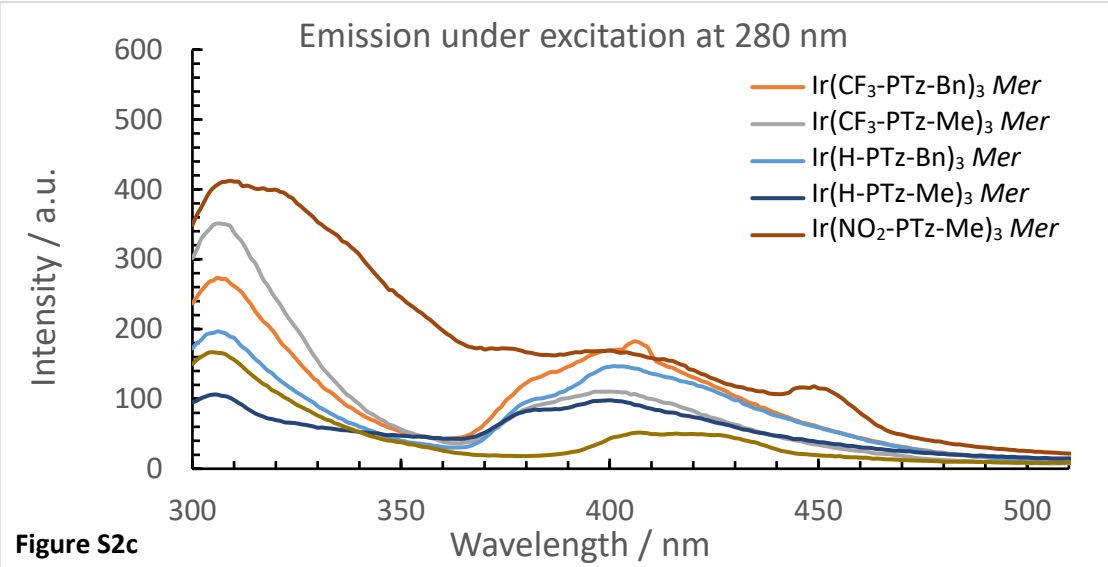

Figure S2c

Figure S2a-c: The emission spectra of the isolated *mer/fac* Ir(III) complexes recorded in a MeCN solution exciting at 280nm, split into spectra a-c for ease of comparison. Sample concentrations were adjusted to give absorbance values of 0.1 prior to measurement

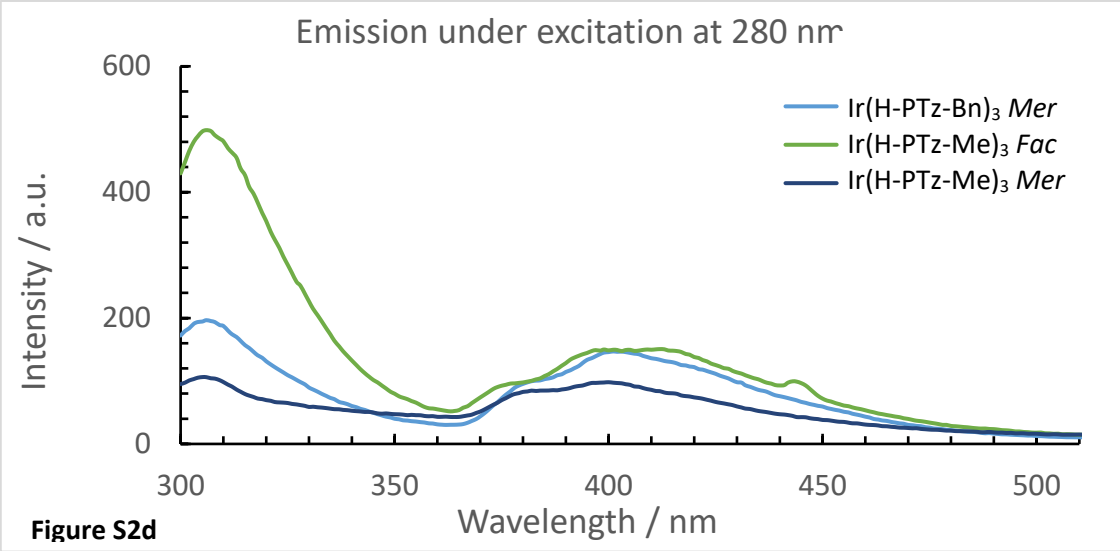

Figure S2d

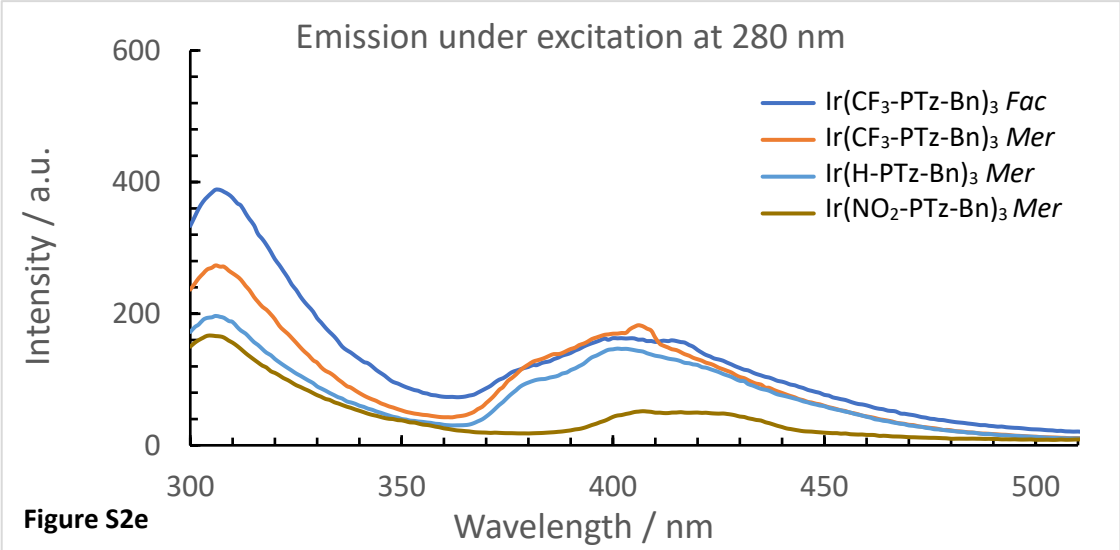

Figure S2e

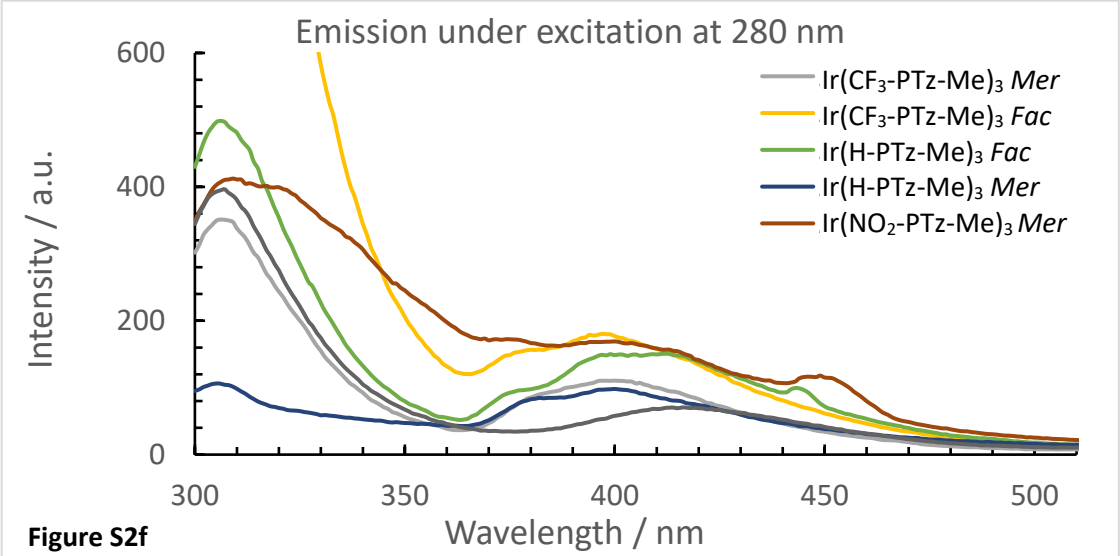

Figure S2f

Figure S2d-f: The emission spectra of the isolated *mer/fac* Ir(III) complexes recorded in a MeCN solution exciting at 280nm, split into spectra d-f for ease of comparison. Sample concentrations were adjusted to give absorbance values of 0.1 prior to measurement

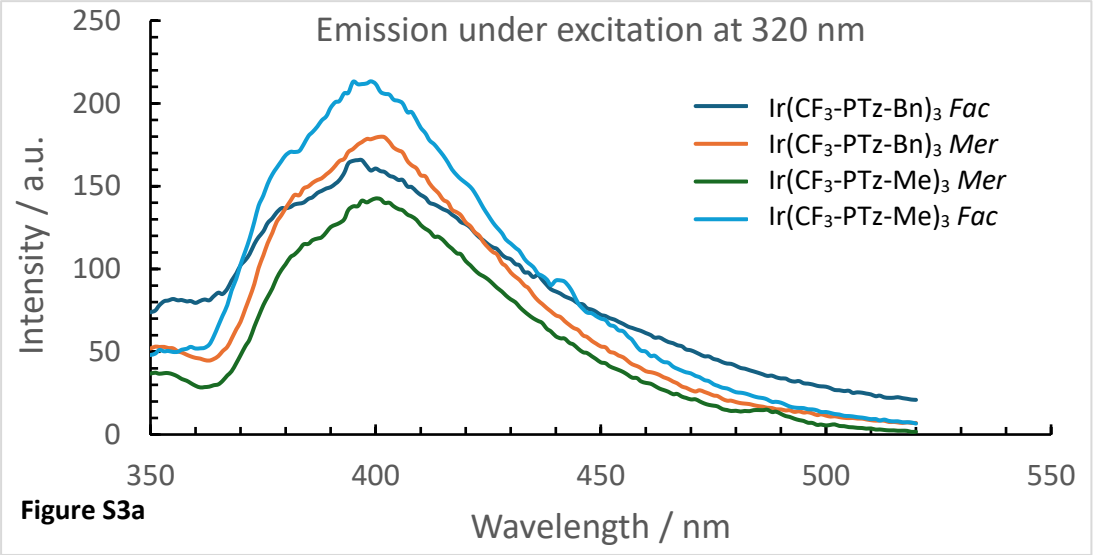

Figure S3a

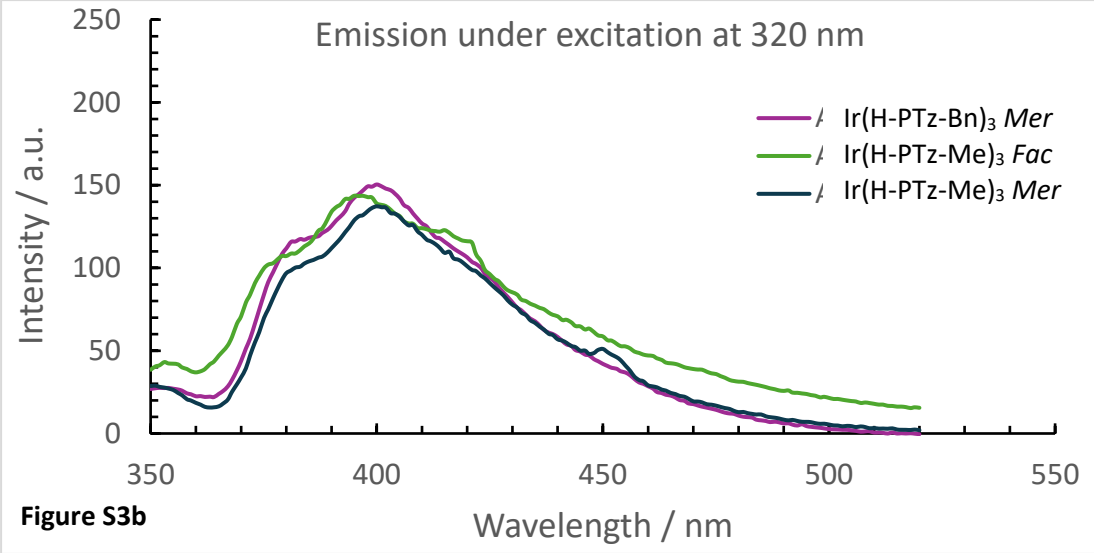

Figure S3b

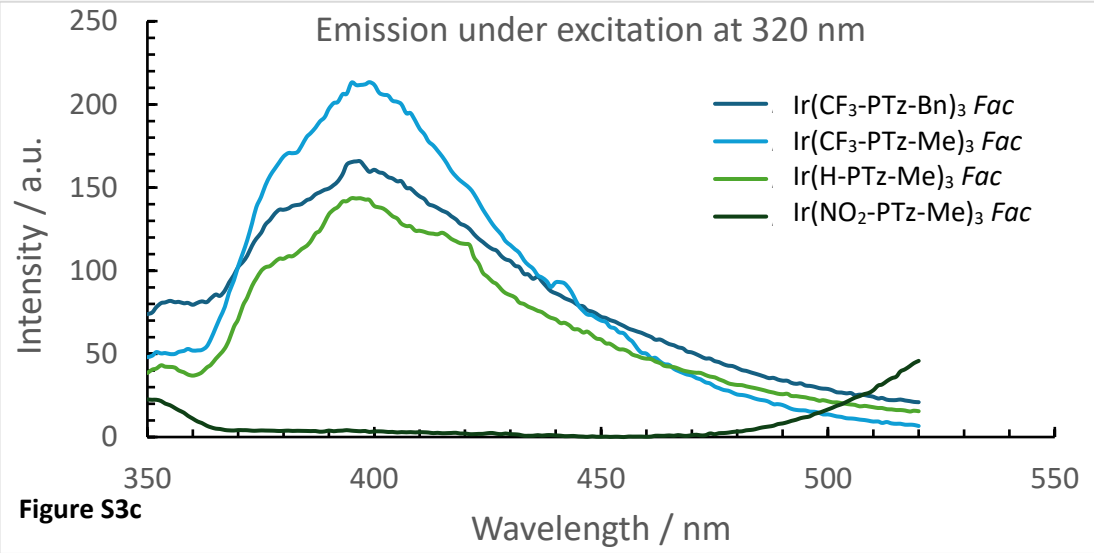

Figure S3c

Figure S3a-c: The Emission spectra of the isolated *mer*/*fac* Ir(III) complexes recorded in a MeCN solution at 320 nm and split into spectra a-e for ease of comparison. Sample concentrations were adjusted to give absorbance values of 0.1 prior to measurement.

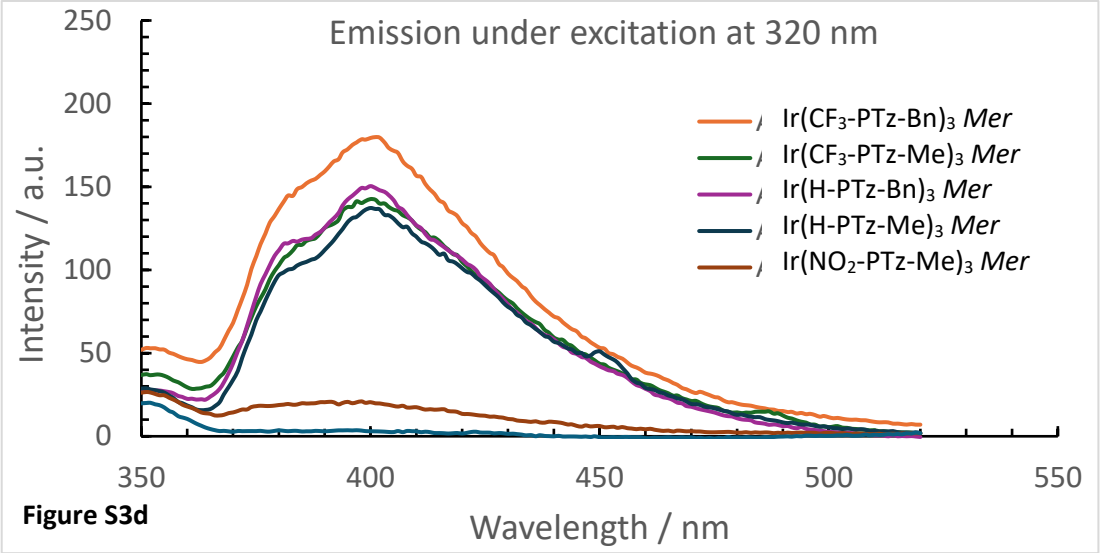

Figure S3d

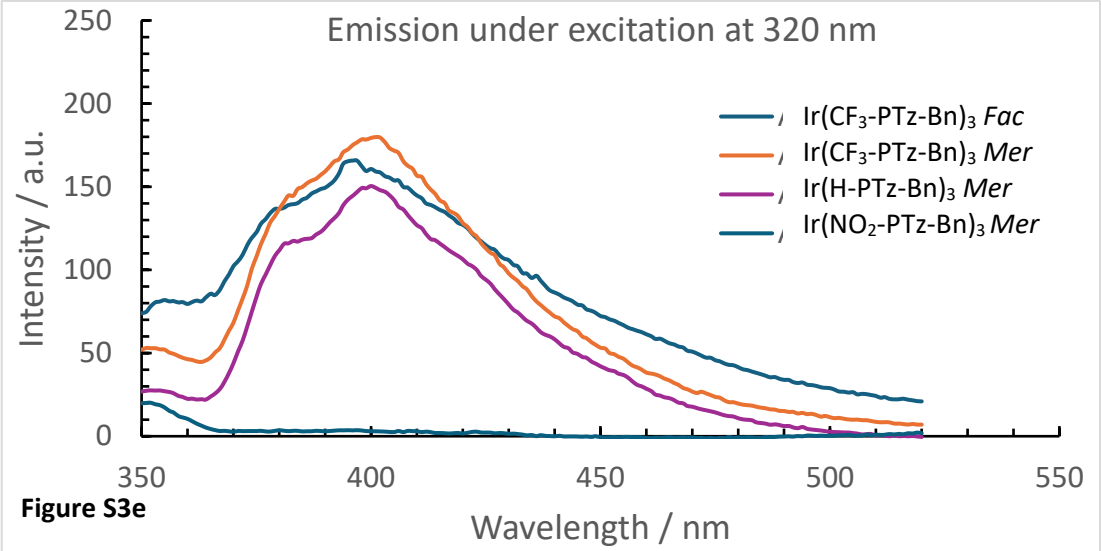

Figure S3e

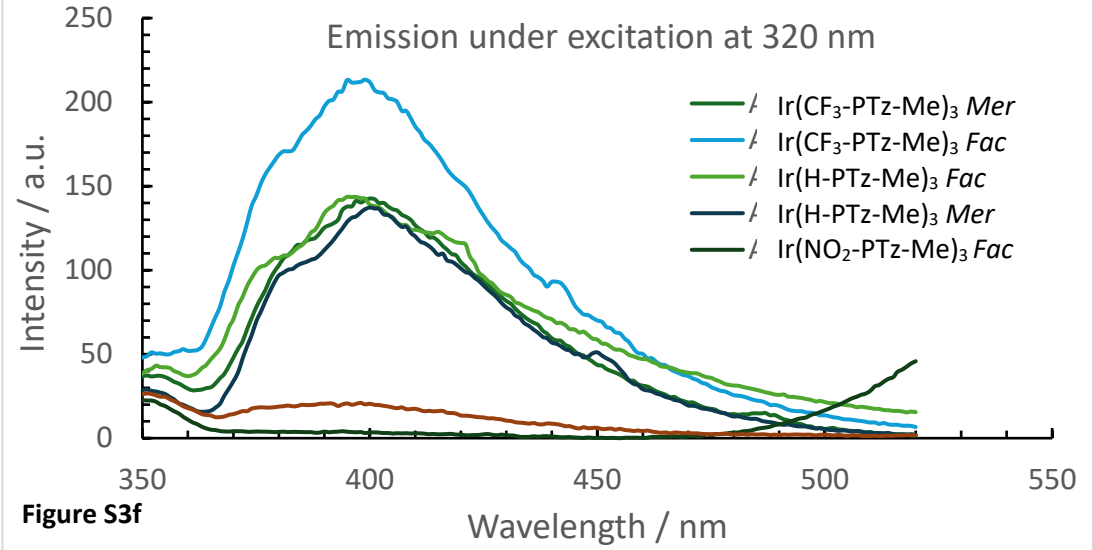

Figure S3f

Figure S3d-f: The Emission spectra of the isolated *mer*/*fac* Ir(III) complexes recorded in a MeCN solution at 320 nm and split into spectra d-f for ease of comparison. Sample concentrations were adjusted to give absorbance values of 0.1 prior to measurement.

7.2. Crystal Data

Table S1: Tabulated data of all 10 isolated mer/fac Ir(III) crystal structures and the isolated tosylate salt crystal.

	$Ir(CF_3\text{-}PTz\text{-}Me)_3$ *Fac* + acetone	$Ir(CF_3\text{-}PTz\text{-}Me)_3$ *Mer* +0.75 water	$Ir(H\text{-}PTz\text{-}Me)_3$ *Fac*	$Ir(H\text{-}PTz\text{-}Me)_3$ *Mer*	$Ir(CF_3\text{-}PTz\text{-}Bn)_3$ *Fac* +chloroform	Tosylate salt
Formula	$C_{33}H_{27}F_9IrN_9O$	$C_{30}H_{21}F_9IrN_9O$	$C_{27}H_{24}IrN_9$	$C_{27}H_{24}IrN_9$	$C_{49}H_{34}C_{13}F_9IrN_9$	$C_7H_7NaO_{3.50}S$
Formula Moiety	$C_{30}H_{21}F_9IrN_9$, C_3H_6O	$C_{30}H_{21}F_9IrN_9$, 0.75 H_2O	$C_{27}H_{24}IrN_9$	$C_{27}H_{24}IrN_9$	$C_{48}H_{33}F_9IrN_9$, C H C_{13}	$C_7H_7NaO_{3.50}S$
M (g/mol)	928.83	886.76	666.75	666.75	1218.40	202.18
Crystal Colour	Colourless	Colourless	Colourless	Colourless	Colourless	Colourless
Crystal Size (min,mid,max)	0.04, 0.05, 0.14	0.05, 0.06, 0.18	0.04, 0.06, 0.09	0.11, 0.12, 0.14	0.06, 0.08, 0.14	0.02,0.06,0.07
Crystal system	Monoclinic 14	Monoclinic 14	Triclinic 2	Orthorhombic 33	Triclinic 2	Monoclinic 14
Space group	P 1 21/c 1	P 1 21/n 1	P -1	P n a 21	P -1	P 1 21/c 1
a (Å)	11.46850	11.16340	9.7135	16.6933	11.7749	17.8243
b (Å)	19.17030	17.7407	11.2263	14.05564	13.4960	14.610017
c (Å)	15.70610	15.9857	14.1452	10.56950	15.6037	6.70639
α (o)	90	90	89.514	90	75.727	90
β (o)	96.9510	97.7460	89.554	90	73.937	90.94115
γ (o)	90	90	83.307	90	79.425	90
V ($Å^3$)	3427.68	3137.02	1531.88	2479.97	2291.52	1746.24
Density (g cm-3)	1.800	1.878	1.445	1.786	1.766	1.538
Z	4	4	2	4	2	8
Temperature (K)	100.00	100.00	102.00	100.00	100.01	100.00
μ (mm-1)	8.370	9.111	4.387	5.420	7.994	3.577
Radiation type	Cu K\a	Cu K/a	Mo K/a	Mo K/a	Cu K/a	Cu K/a
Radiation Wavelength (Å)	1.54184	1.54184	0.71073	0.71073	1.54184	1.54184
Theta range	3.654, 76.867	3.741, 76.747	3.282, 29.757	3.431, 29.531	3.013, 72.841	3.9070 53.2770
D_{calc}	1.800	1.878	1.446	1.786	1.766	1.538

Refinement program and method	SHELXL 2018/3 (Sheldrick, 2015) refined by full-matrix least-squares on F^2	SHELXL 2018/3 (Sheldrick, 2015) refined by full-matrix least-squares on F^2	SHELXL 2018/3 (Sheldrick, 2015) refined by full-matrix least-squares on F^2	SHELXL 2018/3 (Sheldrick, 2015) refined by full-matrix least-squares on F^2	SHELXL 2014/6 (Sheldrick, 2015) refined by full-matrix least-squares on F^2	SHELXL 2014/6 (Sheldrick, 2015) refined by full-matrix least-squares on F^2
Reflns. collected	69380	63410	33417	20212	33889	9555
Ind. reflns. [Rint]	7173 0.0382	6553 0.0361	7734 0.0574	6043 0.0244	8999 0.0625	2467 0.1094
Reflns. observed	6835	6354	7288	5632	8252	1603
Reflns. used in refinement, n	7173	6553	7734	6043	8999	2467
LS parameters, restraints	480, 0	460, 0	334, 0	337, 1	650, 3	228,0
R1 (for $I > 2\sigma$)	0.0284	0.0500	0.0232	0.0257	0.0446	0.0743
wR2	0.0753	0.1062	0.0528	0.0594	0.1189	0.2041
S	1.111	1.308	1.065	1.041	1.020	1.052
Largest difference peak/hole ($e–Å^{-3}$)	-2.447, 0.868	-1.429, 1.417	-1.442, 1.145	-1.412, 1.125	-1.765, 3.414	-0.487, 0.982
	$Ir(CF_3\text{-}PTz\text{-}Bn)_3$ *Mer*	$Ir(H\text{-}PTz\text{-}Bn)_3$ *Mer* +solvents	$Ir(NO_2\text{-}PTz\text{-}Me)_3$ *Fac* + 0.75 water	$Ir(NO_2\text{-}PTz\text{-}Me)_3$ *Mer*	$Ir(NO_2\text{-}PTz\text{-}Bn)_3$ *Mer* + water	
Formula	$C_{48}H_{33}F_9IrN_9$	$C_{45}H_{36}IrN_9$	$C_{27}H_{22.5}IrN_{12}O_{6.75}$	$C_{27}H_{21}IrN_{12}O_6$	$C_{45}H_{35}IrN_{12}O_7$	
Formula Moiety	$C_{48}H_{33}F_9IrN_9$	$C_{45}H_{34}IrN_9$,	$C_{27}H_{21}IrN_{12}O_6$,	$C_{27}H_{21}IrN_{12}O_6$	$C_{45}H_{33}IrN_{12}O_6$, H_2O	
M (g/mol)	1099.03	895.03	815.27	801.76	1048.05	
Crystal Colour	Colourless	Colourless	Yellow	Colourless	Colourless	
Crystal Size (min,mid,max)	0.06, 0.09, 0.11	0.04, 0.05, 0.08	0.08, 0.1, 0.13	0.05, 0.08, 0.12	0.03, 0.04, 0.09	
Crystal system	Monoclinic 14	Monoclinic 15	Monoclinic 14	Monoclinic 14	Monoclinic 14	
Space group	P 1 21/c 1	C 1 2/c 1	P 1 21/n 1	P 1 21/c 1	P 1 21/c 1	
a (Å)	18.30370	38.4189	15.79100	11.2165	15.3730	
b (Å)	22.18010	9.35242	13.56110	20.5659	13.2769	
c (Å)	21.31420	21.8265	27.9666	17.0167	20.8302	
α (o)	90	90	90	90	90	

β (o)	98.44	102.7717	97.3790	107.257	103.426	
γ (o)	90	90	90	90	90	
V ($Å^3$)	8559.34	7648.42	5939.26	3748.66	4135.34	
Density (g cm-3)	1.706	1.555	1.824	1.421	1.683	
Z	8	8	8	4	4	
Temperature (K)	100.00	100.00	100.00	100.00	100.00	
μ (mm-1)	6.802	7.115	9.290	3.612	6.836	
Radiation type	Cu K/a	Cu K/a	Cu K/a	Mo K/a	Cu K/a	
Radiation Wavelength (Å)	1.54184	1.54184	1.54184	0.71073	1.54184	
Theta range	2.440, 76.506	4.154, 76.568	3.057, 76.739	3.317, 28.777	2.955, 73.939	
D_{calc}	1.706	1.555	1.824	1.421	1.683	
Refinement program and method	SHELXL 2018/3 (Sheldrick, 2015) refined by full-matrix least-squares on F^2	SHELXL 2018/3 (Sheldrick, 2015) refined by full-matrix least-squares on F^2	SHELXL 2018/3 (Sheldrick, 2015) refined by full-matrix least-squares on F^2	SHELXL 2018/3 (Sheldrick, 2015) refined by full-matrix least-squares on F^2	SHELXL 2018/3 (Sheldrick, 2015) refined by full-matrix least-squares on F^2	
Reflns. collected	208066	53763	75247	52642	16498	
Ind. reflns. [Rint]	17875 0.0362	7921, 0.0871	12379 0.0277	8736 0.0566	8140 0.0511	
Reflns. observed	16926	6203	11927	6949	6279	
Reflns. used in refinement, n	17875	7921	12379	8736	8140	
LS parameters, restraints	1284, 72	493, 0	829, 0	418, 0	589, 12	
R1 (for I > 2σ)	0.0339	0.0381	0.0194	0.0504	0.0641	
wR2	0.0826	0.0948	0.0499	0.1150	0.1493	
S	1.104	1.025	1.036	1.077	1.069	
Largest difference peak/hole (e–$Å^{-3}$)	-1.918, 2.692	-1.363, 1.639	-0.878, 0.867	-1.817, 1.929	-2.343, 3.451	